Gallium-hydrides in zeolites for catalytic dehydrogenative transformation of alkanes

（ゼオライト中のガリウム水素化物を用いたアルカン脱水素反応）

Huang Mengwen

Graduate School of Chemical Sciences and Engineering
Hokkaido University

2024

Table of contents

Chapter 1

General Introduction

1.1. Ga-exchanged zeolites for light alkane transformation

Heterogeneous catalysts are indispensable as key materials in the modern chemical industry to promote and control chemical reactions and reduce the energy consumption in chemical processes, including separation/purification. Among the heterogeneous catalysts, zeolites have been widely applied in several chemical processes[1–6] and environmental cleanups.[7–12] One of their features is a crystalline microporous structure consisting of connections between corner sharing tetrahedral SiO_4 units. Various metal species can be incorporated into their frameworks to afford heteroatomic zeolites. When trivalent metal species such as Al are incorporated, the frameworks possess a negative charge owing to the isomorphic substitution of SiO_4 units with AlO_4 units (Al sites). To compensate for the negative charge, extra-framework cationic species, such as H^+ and NH_4^+ , are accommodated at the Al sites in zeolites. These cations can be exchanged with metal cations to synthesize metal-exchanged zeolites, in which the generated cationic species are isolated by zeolite pores. Zeolites have great potential to form unique active metal species and their catalysis can be investigated to develop effective heterogenous catalysts.[13–15]

Group 13 metal-exchanged zeolites have attracted considerable attention for light alkane transformations, such as Cyclar process.[16–18] Ga-exchanged MFI (Ga-MFI) is one of the most widely studied zeolites for light alkane transformations. Ono et al. synthesized Ga-MFIs using a liquid-phase ion-exchange method and subsequently used it for the dehydrocyclodimerization (DHCD) of propane to aromatics.[19] To improve the activity of Ga-MFI by loading larger amounts of Ga species, reductive solid-state ion-exchange (RSSIE) under H_2 flow was investigated.[20] Several reduced Ga species, such as Ga^+ cations and Ga-hydrides ($[GaH]^{2+}$ and $[GaH_2]^+$), are considered as catalytically active species for propane (C_3H_8) dehydrogenation (PDH) in the absence of an oxidant.[21–23] Two isolated Ga-hydrides are distinguishable by Fourier-transform infrared (FTIR) measurement because their Ga–H stretching vibration peaks are observed at different wavenumbers.[22] Bell and co-workers reported that $[GaH]^{2+}$, as opposed to $[GaH_2]^+$ ions, are active species by using a combination of kinetic, spectroscopic, and theoretical studies,[24] whereas Lewis–Brønsted acid pairs (Ga^+ and H^+) have been proposed as active sites by the Lercher's group based on characterization and catalytic investigation of a series of Ga-MFIs with different Ga/Al ratios and theoretical investigations.[25] Various Ga-exchanged zeolites, including Ga-MFIs, have been applied to the transformation of other light alkanes to aromatic compounds, dehydrogenation of light alkanes, and reactions of CH_4 with light alkenes to produce higher hydrocarbons.[26–28] Studies on

the use of oxidized Ga species for alkane activation have also been reported. For example, the formation and catalysis of Ga-oxo clusters during H_2O-accelerated alkane dehydrogenation were discussed by Hensen et al.[29,30] Regardless of whether they are reduced and oxidized, the reaction mechanism of alkane activation over possible Ga species has been theoretically discussed.[31–35] Several reaction pathways, including alkyl, carbenium, or concerted mechanisms over possible reduced Ga cations (Ga^+ , $[GaH]^{2+}$, and/or $[GaH_2]^+$) have been considered in the density functional theory (DFT) studies for non-oxidative alkane dehydrogenation utilizing cluster models.[32,33,35] A recent study using a hybrid quantum mechanics/molecular mechanics model provided reasonable activation barrier values similar to the experimentally obtained ones where isolated Ga-hydrides were predicted to be more active than Ga^+ cations.[31] A few oxidized Ga cations, such as $[GaO]^+$ and $[Ga_2O_2]^{2+}$, were considered as possible active sites for alkane dehydrogenation in the presence of oxidants.[34] Based on this perspective, the speciation of active Ga species in zeolites for light-alkane transformation based on a combination of experimental and theoretical investigations is briefly introduced.

1.2. Ga-hydrides formation in MFI zeolites

Recent research has significantly advanced our understanding of hydrides in/on solid materials, particularly in catalysis.[43-50] Metal hydrides on solid supports are key in hydrogenation and dehydrogenation reactions using heterogeneous catalysts.[49,50] Despite their importance, the complex surface structures of metals/metal oxides and the transient nature of metal hydrides make their analysis challenging. Surface organometallic chemistry offers a way to design well-defined metal hydrides, but high-temperature conditions often cause their thermal decomposition, limiting their catalytic applications.

Ga-loaded zeolites, specifically Ga-exchanged MFI (Ga-MFI), have emerged as promising catalysts for light alkane transformations.[16-18] Ga-MFI is prepared by immobilizing Ga_2O_3 on MFI, followed by H_2 treatment. This process leads to various Ga species, both reduced (Ga^+ cations and isolated Ga hydrides) and oxidized (Ga oxides), which are proposed as active sites for light alkane dehydrogenation.[51-56] However, Ga-oxide-based catalysts tend to deactivate quickly, while Ga hydrides show more activity under reductive conditions. The presence of Ga hydrides was first suggested through in situ X-ray absorption spectroscopy,[21] and further detailed through in situ infrared spectroscopy,[22] identifying $[GaH]^{2+}$ and $[GaH_2]^+$ ions. However, the detailed Ga speciation, including remaining Ga-oxides, and dehydrogenation catalysis are yet to be extensively investigated.

1.3. Ga-hydrides in different zeolite frameworks

Zeolites are crystalline aluminosilicates with porous structures formed by tetrahedral SiO_4 and AlO_4

units. The substitution of Si^{4+} with Al^{3+} in these frameworks introduces a negative charge, balanced by cations like protons. This feature allows for ion-exchange methods to introduce metal species, creating metal-exchanged zeolites used in various catalytic reactions.[57-66] In the development of zeolite-based catalysts, the framework type often affects the formation of active metal cation species, resulting in different catalytic performances.[67-72]

The formation of Ga-hydrides was first suggested by Iglesia's group using in situ XAS. Subsequent studies have focused on the speciation of these hydrides and their role in alkane transformations. Other Ga catalysts supported by different zeolites have been explored. Buckles et al. studied Ga-exchanged Y zeolites for propane dehydrogenation, finding lower activity compared to Ga-MFI.[55] Hensen et al. used DFT calculations to study Ga-oxo cations in MOR zeolites, concluding that cyclic $Ga_2O_2^{2+}$ ions are more stable and effective for alkane dehydrogenation than isolated GaO^+ ions.[30] Machado's and Vazhnova's research further compared the activity of Ga-loaded zeolites in various reactions, highlighting the versatility of these materials.[73]

Although a few examples of Ga species in zeolites have been reported, the effect of zeolite frameworks on Ga-hydride formation and subsequent catalysis remains an unexplored area, presenting opportunities for further research in this field.

1.4. In situ Ga K-edge XANES study of Ga-exchanged zeolite

Several research groups have investigated the formation of reduced Ga species in different ratios by Fourier transform infrared (FTIR) spectroscopy using probe molecules as well as their relationship with the dehydrogenation catalysis of Ga-exchanged zeolites.[23, 24, 27, 31] However, the pressure and temperature for catalytic reaction conditions (atmospheric alkane flow conditions and >600 °C) are often different from those for catalyst characterization (vacuum conditions, <300 °C). Besides, unreacted GaOx species often remained especially in the Ga-MFIs prepared under high Ga loading and/or reported temperature (500-600 °C), [25,74] which hinders the elucidation of active Ga species. Although the aforementioned spectroscopic studies have provided important insights into the formation and presence of Ga hydrides upon H_2 treatment, the characterization of Ga-exchanged zeolites under operating conditions has rarely been investigated.

X-ray absorption spectroscopy (XAS) is a physicochemical characterization technique used to study the local structure of materials because it is sensitive to the electronic structure of the targeted atoms. One of the advantages of XAS over other characterization techniques is its applicability to in situ spectroscopic studies under operational conditions, such as heterogeneous catalytic reactions.[75] In the context of in situ X-ray absorption spectroscopy (XAS) studies focused on Ga-exchanged zeolites, several research groups

have observed a lower-energy shift in the X-ray absorption near edge structure (XANES) spectra following hydrogen (H_2) activation, including during the reductive solid-state ion-exchange (RSSIE) process. Iglesia et al. proposed the formation of Ga-hydride species based on the energy shift and disappearance of the extended X-ray absorption fine structure (EXAFS) features,[21] whereas the formation of Ga^+ cations was considered by other research groups[76,77]. Hock et al. recently discussed this shift in XANES spectra based on organometallic model Ga complexes where the lower energy shift can be ascribed to the formation of both reduced Ga species[78]. Despite considerable effort devoted to XANES studies on reduced Ga species in zeolites, their speciation (Ga^+ cations or Ga hydrides) remains controversial.

1.5. Ga-zeolites for anaerobic ammodehydrogenation of ethane

Acetonitrile (CH_3CN) production, typically a byproduct of propylene ammoxidation to acrylonitrile (CH_2=CHCN), depends heavily on acrylonitrile demand.[79,80] An independent method for producing CH_3CN from abundant ethane (C_2H_6) offers a promising alternative.[81-89] Previously, pioneering works by Li and Armor[85,90,91] showed the selective formation of CH_3CN by the ammoxidation of C_2H_6 ($C_2H_6 + NH_3 + O_2$ reaction) over Co-exchanged zeolites. Recently, Xiang et al. developed an alternative route: direct CH_3CN synthesis by the anaerobic ammodehydrogenation of C_2H_6 ($C_2H_6 + NH_3$ reaction) over Pt- and Co-Pt-loaded MFI zeolites.[92,93] Although the formation of CH_3CN from C_2H_6 and NH_3 is thermodynamically less favorable than the ammoxidation of C_2H_6, Xiang et al. demonstrated that the ammodehydrogenation method affords higher activity and selectivity to CH_3CN than the conventional ammoxidation process[93]. To date, only two catalysts (Pt/MFI and Co-Pt-loaded MFI) have been reported for the ammodehydrogenation of C_2H_6.[92,93] This highlights the challenges in developing efficient catalysts for this new catalytic reaction.

Mechanistic studies by Xiang et al. showed a tandem dehydrogenation–amination–dehydrogenation mechanism; the initial C_2H_6 dehydrogenation over the metal sites was followed by amination between C_2H_4 and NH_3 to form ethylamine ($CH_3CH_2NH_2$), which underwent further dehydrogenation on the metal sites. Our group reported a series of studies on the anaerobic dehydrogenation of C_2H_6 over Ga- and In-loaded zeolites. Knowing the high dehydrogenation activity of these catalysts, we hypothesized that Ga- and In-loaded zeolites could be effective catalysts for C_2H_6 ammodehydrogenation.

1.6. Constitution of thesis

Based on these backgrounds, this thesis investigates the speciation of active Ga species in zeolites for selective ethane dehydrogenation and anerobic ethane ammodehydrogenation based on a combination

of experimental and theoretical investigations.

This thesis consists of the following 5 chapters. The outline of each chapter is as follows;

In **chapter 2**, the formation of Ga-hydride species in MFI zeolite and its superior activity for non-oxidative dehydrogenation of ethane were investigated.

In **chapter 3**, the crucial role of zeolite frameworks in Ga-hydride formation and its impact on ethane dehydrogenation catalysis were investigated.

In **chapter 4**, the findings from in situ XANES measurements under various conditions, and the role of whiteline intensity in indicating the presence of hydride sources in Ga-exchanged zeolites were investigated.

In **chapter 5**, the production of CH_3CN from C_2H_6 and NH_3 using various Ga-loaded zeolites and the superior performance of the Ga/HFER zeolite were investigated.

In **chapter 6**, the summary of each chapter and the outlook for further development.

Reference

1. E. T. C. Vogt and B. M. Weckhuysen, Chem. Soc. Rev., 2015, 44, 7342–7370.
2. C. Wei, Q. Yu, J. Li and Z. Liu, ACS Catal., 2020, 10, 4171–4180.
3. J. Zhong, J. Han, Y. Wei, P. Tian, X. Guo, C. Song and Z. Liu, Catal. Sci. Technol., 2017, 7, 4905–4923.
4. P. Tian, Y. Wei, M. Ye and Z. Liu, ACS Catal., 2015, 5, 1922–1938.
5. U. Olsbye, S. Svelle, M. Bjørgen, P. Beato, T. V. W. Janssens, F. Joensen, S. Bordiga and K. P. Lillerud, Angew. Chem., Int. Ed., 2012, 51, 5810–5831.
6. M. Ye, P. Tian and Z. Liu, Engineering, 2021, 7, 17–21.
7. J. Lee, J. R. Theis and E. A. Kyriakidou, Appl. Catal., B, 2019, 243, 397–414.
8. K. Khivantsev, N. R. Jaegers, L. Kovarik, S. Prodinger, M. A. Derewinski, Y. Wang, F. Gao and J. Szanyi, Appl. Catal., A, 2019, 569, 141–148.
9. J. Wang, H. Zhao, G. Haller and Y. Li, Appl. Catal., B, 2017, 202, 346–354.
10. F. Gao, J. H. Kwak, J. Szanyi and C. H. F. Peden, Top. Catal., 2013, 56, 1441–1459.
11. A. M. Beale, F. Gao, I. Lezcano-Gonzalez, C. H. F. Peden and J. Szanyi, Chem. Soc. Rev., 2015, 44, 7371–7405.
12. D. W. Fickel, E. D'Addio, J. A. Lauterbach and R. F. Lobo, Appl. Catal., B, 2011, 102, 441–448.
13. Q. Zhang, S. Gao and J. Yu, Chem. Rev., DOI: 10.1021/ acs.chemrev.2c00315.
14. J. Lee, J. R. Theis and E. A. Kyriakidou, Appl. Catal. B, 2019, 243, 397–414.
15. Z.-P. Hu, J. Han, Y. Wei and Z. Liu, ACS Catal., 2022, 12, 5060–5076.
16. Y. Ono, Catal. Rev., 1992, 34, 179–226.

17. N. Y. Chen and T. Y. Yan, Ind. Eng. Chem., 1986, 25, 151–155.
18. D. Seddon, Catal Today, 1990, 6, 351–372.
19. H. Kitagawa, Y. Sendoda and Y. Ono, J. Catal., 1986, 101, 12–18.
20. K. M. Dooley, C. Chang and G. L. Price, Appl. Catal., A, 1992, 84, 17–30.
21. G. D. Meitzner, E. Iglesia, J. E. Baumgartner and E. S. Huang, J. Catal., 1993, 140, 209–225.
22. V. B. Kazansky, I. R. Subbotina, R. A. van Santen and E. J. M. Hensen, J. Catal., 2004, 227, 263–269.
23. N. M. Phadke, J. van der Mynsbrugge, E. Mansoor, A. B. Getsoian, M. Head-Gordon and A. T. Bell, ACS Catal., 2018, 8, 6106–6126.
24. N. M. Phadke, E. Mansoor, M. Bondil, M. Head-Gordon and A. T. Bell, J. Am. Chem. Soc., 2019, 141, 1614–1627.
25. M. W. Schreiber, C. P. Plaisance, M. Baumga¨rtl, K. Reuter, A. Jentys, R. Bermejo-Deval and J. A. Lercher, J. Am. Chem. Soc., 2018, 140, 4849–4859.
26. N. M. Phadke, E. Mansoor, M. Head-Gordon and A. T. Bell, ACS Catal., 2021, 11, 2062–2075.
27. Y. Yuan, J. S. Lee and R. F. Lobo, J. Am. Chem. Soc., 2022, 144, 15079–15092.
28. L. Ni, R. Khare, R. Bermejo-Deval, R. Zhao, L. Tao, Y. Liu and J. A. Lercher, J. Am. Chem. Soc., 2022, 144, 12347–12356.
29. E. J. M. Hensen, E. A. Pidko, N. Rane and R. A. van Santen, Angew. Chem., Int. Ed., 2007, 46, 7273–7276.
30. E. A. Pidko, R. A. van Santen and E. J. M. Hensen, Phys. Chem. Chem. Phys., 2009, 11, 2893–2902.
31. E. Mansoor, M. Head-Gordon and A. T. Bell, ACS Catal., 2018, 8, 6146–6162.
32. Y. V. Joshi and K. T. Thomson, Catal. Today, 2005, 105, 106–121.
33. M. S. Pereira and M. A. C. Nascimento, Chem. Phys. Lett., 2005, 406, 446–451.
34. E. A. Pidko, R. A. van Santen and E. J. M. Hensen, Phys. Chem. Chem. Phys., 2009, 11, 2893–2902.
35. Z. Maeno, S. Yasumura, C. Liu, T. Toyao, K. Kon, A. Nakayama, J. Hasegawa and K. Shimizu, Phys. Chem. Chem. Phys., 2019, 21, 13415–13427.
36. Z. Maeno, S. Yasumura, X. Wu, M. Huang, C. Liu, T. Toyao and K. Shimizu, J. Am. Chem. Soc., 2020, 142, 4820–4832.
37. S. Yasumura, M. Huang, X. Wu, C. Liu, T. Toyao, Z. Maeno and K. Shimizu, Catal. Today, 2020, 352, 118–126.

38. M. Huang, S. Yasumura, L. Li, T. Toyao, Z. Maeno and K. Shimizu, Catal. Sci. Technol., 2022, 12, 986–995.
39. Z. Maeno, X. Wu, S. Yasumura, T. Toyao, Y. Kanda and K. Shimizu, Catalysts, 2020, 10, 807.
40. M. Huang, Z. Maeno, T. Toyao and K. Shimizu, Catal. Today, 2023, 411-412, 113824. 50 M. H. Groothaert, P. J. Smeets, B. F. Sels, P. A. Jacobs and R. A. Schoonheydt, J. Am. Chem. Soc., 2005, 127, 1394–1395.
41. J. S. Woertink, P. J. Smeets, M. H. Groothaert, M. A. Vance, B. F. Sels, R. A. Schoonheydt and E. I. Solomon, Proc. Natl. Acad. Sci. U. S. A., 2009, 106, 18908–18913.
42. Z. Maeno, S. Yasumura, X. Wu, M. Huang, C. Liu, T. Toyao and K. Shimizu, J. Am. Chem. Soc., 2020, 142, 4820–4832
43. R. Mohtadi and S. I. Orimo, Nat. Rev. Mater., 2016, 2, 1–16.
44. H. Hosono and M. Kitano, Chem. Rev., 2021, 121, 3121–3185.
45. S. R. Ovshinsky, M. A. Fetcenko and J. Ross, Science, 1993, 260, 176–181.
46. L. Schlapbach and A. Züttel, Nature, 2001, 414, 353–359.
47. P. Chen, Z. Xiong, J. Luo, J. Lin and K. Lee Tan, Nature, 2002, 420, 302–304.
48. H. Kageyama, K. Hayashi, K. Maeda, J. P. Attfield, Z. Hiroi, J. M. Rondinelli and K. R. Poeppelmeier, Nat. Commun., 2018, 9, 772.
49. C. Copéret, D. P. Estes, K. Larmier and K. Searles, Chem. Rev., 2016, 116, 8463–8505.
50. P. Serna and B. C. Gates, Acc. Chem. Res., 2014, 47, 2612–2620.
51. B. S. Kwak and W. M. H. Sachtler, J. Catal., 1994, 145, 456–463.
52. A. Biscardi and E. Iglesia, Catal. Today., 1996, 31, 207–231.
53. G. L. Price and V. Kanazirev, J. Catal., 1990, 126, 267–278.
54. P. Meriaudeau and C. Naccache, J. Mol. Catal., DOI:10.1016/0304-5102(90)85100-V.
55. G. Buckles, G. J. Hutchings and C. D. Williams, Catal. Lett., 1991, 11, 89–93.
56. G. L. Price, V. Kanazirev, K. M. Dooley and V. I. Hart, J. Catal., 1998, 173, 17–27.
57. Marberger, A. et al. Time-resolved copper speciation during selective catalytic reduction of NO on Cu-SSZ-13. Nat. Catal. 1, 221–227 (2018).
58. Moliner, M. & Corma, A. From metal-supported oxides to well-defined metal site zeolites: The next generation of passive NOx adsorbers for low-temperature control of emissions from diesel engines. React. Chem. Eng. 4, 223–234 (2019).
59. Song, J. et al. Toward Rational Design of Cu/SSZ-13 Selective Catalytic Reduction Catalysts: Implications from Atomic-Level Understanding of Hydrothermal Stability. ACS Catal. 7, 8214–8227 (2017).

60. Battiston, A. A., Bitter, J. H. & Koningsberger, D. C. Reactivity of binuclear Fe complexes in over-exchanged Fe/ZSM5, studied by in situ XAFS spectroscopy 2. Selective catalytic reduction of NO with isobutane. J. Catal. 218, 163–177 (2003).
61. Kosinov, N., Liu, C., Hensen, E. J. M. & Pidko, E. A. Engineering of Transition Metal Catalysts Confined in Zeolites. Chem. Mater. 30, 3177–3198 (2018).
62. Luo, W. et al. Zeolite-supported metal catalysts for selective hydrodeoxygenation of biomass-derived platform molecules. Green Chem. 21, 3744–3768 (2019).
63. Harris, J. W. et al. Molecular Structure and Confining Environment of Sn Sites in Single-Site Chabazite Zeolites. Chem. Mater. 29, 8824–8837 (2017).
64. Ichihashi, H. & Sato, H. The development of new heterogeneous catalytic processes for the production of ε-caprolactam. Appl. Catal. A Gen. 221, 359–366 (2001).
65. Nakamura, K. et al. Direct Methylation of Benzene with Methane Catalyzed by Co/MFI Zeolite. ChemCatChem 10, 4113–4119 (2018).
66. Tomkins, P., Ranocchiari, M. & Van Bokhoven, J. A. Direct Conversion of Methane to Methanol under Mild Conditions over Cu-Zeolites and beyond. Acc. Chem. Res. 50, 418–425 (2017).
67. Shi, J., Wang, Y., Yang, W., Tang, Y. & Xie, Z. Recent advances of pore system construction in zeolite-catalyzed chemical industry processes. Chem. Soc. Rev. 44, 8877–8903 (2015).
68. Dusselier, M. & Davis, M. E. Small-Pore Zeolites: Synthesis and Catalysis. Chem. Rev. 118, 5265–5329 (2018).
69. Deka, U., Lezcano-Gonzalez, I., Weckhuysen, B. M. & Beale, A. M. Local environment and nature of Cu active sites in zeolite-based catalysts for the selective catalytic reduction of NOx. ACS Catal. 3, 413–427 (2013).
70. Gounder, R. & Iglesia, E. The Roles of Entropy and Enthalpy in Stabilizing Ion-Pairs at Transition States in Zeolite Acid Catalysis. Acc. Chem. Res. 45, 229–238 (2012).
71. Mahyuddin, M. H., Staykov, A., Shiota, Y., Miyanishi, M. & Yoshizawa, K. Roles of Zeolite Confinement and Cu-O-Cu Angle on the Direct Conversion of Methane to Methanol by [Cu2(μ-O)]2+-Exchanged AEI, CHA, AFX, and MFI Zeolites. ACS Catal. 7, 3741–3751 (2017).
72. Lusardi, M. et al. Carbonylation of Dimethyl Ether to Methyl Acetate over SSZ-13. ACS Catal. 10, 842–851 (2020).
73. Machado, F. J., López, C. M., Campos, Y., Bolívar, A. & Yunes, S. The transformation of n-butane over Ga/SAPO-11 - The role of extra-framework gallium species. Appl. Catal. A Gen. 226, 241–252 (2002).
74. Y. Yuan, C. Brady, L. Annamalai, R. F. Lobo and B. Xu, J. Catal., 2021, 393, 60–69.

75. G. T. Whiting, F. Meirer and B. M. Weckhuysen, in XAFS Techniques for Catalysts, Nanomaterials, and Surfaces, eds. Y. Iwasawa, K. Asakura and M. Tada, Springer International Publishing, Cham, 2017, pp. 167–191.
76. A. C. Jr. Faro, V. de O. Rodrigues and J.-G. Eon, J. Phys. Chem. C, 2011, 115, 4749–4756.
77. E. J. M. Hensen, M. García-Sánchez, N. Rane, P. C. M. M. Magusin, P.-H. Liu, K.-J. Chao and R. A. van Santen, Catal. Lett., 2005, 101, 79–85.
78. A. “Bean” Getsoian, U. Das, J. Camacho-Bunquin, G. Zhang, J. R. Gallagher, B. Hu, S. Cheah, J. A. Schaidle, D. A. Ruddy, J. E. Hensley, T. R. Krause, L. A. Curtiss, J. T. Miller and A. S. Hock, Catal. Sci. Technol., 2016, 6, 6339–6353.
79. Deepa, H. A., Anusha, R. & Asha, P. Evaluation on Production and Economics of Acrylonitrile by Sohio Process. Int. J. Eng. Res. Technol. 4, 1–6 (2016).
80. Bell, A. T. Insights into the mechanism and kinetics of propene oxidation and ammoxidation over bismuth molybdate catalysts derived from experiments and theory. J. Catal. 408, 436–452 (2022).
81. Denton, W. I. & Bishop, R. B. Production of Acetonitrile and Other Low Molecular Weight Nitriles. Ind. Eng. Chem. 45, 282–286 (1953).
82. Catani, R. & Centi, G. Selective ethane ammoxidation to acetonitrile on alumina-supported niobium-antimony oxides. J. Chem. Soc. Chem. Commun. 1081–1083 (1991) doi:10.1039/C39910001081.
83. Liang, T. et al. Highly selective Sn/HZSM-5 catalyst for ethane ammoxidation to acetonitrile and ethylene. Appl. Catal. A Gen. 610, 117942 (2021).
84. Liu, X. et al. Ammoxidation of Ethane to Acetonitrile and Ethylene: Reaction Transient Analysis for the Co/HZSM-5 Catalyst. ACS Omega 5, 1669–1678 (2020).
85. Li, Y. & Armor, J. N. A reaction pathway for the ammoxidation of ethane and ethylene over Co-ZSM-5 catalyst. J. Catal. 176, 495–502 (1998).
86. Bondareva, V. M. et al. Ammoxidation of ethane on V-Mo-Nb oxide catalysts. React. Kinet. Catal. Lett. 87, 377–386 (2006).
87. Rojas, E., Guerrero-Pérez, M. O. & Bañares, M. A. Direct ammoxidation of ethane: An approach to tackle the worldwide shortage of acetonitrile. Catal. Commun. 10, 1555–1557 (2009).
88. Rubio-Marcos, F. et al. Tuning of Active Sites in Ni-Nb-O Catalysts for the Direct Conversion of Ethane to Acetonitrile or Ethylene. ChemCatChem 3, 1637–1645 (2011).
89. Essid, S. et al. Improvement of the conventional preparation methods in Co/BEA zeolites: Characterization and ethane ammoxidation. Solid State Sci. 93, 13–23 (2019).

90. Li, Y. & Armor, J. N. Ammoxidation of Ethane to Acetonitrile over Metal–Zeolite Catalysts. J. Catal. 173, 511–518 (1998).
91. Li, Y. & Armor, J. N. Ammoxidation of ethane to acetonitrile over Co-beta zeolite. Chem. Commun. 2013–2014 (1997).
92. Chen, G. et al. Acetonitrile formation from ethane or ethylene through anaerobic ammodehydrogenation. Catal. Today 113751 (2022) doi:10.1016/j.cattod.2022.05.016.
93. Chen, G. et al. Catalytic Light Alkanes Conversion through Anaerobic Ammodehydrogenation. ACS Catal. 11, 7987–7995 (2021).

Chapter 2

High-loading Ga-exchanged MFI zeolites as selective and coke-resistant catalysts for nonoxidative ethane dehydrogenation

2.1. Introduction

Hydrides in/on solid materials have garnered increasing attention and interest in various research fields.[1–8] In the field of catalysis, isolated metal hydrides on solid supports have been recognized as key species for hydrogenation and dehydrogenation reactions using heterogeneous catalysts since the 1970s.[7,8] On metals[10–16] and metal oxides[17–25], H_2 is cleaved in a homolytic or heterolytic manner to form metal–hydrogen (M−H) bonds. However, their analysis is difficult owing to the complexity of the surface structures of metals/metal oxides, as well as the instability of generated hydride species. In addition, the elucidation of their catalysis is complicated because metal hydrides are often formed as transient species during catalytic reactions. To design well-defined metal hydrides, an alternative method that utilizes surface organometallic chemistry has been explored.[26–29] Although various transition metal hydrides were successfully synthesized, they were thermally decomposed under high-temperature conditions, thus limiting their catalytic applications. The study of the formation and catalysis of surface metal hydrides under high-temperature conditions is still a formidable task.

Ga-loaded zeolites, such as Ga-exchanged MFI (Ga-MFI), have been utilized as promising catalysts for light alkane transformations.[30–32] Ga-MFI is typically prepared by immobilization of Ga_2O_3 on MFI via impregnation of $Ga(NO_3)_3$ and calcination, followed by H_2 treatment to promote reductive solid-state ion-exchange (RSSIE) reactions. Various types of Ga species, including those reduced (Ga^+ cations and isolated Ga hydrides) and those oxidized (Ga oxides, $[GaO]^+$, and $[Ga(OH)_2]^+$), are possibly formed and proposed as active sites for the dehydrogenation of light alkanes and several reaction mechanisms are proposed. [33–38] Alkane dehydrogenation on Ga oxides has been explored regardless of differences in structure and supports [39–46]; however, Ga-oxide-based catalysts often suffer from quick deactivation. Under reductive conditions without any oxidant, Ga hydrides are considered to be more active sites than Ga^+ cations. The presence of Ga hydrides was first proposed by Iglesia based on *in situ* X-ray absorption spectroscopy (XAS) measurement of Ga-MFI with Ga/Al = ca. 0.3 under H_2 flow at around 500 °C.[47] Kazansky et al. revealed the structure of Ga hydrides formed in the H_2 treated Ga-MFI with Ga/Al = 1.0 using *in situ* infrared (IR) spectroscopy, where $[GaH]^{2+}$ and $[GaH_2]^+$ ions were identified and the proportion of $[GaH_2]^+$ increased by increasing the treatment temperature from 300 to 500 °C.[48] However, the detailed Ga speciation, including remaining Ga-oxides, and the dehydrogenation catalysis have not

been extensively investigated. The effects of Ga/Al (0−1.7) and Si/Al ratios on the formation of Ga species were determined by Xu et al. where the partially reduced Ga oxide (GaO_X) oligomers/aggregation remained for high Ga loading (Ga/Al > 0.45) after H_2 treatment at 500 °C.[49]. Bell et al. prepared Ga-MFI containing only Ga species via the vapor-phase ion-exchange reaction of H-MFI with $GaCl_3$ (Ga/Al = 0.05−0.6) followed by H_2 treatment at 550 °C. $[GaH]^{2+}$ ions were mainly formed in the Ga-MFI with a low Ga/Al ratio of 0.2, and an increase in Ga/Al above 0.5, affording a mixture of $[GaH]^{2+}$ and $[GaH_2]^+$ ions.[50] $[GaH]^{2+}$ ions are more active species than $[GaH_2]^+$ ions for C_3H_8 dehydrogenation (PDH) although $[GaH_2]^+$ and $[GaH]^{2+}$ ions exhibited similar activities in C_2H_6 dehydrogenation (EDH).[51,52] Lercher et al. investigated the Ga/Al dependency (Ga/Al = 0−1.5) of the reaction rate for PDH and compared it with that of the amounts of Ga^+, Brønsted acid sites (BASs), and GaO_X oligomers. The medium loading Ga-MFI with Ga/Al = 0.5 exhibited the highest reaction rate. The pair of Ga cations and BASs is proposed as the active site for PDH, where $[GaH]^{2+}$ ions are formed from the Ga^+ cations-BASs pairs and thereafter activate C_3H_8.[53] The similar conclusion was proposed by Xu et al.[54] The formation of active Ga hydrides ($[GaH]^{2+}$ ions and H^+-$[GaH_2]^+$ pair) from Ga^+ cations with BASs under reductive conditions was also discussed by Bell et al. [51,52] Aforementioned studies have mainly focused on the characterization and dehydrogenation catalysis of low- to medium-loading Ga-MFIs [33,34,47,50–53] and the reports on the Ga-MFIs with high Ga loading (Ga/Al = ca. 1.0) have been limited. [48,49] The dehydrogenation catalysis of high-loading Ga-MFIs have been rarely explored.[38]

We have recently reported the formation of isolated In-hydrides in the form of $[InH_2]^+$ by high-temperature H_2 treatment of In-exchanged CHA zeolite (In-CHA) prepared via the RSSIE reaction. In-CHA exhibited high selectivity owing to low coke formation and good durability for EDH, where $[InH_2]^+$ ions serve as the catalytically active sites rather than In^+ cations and $[InH]^{2+}$ ions.[55] In contrast, Ga-CHA exhibited low selectivity and durability owing to severe coke formation, although the apparent activation barrier for dehydrogenation is much lower than that for In-CHA. The high selectivity of In-CHA can be interpreted as the formation of $[InH_2]^+$ ions rather than $[InH]^{2+}$ ions based on transition state (TS) calculations. Our calculation results demonstrate that the *in situ* generated BASs are relatively stable during the EDH on $[InH]^{2+}$ ions, whereas the reaction on $[InH_2]^+$ ions does not involve the *in situ* generation of BASs as stable intermediates. The abundance of *in situ* generated BASs for $[InH_2]^+$ ions is likely less than that of $[InH]^{2+}$ ions, resulting in the low coke formation in the In-CHA-catalyzed EDH. A similar difference in the reaction mechanisms between $[GaH]^{2+}$ and $[GaH_2]^+$ ions is also indicated by the comparison of the TS calculation for EDH by Ga-MFI in a recent paper by Bell et al.[56] These mechanistic insights imply that controlling the formation of $[GaH]^{2+}$ and $[GaH_2]^+$ ions influences the catalytic performance of Ga-zeolites for EDH.

In this paper, we aimed at investigating the effects of Ga loading amount and H_2 treatment temperature on the Ga species, including isolated Ga hydrides, in Ga-MFIs as well as their catalysis in EDH. $[GaH]^{2+}$ ions were preferentially formed in the low-loading Ga-MFI (Ga/Al = 0.3) treated with H_2 at a conventional temperature of 550 °C (Ga-MFI-0.3(550)), whereas the high-loading Ga-MFI (Ga/Al = 1.0) treated at a high temperature of 800 °C (Ga-MFI-1.0(800)) afforded $[GaH_2]^+$ ions as the major Ga hydrides. It is also found that the high temperature H_2 treatment of 800 °C was required to extensively promote the RSSIE for high-loading Ga-MFIs and that the different H_2 treatment temperature affects the proportion of $[GaH]^{2+}$ and $[GaH_2]^+$ ions in high-loading Ga-MFIs. In EDH, Ga-MFI-1.0(800) exhibited higher selectivity owing to much less coke formation compared to low-loading and medium-loading Ga-MFIs. We also discussed the difference between Ga-MFI-0.3(550) and 1.0(800) in *in situ* XAS measurements and kinetic study as well as the influence of different proportion of $[GaH]^{2+}$ and $[GaH_2]^+$ ions in the EDH catalyzed by high-loading Ga-MFIs.

2.2. Experimental

2.2.1. Catalyst preparation

The Ga-exchanged MFI zeolite catalysts were synthesized by the reductive solid-state ion-exchange method (RSSIE). First, a 1g NH_4^+-type MFI (SiO_2/Al_2O_3 = 22.3, Tosoh) was mixed with $Ga(NO)_3 \cdot nH_2O$ (n = 7-9, Wako) in 50 mL of deionized water. The water was removed from the mixture by the rotary evaporator under vacuum conditions. The resulting solid was dried in an oven and then calcined under air flow at 500 ℃ for 1 h to give the Ga_2O_3-modified MFI zeolite. After that, the Ga_2O_3-modified MFI zeolite was treated under 10% H_2/He flow at different temperature for 30 min, affording Ga-MFI-X(Y) where X and Y denotes the Ga/Al ratio and H_2 treatment temperature. The Ga/Al value was determined on the basis of the amounts of $Ga(NO_3)_3 \cdot nH_2O$ and MFI zeolite.

2.2.2 *In situ* FTIR measurement

In situ FTIR spectroscopy studies were carried out using a JASCO FT/IR-4600 spectrometer with a mercury cadmium telluride (MCT) detector and a flow-type quartz IR cell connected to a flow system. For characterization of Ga hydrides, the background spectrum was taken under 50 °C without catalyst in He atmosphere. The IR pellet of Ga-MFI-X(Y) was *in situ* obtained through the preparation of self-supported pellet of the corresponding Ga_2O_3-modified zeolite (Ga/Al = 0.3, 0.5, and 1.0) and set into the IR cell followed by H_2 treatment at different temperature (10% H_2/He flow at 550, 700 and 800 °C). Note that the same amount (40 mg) of Ga-MFIs was used for these IR experiments regardless of different Ga loading amount. The temperature was decreased to 50 °C under a H_2/He flow and the FTIR spectrum was recorded without exposure to air. After that, the sample was treated under He flow at 800 °C to decompose

Ga hydrides and then the IR spectrum was recorded again at 50 °C. Subtracting the IR spectrum after He treatment from the one before He treatment afforded the difference spectrum showing the peak derived from Ga hydrides. For pyridine (Py) adsorption experiments, the IR pellet was made *in situ* in the same manner as described above and cooled down to 150 °C in H_2/He atmosphere. Subsequently, purging with He to remove the H_2 and taking the background spectrum. Py was repeatedly introduced until the intensity of the bands derived from adsorbed Py species reached its saturation and then purged with He, followed by obtaining the IR spectra for adsorbed Py species. For NH_3 adsorption experiments, after the *in situ* preparation of IR pellet of Ga-MFI-X(Y), temperature was decreased to 50 °C under H_2/He flow and then purging by He to remove H_2. Prior to the NH_3 adsorption (10% NH_3/He), the background spectra were obtained under He flow at 50 °C. The IR spectra were obtained after the saturation of the peak area for adsorbed NH_3 and purging with He for 15 min.

2.2.3. *In situ* XAS measurement

A Ga K-edge XAS measurement was conducted in transmission mode in the BL14B2 station attached to a Si(311) monochromator at SPring-8 (JASRI), Japan (Proposal No. 2020A1695). The self-supported disk of a Ga_2O_3-modified MFI (Ga/Al = 0.3 or 1.0) was prepared and then put in a flow-type quartz cell with a flow reaction system was used. The XAS spectra were continuously recorded during the RSSIE reaction under 10% H_2/He flow with increasing the temperature from 200 to 550 or 800 °C. Note that the same amount (80 mg) of Ga-MFIs was used for these IR experiments regardless of different Ga loading amount. The absorption edge (E_0) was defined as the 1st inflection point.

2.2.3. EDH reactions

The catalyst test of C_2H_6 dehydrogenation over Ga-MFI-X(Y) was carried out at 660 °C in flow type reactor under atmospheric pressure conditions. Prior to the reaction, the corresponding Ga_2O_3-modified MFI catalyst with the loading of 0.1 g was pretreated with 10% H_2/He (10 mL/min) at different temperature for 30 min. After purging with He to remove H_2, the gas reactant (10 mL/min of 10% C_2H_6/He) was introduced to the flow type system at 660 °C. The conversion, selectivity, and carbon balance were determined by gas chromatography (GC) analysis which conducted by using Shimadzu GC-14B with a flame ionization detector (FID) and a Unipack S column. The details for determination were described in ESI†.

2.2.4. TPO measurement

TPO measurement was performed using BELCAT II (MicrotracBEL). 40 mg of the Ga-MFI-X(Y) after 2 h reaction was used for the TPO experiment. First, the sample was pretreated at 150 °C for 30 min under He atmosphere. Then switching the gas flow to 2% O_2/He (40 mL/min) and subsequently increasing the

temperature to 800 °C at 5 °C/min. During the measurement, the CO_2 generated through coke oxidation (m/z = 44) was monitored by mass spectroscopy (BELmass, MicrotracBEL).

2.3. Results and Discussion

2.3.1. Characterization of Ga species by *in situ* FTIR spectroscopy

In situ FTIR spectroscopy of a series of Ga-MFI was performed to examine the different Ga hydrides in MFI zeolites. In the previous literature, Ga-MFI was prepared conventionally under low to medium Ga loading (Ga/Al = 0.3−0.5) and H_2 treatment at around 500−600 °C, and two types of Ga hydrides are formed: $[GaH]^{2+}$ and $[GaH_2]^+$ ions.[48] The Ga hydrides exhibit peaks assignable to Ga−H stretching vibrations at around 2060 and 2040 cm^{-1}, respectively. [48,50] A recent theoretical study supports these peak assignments and shows that isolated Ga hydrides is kinetically trapped at high temperatures despite the thermodynamically favored formation of Ga^+ cations [56] although these vibration frequencies are higher than those reported in inorganic Ga hydride complexes. [57,58] Even though a few reports on Ga speciation for Ga-MFI with high Ga loading amount have appeared, [48,49,53] a high-loading Ga-MFI treated with H_2 at higher temperatures has been rarely investigated.

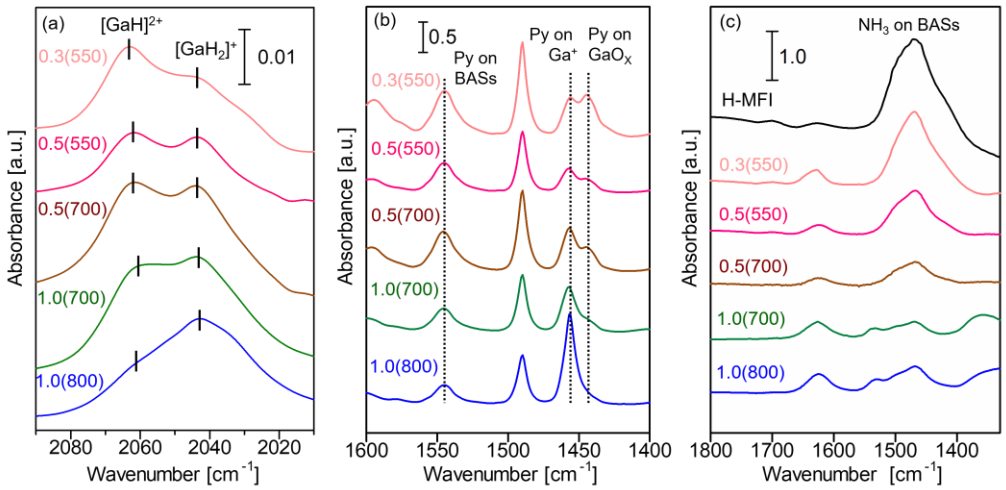

Fig. 1. Characterization of Ga species in Ga-MFI-X(Y) (X: Ga/Al ratio, Y: H_2 treatment temperature). (a) Difference IR spectra obtained at 50 °C without exposure to air. (b) IR spectra of adsorbed pyridine (Py) species at 150 °C. (c) IR spectra of adsorbed NH_3 species at 50 °C. The same amount (40 mg) of Ga-MFIs was used for these IR experiments regardless of different Ga loading amount. For (a), the IR spectrum after H_2 treatment at different temperature was recorded at 50 °C and then the sample was further treated at 800 °C under He flow followed by cooling to 50 °C to record the spectrum. The difference IR spectra were obtained by subtracting the spectra after He treatment from the ones after H_2 treatment. For (b) and

(c), the spectra were recorded after the saturation of Py or NH_3 adsorption followed by He purge. Prior to the adsorption experiment, the background spectra were taken under He flow.

The IR spectra were recorded at 50 °C after H_2 treatment for 1 h at different temperatures. Afterwards, the sample was treated under He at 800 °C for 1 h and subsequently cooled to 50 °C again to obtain the spectra. The difference spectrum was obtained by subtracting the spectra taken after He treatment from those taken after H_2/He treatment for each sample (**Fig. 1a**, the wide-range spectra are shown in **Fig. S1** in ESI†). The IR spectrum for Ga-MFI-0.3(550) exhibited a stronger band at 2063 cm^{-1} derived from $[GaH]^{2+}$ ions with a weaker band at 2043 cm^{-1} derived from $[GaH_2]^+$ ions. For Ga-MFI-0.5(550), both bands were clearly observed, where the band intensity derived from $[GaH_2]^+$ ions is similar to that of $[GaH]^{2+}$ ions. The increase in the H_2 treatment temperature from 550 to 700 °C increased both bands in intensity, indicating that the amount of both Ga hydrides were increased. When Ga/Al ratio was increased from 0.5 to 1.0 (Ga-MFI-1.0(700)), the band for $[GaH_2]^+$ ions became higher in intensity than that for $[GaH]^{2+}$ ions. Upon further increasing the H_2 treatment temperature from 700 to 800 °C (Ga-MFI-1.0(800)), the band intensity for $[GaH]^{2+}$ ions decreased, and the band derived from $[GaH_2]^+$ ions was mainly observed. In a separate experiment, Ga hydrides were regenerated by H_2 treatment of the He-treated Ga-MFI-1.0(800) (See **Fig. S2** in ESI†), confirming the decomposition of Ga hydrides by high-temperature He treatment (800 °C) and the formation of Ga hydrides by high-temperature H_2 treatment (800 °C). To further support the formation of Ga hydrides, the exchange reaction with D_2 was performed for Ga-MFI-1.0(800). The main band derived from $[GaD_2]^+$ ions and the minor band assignable to $[GaD]^{2+}$ ions appeared around 1460 and 1470 cm^{-1}, respectively, with the negative bands for $[GaH_2]^+$ and $[GaH]^{2+}$ ions observed at 2043 cm^{-1} and 2063 cm^{-1}. (**Fig. S3** in ESI†), supporting the formation of $[GaH]^{2+}$ and $[GaH_2]^+$ ions by high temperature H_2 treatment. The XRD measurements of a series of Ga-MFIs revealed that the diffraction pattern of MFI zeolites was maintained (**Fig. S4** in ESI†), which confirmed the preservation of zeolite frameworks after RSSIE reactions.

Pyridine (Py) adsorption experiments were conducted to investigate other Ga species. BASs, Ga^+ cations, and GaO_X can be identified by the difference in frequencies derived from adsorbed Py species.[49,53] Lercehr et al. extensively performed the pyridine adsorption experiments for Ga speciation in Ga-MFIs with a wide-range of Ga/Al (0−1.5) prepared by H_2 treatment at 600 ˚C. In their system, partially reduced Ga oxide (GaO_X) oligomers/aggregation remained for high Ga loading (Ga/Al ≥ 0.5).[53] Xu et al. reported the FTIR spectroscopic study for Ga-MFIs with a wider-range of Ga/Al (0−1.7). The temperature of H_2 treatment for reductive solid-state ion-exchange (RSSIE) reaction was limited to 500 ˚C and GaO_X remained for high Ga loading (Ga/Al > 0.45).[49] The sample was prepared *in situ* under H_2/He flow in the

same manner as described above and cooled to 150 °C under H_2/He flow. After taking the background spectra under He flow, Py was repeatedly introduced until the intensity of the bands for adsorbed Py species reached saturation and thereafter purged with He, followed by recording the IR spectra. The spectrum for Ga-MFI-0.3(550) (**Fig. 1b**) exhibited three peaks derived from Py on BASs, Ga^+ cations, and GaO_X at 1555, 1457, and 1446 cm^{-1}, respectively.[53] Note that other adsorbed Py species on strong Lewis acid sites, such as Al^{3+} cations, or defect sites of zeolites also possibly contribute to the absorption bands.[53] For Ga-MFI-0.5, the higher temperature treatment resulted in higher peak intensities for Ga^+ cations and GaO_X, indicating that the reduction of Ga_2O_3 was facilitated. When the Ga/Al ratio was increased to 1.0 (Ga-MFI-1.0(700)), the peak intensity for Ga^+ cations increased with the decrease of other peaks for BASs and GaO_X. A further increase in the H_2 treatment temperature to 800 °C afforded the highest peak intensity for Ga^+, although the peak derived from GaO_X was scarcely observed, indicating that the RSSIE reaction almost completely occurred.

Furthermore, NH_3 adsorption experiments were conducted to quantify the amount of the remaining BASs. The *in situ* prepared samples were exposed to 10% NH_3/He flow at 50 °C until the saturation of the peak area for the adsorbed NH_3 on the BASs (NH_4^+)[59] at around 1450 cm^{-1} and then purged with He for at least 15 min. Prior to NH_3 adsorption, background spectra were obtained under He flow at the same temperature. The amount of the remaining BASs was normalized by the peak area for NH_4^+ in H-MFI, prepared by He treatment of NH_4-MFI at 700 °C. The IR spectra for NH_3-adsorbed Ga-MFI-0.3(550) exhibited a moderate peak for NH_4^+, where the normalized area (denoted as $H^+/H^+_{H\text{-}MFI}$) was calculated to be 70% (**Fig. 1c**). Considering the formation of $[GaH]^{2+}$ ions that are charge-compensated by paired Al sites and the presence of remaining GaO_X, the RSSIE reaction was incomplete. For Ga-MFI-0.5, the $H^+/H^+_{H\text{-}MFI}$ value decreased from 38% to 18% with an increase in the H_2 treatment temperature from 550 to 700 °C. When Ga/Al was increased to 1.0, $H^+/H^+_{H\text{-}MFI}$ was low (12% and 18% at 700 °C and 800 °C, respectively). The higher $H^+/H^+_{H\text{-}MFI}$ value for Ga-MFI-1.0(800) than (700) is ascribed to the higher proportion of $[GaH_2]^+$ ions that require one Al sites.

From the above results, the speciation of Ga species in Ga-MFI prepared under different Ga/Al ratios and H_2 treatment temperatures is summarized as follows. $[GaH]^{2+}$ ions were preferentially formed in the low Ga loading (Ga/Al = 0.3), whereas the middle Ga loading (Ga/Al = 0.5) resulted in the moderate formation of both $[GaH]^{2+}$ and $[GaH_2]^+$ ions. In the high-loading Ga-MFI (Ga/Al = 1.0) treated with H_2 at a high temperature of 800 °C, the proportion of $[GaH_2]^+$ ions was the highest. In addition, the RSSIE reaction almost completely occurred, leading to the predominant formation of $[GaH_2]^+$ ions and Ga^+ cations as Ga hydrides and other Ga species, respectively. This result can be ascribed to the preferential formation of

monovalent Ga species ($[GaH_2]^+$ ions and Ga^+ cations) rather than divalent Ga species ($[GaH]^{2+}$ ions) under high Ga loading conditions above Ga/Al = 0.5.

2.3.2. *In situ* XAS measurements for Ga-MFI-0.3(550) and 1.0(800)

Iglesia et al. proposed the formation of Ga hydrides in Ga-MFI based on the lower energy shift in the XANES spectrum and the disappearance of EXAFS features[47] while Hensen et al. attributed the shift to the formation of Ga^+ cations.[60] Wilkinson reported the XAS spectra for Ga^+ cations supported on β''-Al_2O_3 or in $GaZr_2(PO_4)_3$, where their absorption edge energies were much lower than that for Ga^{3+} in $ZnGa_2O_4$.[61] Hock et al. recently performed the synthesis and XAS measurements of several organometallic model Ga complexes and concluded that the lower energy shift is equally interpreted as the formation of Ga^+ cations and Ga hydrides.[62]

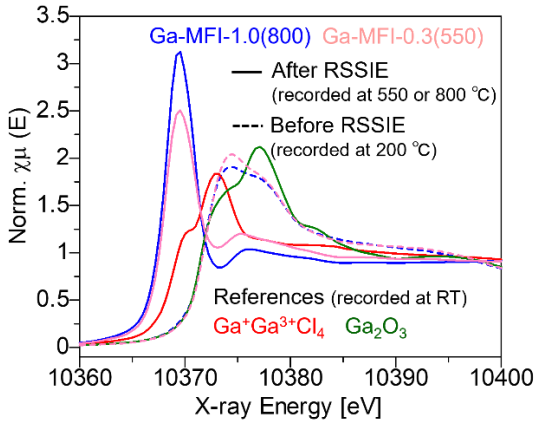

Fig. 2. *In situ* Ga K-edge XAS spectra of Ga-MFI-0.3(550) and 1.0(800) (pink and blue lines, respectively) before and after RSSIE (dot and solid lines, respectively). The spectra before RSSIE were obtained at 200 ˚C whereas the ones after RSSIE were recorded at the same temperature as H_2 treatment. For references (Ga_2O_3, $Ga^+Ga^{3+}Cl_4$), the spectra were obtained at room temperature.

In this work, *in situ* XAS measurements of Ga-MFI-0.3(550) and 1.0(800) were conducted and then the obtained spectra were compared. The self-supported disk of the corresponding Ga_2O_3-modified MFI zeolite after calcination was exposed to a 10% H_2/He flow at 200 °C and thereafter heated to 550 or 800 °C in a quartz cell to promote RSSIE reactions, as mentioned above. During the H_2 treatment, the XAS spectra were continuously recorded until the spectrum remained unchanged. The absorption edge of the XANES spectrum of Ga-MFI-0.3(550) and 1.0(800) before RSSIE was quite similar to that of bulk Ga_2O_3 (**Fig. 2**, E_0 = 10372.0, 10371.8, and 10371.6 eV, respectively. E_0 denotes the energy of the absorption edge,

defined as the first inflection point). Note that the XAS measurements of Ga-MFIs before RSSIE were performed at 200 °C while the XAS spectra of reference samples were obtained at room temperature.

After the H_2 treatment at each temperature, the XAS spectra were recorded without exposure to air at the same temperatures (550 or 800 °C). The absorption edge shifted to a lower value in the energy in both cases (E_0 = 10368.1 and 10368.3 eV for Ga-MFI-0.3(550) and 1.0(800), respectively), which are almost the same as that of Ga^+ in $Ga^+Ga^{3+}Cl_4$ (E_0 = 10369.3 eV)[53,62] (**Fig. 2**). However, the intensity of the peak around 10370 eV is much higher for Ga-MFI-1.0(800) than Ga-MFI-0.3(550). The stronger peak for Ga-MFI-1.0(800) is ascribed to the occurrence of sufficient RSSIE reaction and the exclusive formation of isolated Ga species ($[GaH]^{2+}$ and $[GaH_2]^+$ ions as well as Ga^+ cations), which is consistent with the FTIR results as discussed above.

2.3.3. EDH reaction using Ga-MFI-X(Y)

Next, the catalysis of a series of Ga-MFIs was compared in EDH reaction. This transformation is promising for obtaining C_2H_4, which is one of the most important bulk chemicals in industries, because of the increasing availability of cheap C_2H_6 from shale gas.[63–65] In comparison with the oxidative EDH, the high selectivity for C_2H_4 is obtained owing to the absence of an oxidant. Cracking reactions without catalysts are commercially operated, but severe reaction conditions above 1000 °C are required. In addition, rapid cooling of the outlet gas is necessary below 800 °C to suppress the successive reaction of C_2H_4. To decrease the reaction temperature, catalytic EDH has been investigated using mainly Pt-based alloys, Cr, and Ga catalysts.[63–65] However, most catalysts are easily deactivated owing to coke formation. In the context of EDH using Ga-MFI, the Ga-MFI with low-to-medium Ga/Al values have been studied previously[39,52], but the dehydrogenation catalysis of high-loading Ga-MFI has been rarely investigated.

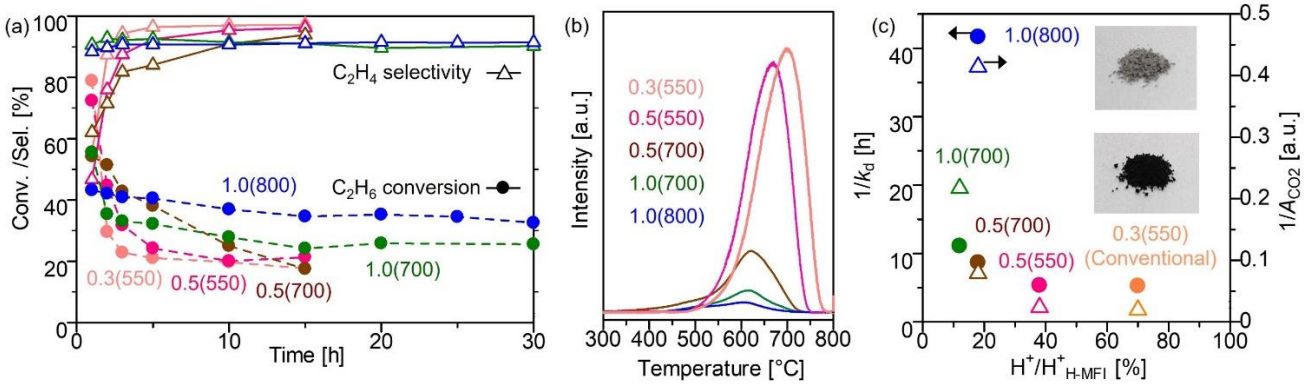

Fig. 3. (a) Conversion and selectivity in EDH using different Ga-MFI-X(Y). Reaction conditions: 100 mg of Ga-MFI-X(Y), 10 mL/min of 10% C_2H_6/He, and 660 °C. (b) TPO profiles of a series of Ga-MFI after

reaction for 2 h. (c) Plots of reciprocals of k_d in dehydrogenation tests and A_{CO2} in TPO experiments (indexes of durability and coking suppression, respectively) as a function of relative amount of the remaining BASs based ($H^+/H^+_{H\text{-}MFI}$). Upper and lower inset pictures are the Ga-MFI-1.0(800) and 0.3(550) after reactions for 2 h, respectively.

Table 1. Conversion, selectivity, and carbon balance values at 1, 15, and 30 h in EDH catalyzed by Ga-MFI-X(Y)[a]

Catalyst	Time [h]	Conv. [%][b]	Sel. [%][b]	Carbon balance [%][b]	k_d [h^{-1}][c]
GaMFI-0.3(550)	1	79	55	34	0.190
	15	18	97	96	
GaMFI-0.5(550)	1	72	47	52	0.187
	15	21	96	100	
GaMFI-0.5(700)	1	54	62	62	0.115
	15	18	94	97	
GaMFI-1.0(700)	1	56	91	61	0.090
	15	26	91	99	
	30	25	90	97	
GaMFI-1.0(800)	1	43	89	85	0.024
	15	35	91	99	
	30	33	91	98	

[a]Reaction conditions: 100 mg of Ga-MFI-X(Y), 10 mL/min of 10% C_2H_6/He, and 660 °C. [b]Determined by GC-FID. More information is presented in SI. [c]Deactivation rate for 15 h of reaction. The determination is described in SI.

The EDH using Ga-MFI-X(Y) was carried out at 660 °C (**Fig. 3a** and **Table 1**). Ga-MFI-0.3(550), prepared under conventional conditions, exhibited a high initial conversion (78%), but the selectivity for C_2H_4 was quite low (55%) at 1 h. The conversion of Ga-MFI-0.3(550) immediately decreased to about 20% within 3 h. Ga-MFI-0.5(550) also exhibited a similar initial conversion and selectivity (72% and 47%, respectively), whereas the conversion decreased to 22% after 8 h. Increasing the H_2 treatment temperature from 550 to 700 °C (Ga-MFI-0.5(700)) improved the C_2H_4 selectivity to 62% with a slight decrease in the initial conversion to 55%, leading to slightly better durability. When Ga/Al was increased from 0.5 to 1.0, the C_2H_4 selectivity was significantly enhanced, reaching about 90%. Although the initial conversion of Ga-MFI-1.0(800) (43%) was lower than that of Ga-MFI-1.0(700) (55%), the durability of Ga-MFI-1.0(800) was much better. The conversion of Ga-MFI-1.0(800) after 30 h of reaction was still higher than 30%, whereas that for Ga-MFI-1.0(700) decreased to less than 30% at 10 h. The deactivation rate (k_d)[65] for the 15 h reaction was calculated and thereafter compared among a series of Ga-MFIs. The k_d value increased in the order of Ga-MFI-1.0(800) < 1.0(700) < 0.5(700) < 0.5(550) < 0.3(550), indicating that Ga-MFI-1.0(800) exhibited the highest durability. Under the optimized reaction conditions using Ga-MFI-1.0(800), the C_2H_4 formation rate reached 72.1 mmol/(g·h) with good conversion and selectivity values (28.5% and 92.6%, respectively) as well as a low deactivation rate (0.014 h^{-1}) (**Fig. 4**). This formation rate is the highest among the reported Pt-free catalysts (**Table S1** in in ESI†)[55,66,75,67–74]. After the reaction, Ga-MFI-1.0(800) could be regenerated by oxidation treatment (a 5% O_2/He flow at 600 °C for 1.5 h) followed by H_2 treatment at 800 °C. The regenerated catalyst exhibited similar initial conversion and selectivity values to the original values (See **Fig. S5** in ESI†).

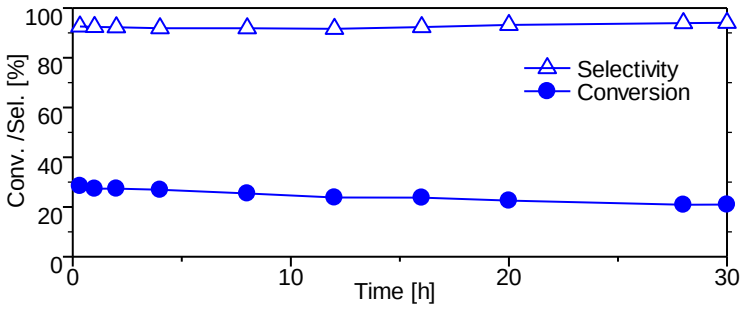

Fig. 4. Ga-MFI-1.0(800)-catalyzed EDH under optimized conditions. Reaction conditions: 50 mg of Ga-MFI-1.0(800), 10 mL/min of 50% C_2H_6/He, and 660 °C.

Temperature-programmed oxidation (TPO) experiments were conducted for the Ga-MFI-X(Y) used for the 2 h reaction. The generated CO_2 by coke oxidation was monitored by mass spectroscopy (m/z = 44), and the corresponding peaks were compared. The peak areas (A_{CO2}) for Ga-MFI-0.3(550) and 0.5(550) were much larger than those for others, and the A_{CO2} for Ga-MFI-1.0(800) was the lowest (**Fig. 3b**). These results demonstrate that coke formation was suppressed by the increase in Ga loading and H_2 treatment temperature. To further discuss the reason for coke formation, the reciprocal of k_d as an index of durability and that of A_{CO2} as an index of coking suppression were plotted as a function of the remaining BASs, $H^+/H^+_{H\text{-}MFI}$ (**Fig. 3c**). The trends of these plots were similar, which clearly shows that coke formation was the main cause of deactivation. This is also supported by a comparison of the color of the used Ga-MFI. The Ga-MFI-0.3(550) changed from white to black owing to coke formation after 2 h of reaction, whereas the most durable Ga-MFI-1.0(800) exhibited a gray color (the inset pictures in **Fig. 3c**). Among the tested Ga-MFI except for Ga-MFI-1.0(800), the $1/A_{CO2}$ value increased with a decrease in $H^+/H^+_{H\text{-}MFI}$, indicating that the remaining BASs induce coke formation. However, the $1/A_{CO2}$ value for Ga-MFI-1.0(800) was much higher than that for Ga-MFI-1.0(700) despite the same Ga loading and a higher $H^+/H^+_{H\text{-}MFI}$ value. The higher proportion of $[GaH_2]^+$ ions among isolated Ga hydrides ($[GaH_2]^+$ and $[GaH]^{2+}$ ions) might be the reason for lower coke formation for Ga-MFI-1.0(800). Although the high-loading Ga-MFIs treated with H_2 at lower temperature below 600 °C has been studied as proton-poor Ga-MFI for cyclodimerization of propane by Price et al. the characterization of Ga species and BASs as well as their effects on catalysis were not investigated. This study revealed the importance of high-temperature H_2 treatment and the influence of proportion of active Ga hydrides in high-loading Ga-MFIs.

2.3.4. Feasibility of isolated Ga hydrides as active sites based on kinetic studies

The reaction mechanism for alkane dehydrogenation has been discussed by several research groups.[53,56,76,77,78]. Lercher et al. theoretically investigated the PDH mechanism on the pair of Ga^+ cations and BASs via the formation of $[GaH]^{2+}$ ions and reported the experimental activation enthalpy for PDH as 106 kJ/mol. [53] Bell et al. show in the recent theoretical study for EDH that $[GaH]^{2+}$ and $[GaH_2]^+$ ions are more plausible catalytically active sites than Ga^+ cations and propose the following reaction mechanisms; alkyl or carbeinum mechanism on $[GaH]^{2+}$ ions, and alkyl or concerted mechanism on $[GaH_2]^+$ ions.[56] Alkyl mechanism involves the C_2H_4 formation from a pair of $[GaH(C_2H_5)]^+/H^+$ as a rate determining step (RDS) with a theoretical activation enthalpy (theoretical $\Delta H^{\ddagger}$) of 150 kJ/mol whereas a theoretical $\Delta H^{\ddagger}$ is predicted as 118 kJ/mol for the carbenium mechanism on $[GaH]^{2+}$ ions where both the C−H activation of C_2H_6 into a pair of $[GaH_2]^+/C_2H_5^+$ and the formation of C_2H_4 and H_2 from $[GaH_2]^+/C_2H_5^+$ are possibly RDSs. For $[GaH_2]^+$ ions, the alkyl mechanism involves C−H activation of C_2H_6 as an RDS with the theoretical $\Delta H^{\ddagger}$ of 115 kJ/mol, and the concerted mechanism does not compete with the alkyl mechanism owing to a high free energy barrier. These distinctions in reaction mechanisms imply that EDH reactions over $[GaH]^{2+}$ and $[GaH_2]^+$ ions show different kinetics. The same group also reported that $[GaH]^{2+}$ and $[GaH_2]^+$ ions exhibited similar activity for EDH using Ga-MFI with a different loading amount (Ga/Al = 0.05-0.6) where $[GaH]^{2+}$ ions and $[GaH_2]^+$-BAS cation pairs are formed from Ga cations.[51] However, the kinetic study was performed for only the medium-loading Ga-MFI (Ga/Al = 0.5) possessing both $[GaH]^{2+}$ and $[GaH_2]^+$ ions, and they discussed the kinetics for EDH over $[GaH_2]^+$ ions.

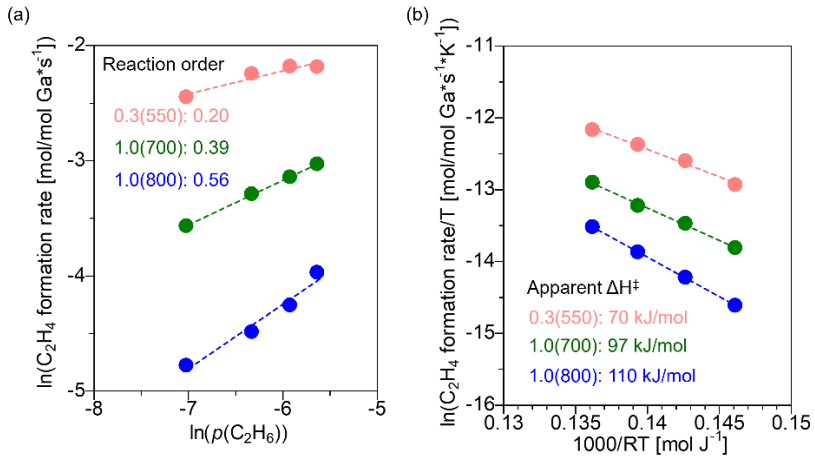

Fig. 5. Kinetic studies using Ga-MFI-0.5(550), 1.0(800), and 1.0(700). C_2H_4 formation rate dependence on (a) $p(C_2H_6)$ and (b) reaction temperature. Reaction condition for (a): 0.1 g of catalyst, 50 mL/min of 2−8% C_2H_6/He, and 600 °C. Reaction condition for (b): 0.1 g of catalyst, 50 mL/min of 4% C_2H_6/He, and 550−610 °C.

In this study, Ga-MFI-1.0(800) and 0.3(550) were used for kinetic studies as Ga-MFIs with the highest proportion of $[GaH_2]^+$ and $[GaH]^{2+}$ ions among tested catalysts, respectively. In the EDH using Ga-MFI-1.0(800), the increase of C_2H_6 partial pressure ($p(C_2H_6)$) increased the formation rate, and the reaction order was 0.56 (**Fig. 5a**), which suggests that the RDS involves C_2H_6 activation. The apparent $\Delta H^{\ddagger}$ determined experimentally from the temperature dependency of the C_2H_4 formation rate was 110 kJ/mol (**Fig. 5b**), which is similar to that in the experimental study reported by Bell et al. using Ga-MFI.[51] These observations support that $[GaH_2]^+$ ions are the active sites in Ga-MFI-1.0(800). In the case of EDH using Ga-MFI-0.3(550), the reaction order with respect to $p(C_2H_6)$ was determined as 0.20 (**Fig. 5a**), and the apparent $\Delta H^{\ddagger}$ was determined to be 70 kJ/mol (**Fig. 5b**), demonstrating the different kinetics from Ga-MFI-1.0(800). Although the obtained $\Delta H^{\ddagger}$ value was lower than the theoretical values reported by Bell et al., the low reaction order value suggest that $[GaH]^{2+}$ ions is more plausible active sites rather than rather $[GaH_2]^+$ ions. Furthermore, the kinetics of Ga-MFI-1.0(700) was investigated to discuss the influence of different proportion of $[GaH_2]^+/[GaH]^{2+}$ ions. The reaction order of $p(C_2H_6)$ was intermediate (0.39) while the apparent $\Delta H^{\ddagger}$ was determined to be 97 kJ/mol, which indicate that both $[GaH_2]^+$ and $[GaH]^{2+}$ ions contribute to the EDH using Ga-MFI-1.0(700). Based on the previous TS calculations reported by Bell et al.,[56] the EDH reaction over $[GaH]^{2+}$ ions involve the *in situ* formation of BASs and/or carbocations as relatively stable intermediates, which possibly induce the coke formation. In contrast, *in situ* generated BASs after C−H bond cleavage via alkyl mechanism smoothly reacts with the coordinated hydrides with the small free energy barriers in the EDH via alkyl mechanism on $[GaH_2]^+$ ions. The similar difference in reaction mechanism between $[InH_2]^+$ and $[InH]^{2+}$ was also found in our recent study on EDH using

In-exchanged zeolites.[55] It can be considered that the abundance of *in situ* generated BASs and/or carbocations during EDH is lower for $[GaH_2]^+$ ions than for $[GaH]^{2+}$ ions. Combined with our experimental results and prior discussion, $[GaH_2]^+$ ions are likely to act as more selective and coke-resistant active sites compared to $[GaH]^{2+}$ ions in EDH. The high selectivity and durability of Ga-MFI-1.0(800) is ascribed to both the low amount of remaining BASs and the main formation of $[GaH_2]^+$ ions.

2.4. Conclusion

In summary, we prepared a series of Ga-MFIs with different Ga loading amounts and H_2 treatment temperature and examined the generated Ga species and catalysis for EDH. *In situ* FTIR spectroscopy revealed that $[GaH]^{2+}$ ions were preferentially formed in low-loading Ga-MFI (Ga-MFI-0.3(550)), prepared under conventional conditions, whereas both $[GaH]^{2+}$ and $[GaH_2]^+$ ions were moderately formed in the middle-loading Ga-MFI (Ga/Al = 0.5). In contrast, $[GaH_2]^+$ ions were formed as the major Ga hydride in Ga-MFI-1.0(800). The characterization of other Ga species and BASs indicated that high-temperature H_2 treatment was required to promote the RSSIE sufficiently for high-loading Ga-MFI. In Ga-MFI-1.0(800), monovalent Ga species ($[GaH_2]^+$ ions and Ga^+ cations) are mainly formed. The difference of H_2 treatment temperature between 700 and 800 ˚C also affects the proportion of $[GaH]^{2+}$ and $[GaH_2]^+$ ions in high-loading Ga-MFI. In EDH, Ga-MFI-1.0(800) exhibited high selectivity owing to much less coke formation, resulting in the highest durability. Under the optimized reaction conditions, the highest C_2H_4 formation rate was achieved among the reported Pt-free catalyst systems. The kinetic study revealed that isolated Ga hydrides serve as active sites rather than Ga^+ cations. The main reason for the high catalytic performance of Ga-MFI-1.0(800) is a low amount of the remaining BASs by introducing the high loading amount of isolated Ga species. Based on the comparison of high-loading Ga-MFIs treated with different temperature (700 or 800 ˚C), the different proportion of active Ga hydrides ($[GaH_2]^+$ and $[GaH]^{2+}$ ions) also influences their catalysis in EDH.

References

1. Mohtadi, R. & Orimo, S. I. The renaissance of hydrides as energy materials. *Nat. Rev. Mater.* **2**, 1–16 (2016).
2. Hosono, H. & Kitano, M. Advances in Materials and Applications of Inorganic Electrides. *Chem. Rev.* **121**, 3121–3185 (2021).
3. Ovshinsky, S. R., Fetcenko, M. A. & Ross, J. A Nickel Metal Hydride battery for electric vehicles. *Science (80-.).* **260**, 176–181 (1993).
4. Schlapbach, L. & Züttel, A. Hydrogen-storage materials for Mobile Applications. *Nature* **414**, 353–359 (2001).
5. Chen, P., Xiong, Z., Luo, J., Lin, J. & Lee Tan, K. Interaction of hydrogen with metal nitrides and imides. *Nature* **420**, 302–304 (2002).
6. Kageyama, H. *et al.* Expanding frontiers in materials chemistry and physics with multiple anions. *Nat. Commun.* **9**, 772 (2018).
7. Copéret, C., Estes, D. P., Larmier, K. & Searles, K. Isolated Surface Hydrides: Formation, Structure, and Reactivity. *Chem. Rev.* **116**, 8463–8505 (2016).
8. Serna, P. & Gates, B. C. Molecular metal catalysts on supports: Organometallic chemistry meets surface science. *Acc. Chem. Res.* **47**, 2612–2620 (2014).
9. Polo-Garzon, F. *et al.* Neutron Scattering Investigations of Hydride Species in Heterogeneous Catalysis. *ChemSusChem* **12**, 93–103 (2019).
10. Kubota, T., Asakura, K. & Iwasawa, Y. Quantitative analysis of hydrogen adsorbed on Pt particles on SiO_2 in the presence of coadsorbed CO by means of L3-edge X-ray absorption near-edge structure spectroscopy. *Catal. Letters* **46**, 141–144 (1997).
11. Oudenhuijzen, M. K., Van Bokhoven, J. A., Miller, J. T., Ramaker, D. E. & Koningsberger, D. C. Three-site model for hydrogen adsorption on supported platinum particles: Influence of support ionicity and particle size on the hydrogen coverage. *J. Am. Chem. Soc.* **127**, 1530–1540 (2005).
12. Teschner, D. *et al.* The roles of subsurface carbon and hydrogen in palladium-catalyzed

alkyne hydrogenation. *Science (80-.).* **320**, 86–89 (2008).

13. Shimizu, K. I., Sugino, K., Sawabe, K. & Satsuma, A. Oxidant-free dehydrogenation of alcohols heterogeneously catalyzed by cooperation of silver clusters and acid-base sites on alumina. *Chem. - A Eur. J.* **15**, 2341–2351 (2009).
14. Juárez, R., Parker, S. F., Concepción, P., Corma, A. & García, H. Heterolytic and heterotopic dissociation of hydrogen on ceria-supported gold nanoparticles. Combined inelastic neutron scattering and FT-IR spectroscopic study on the nature and reactivity of surface hydrogen species. *Chem. Sci.* **1**, 731–738 (2010).
15. Ishida, R., Hayashi, S., Yamazoe, S., Kato, K. & Tsukuda, T. Hydrogen-Mediated Electron Doping of Gold Clusters As Revealed by in Situ X-ray and UV-vis Absorption Spectroscopy. *J. Phys. Chem. Lett.* **8**, 2368–2372 (2017).
16. Noujima, A., Mitsudome, T., Mizugaki, T., Jitsukawa, K. & Kaneda, K. Selective deoxygenation of epoxides to alkenes with molecular hydrogen using a hydrotalcite-supported gold catalyst: Aconcerted effect between gold nanoparticles and basic sites on a support. *Angew. Chemie - Int. Ed.* **50**, 2986–2989 (2011).
17. Hattori, H., Tanaka, Y. & Tanabe, K. A Novel Catalytic Property of Magnesium Oxide for Hydrogenation of 1,3-Butadiene. *J. Am. Chem. Soc.* **98**, 4652–4653 (1976).
18. Gribov, E. N. *et al.* Vibrational and thermodynamic properties of H_2 adsorbed on MgO in the 300-20 K interval. *J. Phys. Chem. B* **108**, 16174–16186 (2004).
19. Wischert, R., Laurent, P., Copéret, C., Delbecq, F. & Sautet, P. γ-Alumina: The essential and unexpected role of water for the structure, stability, and reactivity of 'defect' sites. *J. Am. Chem. Soc.* **134**, 14430–14449 (2012).
20. Wu, Z. *et al.* Direct Neutron Spectroscopy Observation of Cerium Hydride Species on a Cerium Oxide Catalyst. *J. Am. Chem. Soc.* **139**, 9721–9727 (2017).
21. Tsuneoka, H., Teramura, K., Shishido, T. & Tanaka, T. Adsorbed Species of CO_2 and H_2 on Ga_2O_3 for the Photocatalytic Reduction of CO_2. *J. Phys. Chem. C* **114**, 8892–8898 (2010).
22. Kondo, J., Sakata, Y., Domen, K., Maruya, K. I. & Onishi, T. Infrared study of hydrogen

adsorbed on ZrO_2. *J. Chem. Soc. Faraday Trans.* **86**, 397–401 (1990).

23. Tsoukalou, A. *et al.* Hydrogen Dissociation Sites on Indium-Based ZrO2-Supported Catalysts for Hydrogenation of CO2 to Methanol. *Catal. Today* (2021) doi:10.1016/j.cattod.2021.04.010.

24. Wang, L. *et al.* Room-Temperature Activation of H_2 by a Surface Frustrated Lewis Pair. *Angew. Chemie - Int. Ed.* **58**, 9501–9505 (2019).

25. LiBretto, N. J. *et al.* Olefin oligomerization by main group Ga3+ and Zn2+ single site catalysts on SiO2. *Nat. Commun.* **12**, 2322 (2021).

26. Copéret, C., Chabanas, M., Petroff Saint-Arroman, R. & Basset, J. M. Surface organometallic chemistry: Homogeneous and heterogeneous catalysis: Bridging the gap through surface organometallic chemistry. *Angew. Chemie - Int. Ed.* **42**, 156–181 (2003).

27. Copéret, C. *et al.* Surface Organometallic and Coordination Chemistry toward Single-Site Heterogeneous Catalysts: Strategies, Methods, Structures, and Activities. *Chem. Rev.* **116**, 323–421 (2016).

28. Rascón, F., Wischert, R. & Copéret, C. Molecular nature of support effects in single-site heterogeneous catalysts: Silica vs. alumina. *Chem. Sci.* **2**, 1449–1456 (2011).

29. Marks, T. J. Surface-bound metal hydrocarbyls. Organometallic connections between heterogeneous and homogeneous catalysis. *Acc. Chem. Res.* **25**, 57–65 (1992).

30. Ono, Y. Transformation of Lower Alkanes into Aromatic Hydrocarbons over ZSM-5 Zeolites. *Catal. Rev.* **34**, 179–226 (1992).

31. Chen, N. Y. & Yan, T. Y. M2 Forming — A Process for Aromatization of Light Hydrocarbons. 151–155 (1986) doi:10.1021/i200032a023.

32. Seddon, D. Paraffin oligomerisation to aromatics. *Catal. Today* **6**, 351–372 (1990).

33. Kwak, B. S. & Sachtler, W. M. H. Effect of Ga/Proton Balance in Ga/HZSM-5 Catalysts on C3 Conversion to Aromatics. *Journal of Catalysis* vol. 145 456–463 (1994).

34. Biscardi, A. & Iglesia, E. Structure and function of metal cations in light alkane reactions. *Catal. Today.* **31**, 207–231 (1996).

35. Price, G. L. & Kanazirev, V. Ga2O3/HZSM-5 propane aromatization catalysts: Formation of active centers via solid-state reaction. *J. Catal.* **126**, 267–278 (1990).

36. Meriaudeau, P. & Naccache, C. The role of Ga2O3 and proton acidity on the dehydrogenating activity of Ga2O3-HZSM-5 catalysts: evidence of a bifunctional mechanism. *J. Mol. Catal.* **59**, (1990).

37. Buckles, G., Hutchings, G. J. & Williams, C. D. Aromatization of propane over Ga/H-ZSM-5: An explanation of the synergy observed between Ga3+ and H+. *Catal. Letters* **11**, 89–93 (1991).

38. Price, G. L., Kanazirev, V., Dooley, K. M. & Hart, V. I. On the mechanism of propane dehydrocyclization over cation-containing, proton-poor MFI zeolite. *J. Catal.* **173**, 17–27 (1998).

39. Ausavasukhi, A. & Sooknoi, T. Tunable activity of [Ga]HZSM-5 with H2 treatment: Ethane dehydrogenation. *Catal. Commun.* **45**, 63–68 (2014).

40. Saito, H. *et al.* Supported Ga-oxide catalyst for dehydrogenation of ethane. *J. Japan Pet. Inst.* **60**, 203–210 (2017).

41. Searles, K., Siddiqi, G., Safonova, O. V. & Copéret, C. Silica-supported isolated gallium sites as highly active, selective and stable propane dehydrogenation catalysts. *Chem. Sci.* **8**, 2661–2666 (2017).

42. Nakagawa, K., Okamura, M., Ikenaga, N., Suzuki, T. & Kobayashi, T. Dehydrogenation of ethane over gallium oxide in the presence of carbon dioxide. *Chem. Commun.* **3**, 1025–1026 (1998).

43. Cybulskis, V. J. *et al.* The Nature of the Isolated Gallium Active Center for Propane Dehydrogenation on Ga/SiO2. *Catal. Letters* **147**, 1252–1262 (2017).

44. Cheng, Y. *et al.* Ga2O3/HSSZ-13 for dehydrogenation of ethane: Effect of pore geometry of support. *Catal. Commun.* **71**, 42–45 (2015).

45. Castro-Fernández, P. *et al.* Propane Dehydrogenation on Ga2O3-Based Catalysts: Contrasting Performance with Coordination Environment and Acidity of Surface Sites. *ACS Catal.* **11**,

907–924 (2021).

46. Uslamin, E. A., Saito, H., Sekine, Y., Hensen, E. J. M. & Kosinov, N. Different mechanisms of ethane aromatization over Mo/ZSM-5 and Ga/ZSM-5 catalysts. *Catal. Today* 1–9 (2020) doi:10.1016/j.cattod.2020.04.021.

47. Meitzner, G. D., Iglesia, E., Baumgartner, J. E. & Huang, E. S. The Chemical State of Gallium in Working Alkane Dehydrocyclodimerization Catalysts. In Situ Gallium K-Edge X-ray Absorption Spectroscopy. *J. Catal.* **140**, 209–225 (1993).

48. Kazansky, V. B., Subbotina, I. R., Van Santen, R. A. & Hensen, E. J. M. DRIFTS study of the chemical state of modifying gallium ions in reduced Ga/ZSM-5 prepared by impregnation I. Observation of gallium hydrides and application of CO adsorption as a molecular probe for reduced gallium ions. *J. Catal.* **227**, 263–269 (2004).

49. Yuan, Y., Brady, C., Annamalai, L., Lobo, R. F. & Xu, B. Ga speciation in Ga/H-ZSM-5 by in-situ transmission FTIR spectroscopy. *J. Catal.* **393**, 60–69 (2021).

50. Phadke, N. M. *et al.* Characterization of Isolated Ga3+ Cations in Ga/H-MFI Prepared by Vapor-Phase Exchange of H-MFI Zeolite with GaCl3. *ACS Catal.* **8**, 6106–6126 (2018).

51. Phadke, N. M., Mansoor, E., Bondil, M., Head-Gordon, M. & Bell, A. T. Mechanism and Kinetics of Propane Dehydrogenation and Cracking over Ga/H-MFI Prepared via Vapor-Phase Exchange of H-MFI with $GaCl_3$. *J. Am. Chem. Soc.* **141**, 1614–1627 (2019).

52. Phadke, N. M., Mansoor, E., Head-Gordon, M. & Bell, A. T. Mechanism and Kinetics of Light Alkane Dehydrogenation and Cracking over Isolated Ga Species in Ga/H-MFI. *ACS Catal.* 2062–2075 (2021) doi:10.1021/acscatal.0c04906.

53. Schreiber, M. W. *et al.* Lewis-Brønsted Acid Pairs in Ga/H-ZSM-5 to Catalyze Dehydrogenation of Light Alkanes. *J. Am. Chem. Soc.* **140**, 4849–4859 (2018).

54. Yuan, Y., Brady, C., Lobo, R. F. & Xu, B. Understanding the Correlation between Ga Speciation and Propane Dehydrogenation Activity on Ga/H-ZSM-5 Catalysts. *ACS Catal.* **11**, 10647–10659 (2021).

55. Maeno, Z. *et al.* Isolated Indium Hydrides in CHA Zeolites: Speciation and Catalysis for

Nonoxidative Dehydrogenation of Ethane. *J. Am. Chem. Soc.* **142**, 4820–4832 (2020).

56. Mansoor, E., Head-gordon, M. & Bell, A. T. Computational Modeling of the Nature and Role of Ga Species for Light Alkane Dehydrogenation Catalyzed by Ga / H-MFI. (2018) doi:10.1021/acscatal.7b04295.

57. Wang, X. & Andrews, L. Infrared Spectra of Gallium Hydrides in Solid Hydrogen: GaH 1,2,3, Ga2H2,4,6, and the GaH 2,4- Anions. *J. Phys. Chem. A* **107**, 11371–11379 (2003).

58. Grocholl, L., Cullison, S. A., Wang, J., Swenson, D. C. & Gillan, E. G. Synthesis and characterization of an air-stable gallium hydride, [t-Bu(H)Ga(μ-NEt2)]2, and related chloride derivatives. *Inorg. Chem.* **41**, 2920–2926 (2002).

59. Katada, N., Tamagawa, H. & Niwa, M. Quantitative analysis of acidic OH groups in zeolite by ammonia IRMS-TPD and DFT: Application to BEA. *Catal. Today* **226**, 37–46 (2014).

60. Hensen, E. J. M. *et al.* In situ Ga K edge XANES study of the activation of Ga/ZSM-5 prepared by chemical vapor deposition of trimethylgallium. *Catal. Letters* **101**, 79–85 (2005).

61. Wilkinson, A. P. Crystal Chemistry of Gallium (I) in Oxides : Ga + - ″ -Alumina and GaZr 2 (PO 4) 3. **2**, 1602–1607 (1997).

62. Getsoian, A. *et al.* Organometallic model complexes elucidate the active gallium species in alkane dehydrogenation catalysts based on ligand effects in Ga K-edge XANES. *Catal. Sci. Technol.* **6**, 6339–6353 (2016).

63. Saito, H. & Sekine, Y. Catalytic conversion of ethane to valuable products through non-oxidative dehydrogenation and dehydroaromatization. *RSC Adv.* **10**, 21427–21453 (2020).

64. Dai, Y. *et al.* Recent progress in heterogeneous metal and metal oxide catalysts for direct dehydrogenation of ethane and propane. *Chem. Soc. Rev.* (2021) doi:10.1039/d0cs01260b.

65. Sattler, J. J. H. B., Ruiz-Martinez, J., Santillan-Jimenez, E. & Weckhuysen, B. M. Catalytic dehydrogenation of light alkanes on metals and metal oxides. *Chem. Rev.* **114**, 10613–10653 (2014).

66. De, S. *et al.* Stable Cr-MFI Catalysts for the Nonoxidative Dehydrogenation of Ethane: Catalytic Performance and Nature of the Active Sites. *ACS Catal.* 3988–3995 (2021)

doi:10.1021/acscatal.0c05170.

67. Guo, H., Miao, C., Hua, W., Yue, Y. & Gao, Z. Cobaltous oxide supported on MFI zeolite as an efficient ethane dehydrogenation catalyst. *Microporous Mesoporous Mater.* **312**, 110791 (2021).

68. Seki, H. *et al.* Effect of Ba addition to Ga-A-Al2O3 catalyst on structure and catalytic selectivity for dehydrogenation of ethane. *Appl. Catal. A Gen.* **581**, 23–30 (2019).

69. Olsbye, U., Virnovskaia, A., Prytz, O., Tinnemans, S. J. & Weckhuysen, B. M. Mechanistic insight in the ethane dehydrogenation reaction over Cr/Al2O3 catalysts. *Catal. Letters* **103**, 143–148 (2005).

70. Rao, T. V. M., Zahidi, E. M. & Sayari, A. Ethane dehydrogenation over pore-expanded mesoporous silica-supported chromium oxide: 2. Catalytic properties and nature of active sites. *J. Mol. Catal. A Chem.* **301**, 159–165 (2009).

71. Tsyganok, A., Green, R. G., Giorgi, J. B. & Sayari, A. Non-oxidative dehydrogenation of ethane to ethylene over chromium catalysts prepared from layered double hydroxide precursors. *Catal. Commun.* **8**, 2186–2193 (2007).

72. Wang, L. C. *et al.* Non-oxidative dehydrogenation of ethane to ethylene over ZSM-5 zeolite supported iron catalysts. *Appl. Catal. B Environ.* **256**, 117816 (2019).

73. He, Y., Song, Y. & Laursen, S. The Origin of the Special Surface and Catalytic Chemistry of Ga-Rich Ni3Ga in the Direct Dehydrogenation of Ethane. *ACS Catal.* **9**, 10464–10468 (2019).

74. Yang, Z. *et al.* Coking-Resistant Iron Catalyst in Ethane Dehydrogenation Achieved through Siliceous Zeolite Modulation. *J. Am. Chem. Soc.* **142**, 16429–16436 (2020).

75. Wu, Z. *et al.* Pd-In intermetallic alloy nanoparticles: Highly selective ethane dehydrogenation catalysts. *Catal. Sci. Technol.* **6**, 6965–6976 (2016).

76. Pidko, E. A., Kazansky, V. B., Hensen, E. J. M. & van Santen, R. A. A comprehensive density functional theory study of ethane dehydrogenation over reduced extra-framework gallium species in ZSM-5 zeolite. *J. Catal.* **240**, 73–84 (2006).

77. Pereira, M. S., Antonio, M. & Nascimento, C. Theoretical study of the dehydrogenation

reaction of ethane catalyzed by zeolites containing non-framework gallium species : The 3-step mechanism · the 1-step concerted mechanism. **406**, 446–451 (2005).

Chapter 3

Ga speciation and ethane dehydrogenation catalysis of Ga-CHA and MOR: Comparative investigation with Ga-MFI

3.1. Introduction

Zeolites are crystalline aluminosilicates comprising tetrahedral SiO_4 and AlO_4 units. These tetrahedral SiO_4 or AlO_4 units are connected by sharing oxygen atoms to develop uniform porous frameworks. Because the isomorphic substitution of Si^{4+} with Al^{3+} leads to a negative charge in zeolite frameworks, cation species such as protons exist in the pores connecting with Al sites to maintain charge neutrality [1]. Through ion-exchange methods, cationic metal species can be introduced to synthesize metal-exchanged zeolites that can be used as heterogeneous catalysts to promote gas-phase and liquid-phase catalytic reactions [2–11]. Various types of zeolites comprising different frameworks have been developed, and their catalytic performance varies accordingly [12–17].

Group 13 metal-exchanged zeolites for light-alkane transformations have attracted considerable attention. In particular, Ga-exchanged MFI (Ga-MFI) zeolites have been one of the most important research topics for light-alkane dehydrogenation for over 30 years [18–21]. Several Ga species, such as Ga-oxides, GaO^+, Ga^+, and Ga-hydrides, have been reported to be active sites [22–28]. Various types of Ga-oxide-based catalysts have been developed for alkane dehydrogenation; however, the catalysts deactivate quickly owing to coke formation [22,29–35]. Some studies have reported that isolated Ga-hydrides possess alkane dehydrogenation capabilities [36–42]. The possibility of Ga-hydride formation was first proposed by Iglesia's group via an *in situ* XAS study during RSSIE reactions [41]. Several research groups have since comprehensively studied the speciation of Ga-hydrides in MFI and/or catalysis for dehydrogenative alkane transformations. Kazansky's group reported the formation of two kinds of Ga-hydrides in the form of $[GaH_2]^+$ and $[GaH]^{2+}$ via *in situ* infrared (IR) spectroscopy [36]. For propane and butane dehydrogenation, $[GaH]^{2+}$ was independently proposed as the active site rather than $[GaH_2]^+$ by the research groups of Bell [37–39], Lercher [40], and Xu [42]. Both Ga-hydrides, as reported by Bell's group,[39] are active for ethane dehydrogenation.

Ga-hydrides in MFI may also promote the dehydrogenative aromatization of ethylene, as reported by Rimer and co-authors [43]. Other zeolite-supported Ga catalysts have been experimentally and theoretically studied by a few research groups [44,45]. Buckles *et al*. synthesized Ga^{3+}-exchanged Y zeolites via a liquid-phase ion-exchange reaction to study the mechanism of the propane dehydrogenation reaction, where Ga-Y exhibited lower activity than Ga-MFI [44]. Hensen *et al*. conducted DFT calculations of Ga-oxo cations in MOR zeolites. The cyclic $Ga_2O_2^{2+}$ ions were much more stable than the isolated GaO^+ ions in MOR (Si/Al = 23), and *in situ* hydrolysis of the reduced extra-framework Ga species was regarded to promote alkane dehydrogenation facilitating high activity [45]. The excellent activity and selectivity of the SAPO-11 zeolite-supported Ga catalyst in butane dehydrogenation was also reported by Machado and co-authors [46]. Vazhnova *et al*. compared the activity of Ga-loaded MFI and TON zeolites in butane aromatization, where Ga^+ ions are proposed as active species [47]. Despite Ga-hydrides being regarded as active sites for alkane dehydrogenation over Ga-MFI, the possibility of Ga-hydride formation in other zeolites, and their relationship with catalysis have not yet been reported.

Recently, our group investigated In- [48] and Ga- [49] exchanged zeolites for selective ethane dehydrogenation. In-CHA was found to show high selectivity and durability, where $[InH_2]^+$ is the most plausible active site rather than In^+ or $[InH]^{2+}$, as revealed by experimental and theoretical studies. The different zeolite frameworks (CHA, MFI, and MOR of 8-, 10-, 12-membered ring zeolites, respectively) are closely related to ethane dehydrogenation catalysis, and the active $[InH_2]^+$ ions are possibly formed only in CHA zeolites [50]. More recently, the effect of the loading amount on the generation of Ga species in MFI and ethane dehydrogenation has been reported [49]. $[GaH_2]^+$ is mainly formed in the high-loading Ga-MFI (SiO_2/Al_2O_3 = 22.3, Ga/Al = 1.0 with H_2 at 800 °C) and serves as a selective and coke-resistant active site, yielding the highest ethylene formation rate among Pt-free catalyst systems [49]. However, the effect of zeolite frameworks on Ga-hydride formation and ethane dehydrogenation catalysis has not yet been investigated.

Herein, the formation of Ga-hydrides and catalysis in ethane dehydrogenation of Ga-CHA and MOR was investigated using zeolite supports with similar SiO_2/Al_2O_3 ratios (22.3 and 18.3 for CHA and MOR, respectively) and identical preparation conditions (Ga/Al = 0.3, H_2 at 550 °C, and Ga/Al = 1.0, with H_2 at 800 °C, denoted as 0.3(550) and 1.0(800), respectively). It was found that more Ga-hydrides were formed in the MOR than in CHA. In ethane dehydrogenation, the high-loading Ga-MOR exhibited the best ethylene selectivity and durability among the tested Ga-CHA and -MOR catalysts, although the ethane conversion value was lower than that for the high-loading Ga-MFI previously developed [49]. The impact of Ga-hydride formation in different zeolites on ethane dehydrogenation catalysis is also discussed.

3.2. Experimental

3.2.1. Catalyst preparation

A series of Ga-CHA and -MOR were synthesized by the RSSIE method in a similar manner to previous our study [49]. First, Ga_2O_3-modified zeolites were prepared by impregnation of $Ga(NO)_3 \cdot nH_2O$ (n = 7-9, Wako) on NH_4^+-type CHA (SiO_2/Al_2O_3 = 22.3, Tosoh) and H^+-type MOR (SiO_2/Al_2O_3 = 18.3, Tosoh) , followed by drying in an oven and calcination at 500 °C for 1 h under air flow. The Ga/Al ratio (Ga/Al = 0.3 or 1.0) was determined based on the amount of Ga precursor ($Ga(NO)_3.nH_2O$), and zeolite. After the calcined samples were prepared, RSSIE reactions were conducted via H_2 treatment (10 mL/min of 10% H_2/He) for 1 h. The treatment temperatures were 550 °C for Ga/ Al = 0.3 and 800 °C for Ga/Al = 1.0. The obtained samples were denoted as Ga-CHA-X(Y) or Ga-MOR-X(Y) (X: 0.3 or 1.0, Y: 550, or 800).

3.2.2. Characterization

3.2.2.1 X-ray diffraction (XRD)

XRD experiments were performed using a Rigaku MiniFlex II/AP diffractometer with Cu Kα

radiation. H-CHA was prepared by the calcination of NH_4^+-type CHA at 500 ° C for 1 h under air flow. After the RSSIE reaction, Ga-CHA and Ga-MOR were exposed to air and subsequently characterized.

3.2.2.2 Fourier-transform infrared (FT-IR) spectroscopy for Ga-hydrides formation by RSSIE

FT-IR spectroscopy was conducted using a homemade *in situ* quartz cell and FT/IR-4100 (JASCO) with a mercury cadmium telluride (MCT) detector. The Ga_2O_3-modified zeolite (40 mg) was made into a self-supported disk and placed into the cell. The background spectrum was recorded at 50 °C in a He atmosphere prior to the measurement. The disk sample was treated with 10% H_2/He at different temperatures (550 °C for Ga/Al = 0.3 and 800 °C for Ga/Al = 1.0) to promote the RSSIE reaction. In each case, the sample was treated with 10% H_2/He for 1 h and cooled to 50 °C in a H_2 atmosphere without exposure to air. The first IR spectrum was recorded after purging with He. Next, the obtained sample was treated at 800 °C under He flow for 1 h to decompose the generated Ga-hydrides. The second spectrum was recorded at 50 °C. The first spectrum was subsequently subtracted from the second spectrum to obtain a third spectrum.

3.2.2.3 FT-IR spectroscopy for Py and NH_3 adsorption experiments

Disk samples of Ga-CHA or Ga-MOR were prepared *in situ* in a quartz cell as described above. The temperature was decreased to 150 °C to obtain the background spectrum in a He atmosphere. Approximately 1 mL of Py was introduced using a syringe with continuous recording of the IR spectra. This dosing procedure was repeated until the band corresponding to the adsorbed Py was saturated. The final IR spectrum was obtained after purging the sample with He for 15 min. For the NH_3 adsorption experiment, background spectra were obtained at 50 °C in He atmosphere, and then, 10% NH_3/He flow was introduced until the peak at approximately 1450 cm^{-1}, corresponding to adsorbed NH_3 on Brønsted acid sites (BASs), was saturated [51]. After purging with He for 15 min to remove NH_3, the final IR spectrum was recorded.

3.2.2.4 *In situ* XAS measurement

XAS measurements were conducted using the BL14B2 station at SPring-8. The disk sample of Ga_2O_3/CHA or Ga_2O_3/MOR was set into a cell and heated to 550 or 800 °C based on the Ga loading amount as described above, and thereafter, the first spectrum was recorded. Then, 10% H_2/He was introduced to promote the RSSIE reactions of Ga_2O_3/CHA or Ga_2O_3/MOR with continuous recording until the spectrum was saturated.

3.2.2.5 Temperature programed oxidation (TPO) experiment

Temperature programed oxidation (TPO) measurements were conducted 2 h after reaction commencement, using 50 mg of the catalyst. The catalyst was set into a flow-type reactor connected to a BELmass (MicrotracBEL). Initially, the sample was treated with He at 100 °C for 30 min, followed by 10% O_2/He (50 mL/min), with the temperature increasing to 800 °C at 10 °C/min. The amount of CO_2 generated by coke oxidation (m/z = 44) was recorded throughout.

3.2.2.6 H−D exchange experiment

The H−D exchange reactions were carried out for the pellet of Ga-exchanged zeolite after RSSIE using the homemade *in situ* cell described above. Prior to the reaction, the background spectra were obtained under He at 50 °C. The disk samples were treated with 10 mL/min of 10% D_2/He at 400 °C for 30 min. The IR spectra were then recorded at 50 °C under He to monitor a negative band for Ga−H stretching vibration and a positive band for Ga−D stretching vibration.

3.2.3. Catalytic test

3.2.3.1 Non-oxidative ethane dehydrogenation

The ethane dehydrogenation over Ga-exchanged zeolites (Ga-MOR and Ga-CHA) was carried out at 660 °C in a flow-type reactor at atmospheric pressure. Before the catalytic reaction, catalysts were prepared *in situ* under 10% H_2/He flow for 30 min at 550 °C or 800 °C. After cooling to 660 °C under H_2/He flow and subsequent purging with He, the gas reactant (10% C_2H_6/He) was introduced at

660 °C. The conversion, selectivity, and yield were determined by GC and calculated using the following equations:

$$\text{Conv.}\,[\%] = \frac{[ethane]_{init} - [ethane]}{[ethane]_{init}} \times 100$$

$$\text{Selec.}\,[\%] = \frac{[ethylene]}{[ethylene] + [methane]} \times 100$$

$$\text{Yield}\,[\%] = [\text{Conv.}] \times [\text{Selec.}] \times 100$$

The deactivation rate was calculated by the following equation according to previous paper: [52]

$$k_d(h^{-1}) = \frac{\ln\left(\frac{1 - Conv._{end}}{Conv._{end}}\right) - \ln\left(\frac{1 - Conv._{start}}{Conv._{start}}\right)}{t}$$

The $Conv._{start}$ and $Conv._{end}$ represent the initial and end conversions, respectively. t (h) represents the reaction time. A lower K_d value indicates less deactivation and increased durability of the catalyst.

3.2.3.2 Kinetic study for ethane dehydrogenation

The kinetic study of ethane dehydrogenation was conducted in the same flow-type reactor. The reaction conditions were as follows: for C_2H_6 partial pressure (0.02–0.08), balanced with He (total flow rate: 50 mL/min), at a reaction temperature of 600 °C. For the formation rate dependency on reaction temperature (550–610 °C), the partial pressure of C_2H_6 was 0.04, and balanced with He (total flow rate: 50 mL/min).

3.3. Result and discussion

3.3.1. Characterization of Ga-CHA and Ga-MOR

XRD experiments were conducted on Ga-CHA and -MOR to confirm the preservation of the zeolite framework after the RSSIE reactions (**Figure 1**). Any diffraction peak derived from Ga oxide species was not observed in the XRD patterns before RSSIE, suggesting that the small or amorphous Ga oxide species possibly exist after calcination. For CHA zeolites, the spectra of the Ga-exchanged zeolite after RSSIE reactions were almost identical to proton-type zeolites, indicating that the CHA zeolite frameworks were maintained by H_2 treatment at 550 or 800 °C. While in the case of MOR zeolites, the peak intensity for Ga-MOR-0.3(550) remained almost unchanged. However, the peak intensity for Ga-MOR-1.0(800) decreased slightly, implying that the MOR zeolite framework was partially destroyed by high-temperature H_2 treatment at 800 °C. The low angle shift was hardly observed between the H-type zeolites and the Ga-exchanged zeolites in both cases, which indicates that the Ga species are mostly immobilized at Al sites and that the incorporation of Ga species in zeolite framework is unlikely to occur. The similar result was reported by Serykh. [53]

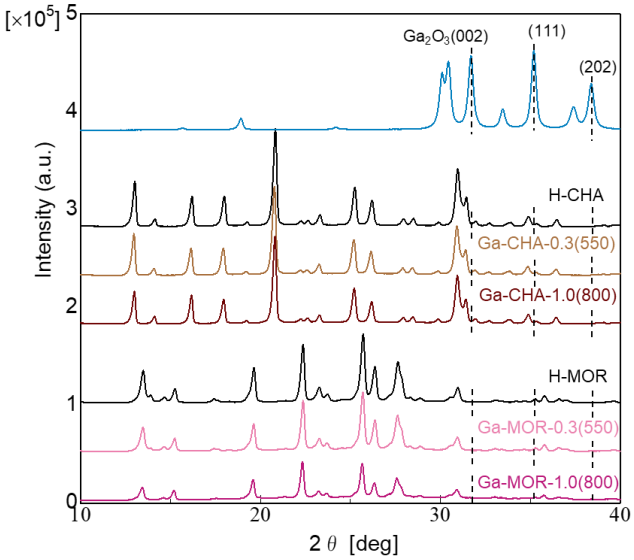

Figure 1. XRD patterns of proton-type and Ga-exchanged CHA and MOR zeolites

In situ FT-IR measurements were performed to investigate the formation of Ga-hydrides in the

Ga-CHA and MOR. IR spectra were obtained using a method similar to that used in our recent work on Ga-MFIs (Figure 2) [49]. Monovalent $[GaH_2]^+$ and divalent $[GaH]^{2+}$ in MFI show an IR peak derived from the Ga−H stretching vibration at approximately 2040 cm^{-1} and 2060 cm^{-1}, respectively [36]. Ga-CHA-0.3(550) showed almost no peak derived from Ga−H stretching vibration, indicating that few Ga-hydrides were formed. Increasing the Ga/Al ratio from 0.3 to 1.0 and H_2 treatment temperature from 550 °C to 800 °C (Ga-CHA-1.0(800)), a peak at 2050 cm^{-1} was detected. In the case of Ga-MOR, low Ga loading Ga-MOR-0.3(550) exhibited two peaks with wavenumbers of 2077 and 2050 cm^{-1}. These peaks were assigned to $[GaH]^{2+}$ and $[GaH_2]^+$, respectively. Contrastingly, Ga-MOR-1.0-(800) showed a main peak assignable to $[GaH_2]^+$ at 2050 cm^{-1}, with a much higher intensity compared to Ga-CHA-1.0(800). These results indicate Ga-hydrides were also formed in other zeolite frameworks, such as CHA and MOR. The formation of Ga-hydrides was supported by H−D exchange reactions. The results are discussed in section 3.5.

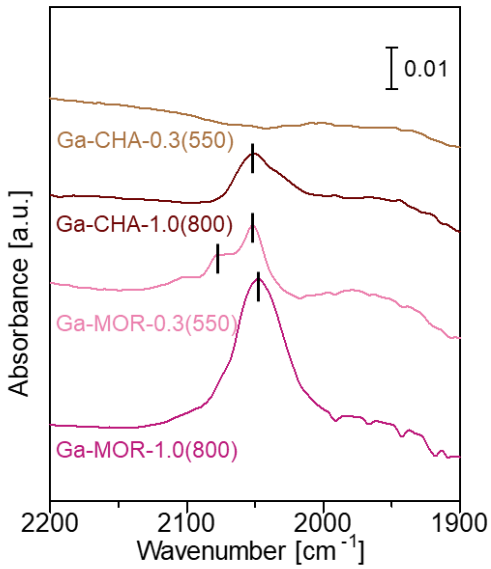

Figure 2. Difference IR spectra of Ga-exchanged CHA and MOR with different loading amounts and H_2 treatment. The spectra were recorded at 50 °C. Difference spectra were obtained by subtracting the spectra after He treatment at 800 °C from that after H_2 treatment.

Py adsorption experiments were conducted to investigate other Ga species after the RSSIE reaction. Py was introduced after recording the background, and the dosing procedure was repeated

until the saturation of the band corresponded to adsorbed Py. The IR spectra were collected after complete adsorption of Py, followed by He purging (**Figure 3**). As recently reported, Py adsorbed onto BASs, Ga^{+}, and GaO_x displayed peaks at approximately 1555, 1457, and 1446 cm^{-1}, respectively [40,49,54]. In our recent study, the peak intensity of GaO_x was hardly observed for Ga-MFI-1.0(800), confirming that the RSSIE occurred completely by high-temperature H_2 treatment. The lower-temperature H_2 treatment for low-loading Ga-MFI, however, resulted in the presence of remaining GaO_x species. A similar result was obtained for Ga-MOR. When the Ga/Al ratio and H_2 treatment temperature were increased from 0.3 to 1.0 and from 550 °C to 800 °C, respectively, the peak intensity of Ga^{+} cations (1457 cm^{-1}) increased while the peak intensity of GaO_x (1445 cm^{-1}) and remaining BASs (1555 cm^{-1}) decreased, suggesting that higher Ga loading and H_2 treatment temperature also improve the RSSIE reaction in the MOR zeolite. The pore size of CHA is the smallest among the three kinds of zeolites. Py might be too large to access into the pore, so that the adsorbed Py was hard to be detected.

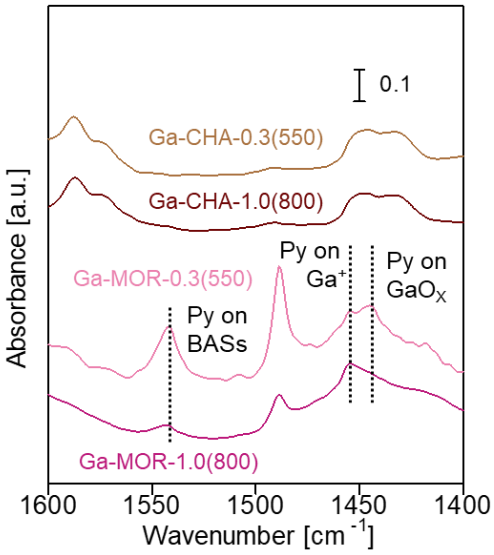

Figure 3. IR spectra of Py adsorbed Ga species in Ga-CHA and Ga-MOR at 150 °C. The spectra were recorded after the Py adsorption was saturated and purged by He.

The remaining BASs after the RSSIE were also measured using NH_3 adsorption experiments. After the RSSIE reaction, the temperature was decreased to 50° C and purged with He, followed by NH_3/He (10%) until the peak at approximately 1450 cm^{-1}, corresponding to adsorbed NH_3 on BASs [51], reached saturation. The IR spectra for adsorbed NH_3 were recorded after He was purged to

remove gaseous NH_3.

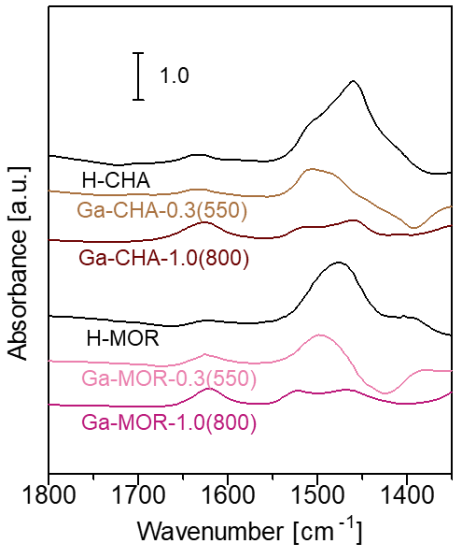

Figure 4. IR spectra of adsorbed NH_3 on Ga-CHA and Ga-MOR recorded at 50 °C. The spectra were recorded after the NH_3 adsorption was saturated and purged by He.

The peak area was normalized to that of the proton-type zeolite (H-CHA or H-MOR) to determine the relative amount of BASs. The remaining BASs over Ga-CHA-0.3(550) were determined to be 48%. An increase in the Ga loading and H_2 treatment temperature (Ga-CHA-1.0(800)) decreased the remaining BAS to 17%. Similar results were obtained for Ga-MOR, where the remaining BASs were 72% and 34% for Ga-MOR-0.3(550) and 1.0(800), respectively. A high Ga loading is effective for reduction of the remaining BASs.

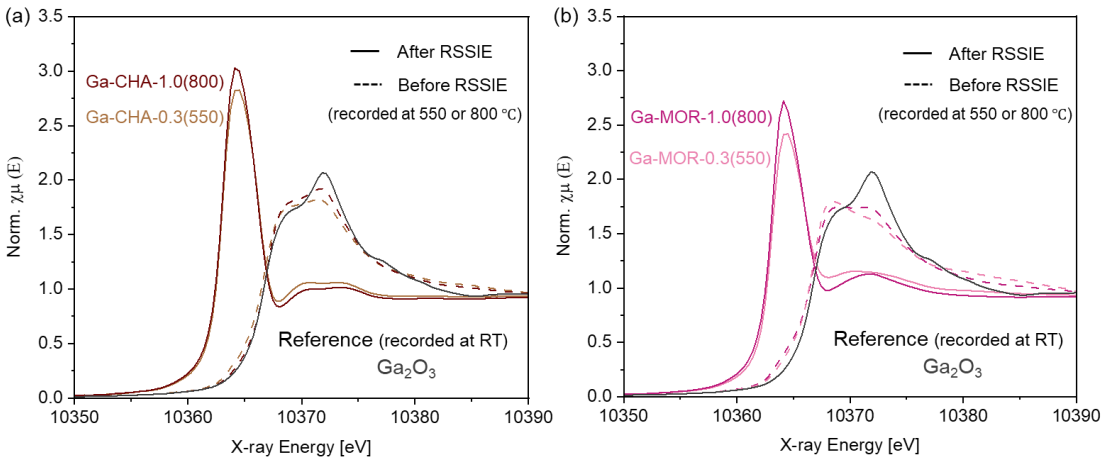

Figure 5. *In situ* Ga K-edge XAS spectra of (a) Ga-CHA and (b) Ga-MOR and reference samples

(Ga_2O_3). The spectra of low and high Ga loading zeolites during RSSIE were obtained at 550 or 800 °C, respectively. Reference spectra were obtained at room temperature. (approximately at 25 °C)

Furthermore, *in situ* XAS measurements were conducted for low- and high-loading Ga-CHA and MOR during RSSIE reactions. The disk of Ga_2O_3-modified zeolite was set into a cell and heated under He to the requisite temperature (550 °C for Ga/Al = 0.3 and 800 °C for Ga/Al = 1.0, respectively). With continuously recording the X-ray absorption near edge structure (XANES) spectra, the gas flow was changed to H_2/He to initiate the RSSIE reaction. The final spectrum was obtained when the spectrum remained unchanged. The absorption energy of Ga-CHA-0.3(550) and 1.0(800) before RSSIE was determined as E_0 = 10366.8 and 10367.0 eV, respectively, which were nearly the same as that of the bulk Ga_2O_3 (E_0 = 10366.9 eV) (**Figure 5a**). In the FT-EXAFS spectra of the Ga-CHA and Ga-MOR (**Figure S1**), the peak derived from Ga−O−Ga shell was much lower in intensity compared to that for Ga_2O_3, supporting the presence of small or amorphous Ga oxide species before RSSIE. After the RSSIE reaction, the XANES spectra of Ga-CHA-0.3(550) and Ga-CHA-1.0(800) showed strong peaks at approximately 10364 eV, and the absorption edge shifted toward lower energy values (E_0 = 10363.1 and 10363.3 eV, respectively). Although the assignment of these species is controversial, the spectral changes were interpreted as the formation of isolated Ga species in zeolites, including Ga^+ [55] and Ga-hydrides [56] ($[GaH]^{2+}$ and $[GaH_2]^+$) [57]. Similar spectral changes induced by RSSIE reactions were observed for Ga-MOR (**Figure 5b**). When the XANES spectra were compared between 0.3(550) and 1.0(800), the intensity of the peak at approximately 10363 eV was higher for 1.0(800) in both cases (Ga-CHA and Ga-MOR). Together with the IR results, high-temperature H_2 treatment was necessary for the formation of isolated Ga species. The similar conclusion was obtained in our previous paper for Ga-MFIs [49].

3.3.2. Comparative investigation of Ga-exchanged zeolites in ethane dehydrogenation

Ethylene is an important building block for producing many chemicals, such as polymers,

oxygenates, and some important chemical intermediates [52,58]. Steam cracking of alkanes is the most widely used method to produce ethylene. However, extremely high temperatures are required, and coke formation is heavy. Catalytic non-oxidative ethane dehydrogenation has been a potential technology to produce ethylene under milder conditions [48,52,59]. In general, Pt- [52,60–63] and Cr- [64–66] based catalysts are widely used in non-oxidative ethane dehydrogenation, but the utilization of these catalysts suffers from poor durability due to coke formation or metal sintering of Pt particles in current reactions. Apart from the commonly used catalysts, other metal-based catalysts, such as Fe- [59,67], Co- [68] loaded zeolites, have also been reported to exhibit a high C_2H_4 formation rate or selectivity, while rapid coke formation is still unavoidable.

Recently, we found that the high-loading Ga-MFI (Ga/Al = 1.0, H_2 at 800 °C, denoted as Ga-MFI-1.0(800)) worked as a selective and coke-resistant catalyst for ethane dehydrogenation. Good initial conversion and selectivity (43% and 89%, respectively) were obtained with a low deactivation rate (0.024 h^{-1} for 15 h) at 660 °C [49]. The high catalytic performance was ascribed to both the low amount of remaining BASs and the main formation of $[GaH_2]^+$ ions as active isolated Ga-hydrides.

In this study, Ga-CHA and Ga-MOR were prepared *in situ* by RSSIE. Catalytic reactions were carried out under the same reaction conditions as those above (**Figure 6** and **Table 1**). Ga-CHA-1.0(800) exhibited better selectivity (90%) than Ga-CHA-0.3(550) (73%), while the initial conversion values were similar (33% and 27%, respectively) (**Figure 6a**). Conversion decreased with increasing reaction time for both Ga-CHA-0.3(550) and 1.0(800). The deactivation rates (k_d) for 220 min were almost identical (0.25 and 0.28 h^{-1}, respectively). Both low- and high-loading Ga-CHA showed low durability despite the decrease in the relative amount of remaining BASs with increasing Ga loading.

Contrastingly, Ga loading strongly affected the durability of Ga-MOR. The low-loading Ga-MOR-0.3(550) catalyst exhibited moderate initial conversion and selectivity values of 37% and 70%, respectively (**Figure 6b** and **Table 1**). However, conversion quickly decreased from 37% to 14% after

220 min, with a k_d of 0.37 h^{-1}. Ga-MOR-1.0(800) showed good selectivity (90%) and maintained the initial conversion (20%) for 220 min, although the conversion was much lower than that of Ga-MFI-1.0(800) (43%, **Table 1**, comparison of the time course is shown in **Figure S2.** The product distribution with considering coke formation is summarized in **Table S1**).

Increased Ga loading improved the durability of Ga-MOR in ethane dehydrogenation. A similar trend was reported for Ga-MFI-1.0(800) and showed increased durability (k_d = 0.013 h^{-1} for 220 min) compared to the low-loading Ga-MFI (Ga/Al = 0.3, H_2 at 550 °C, k_d = 0.65 h^{-1}) [49]. TPO experiments for the catalysts after 2 h (**Figure 7**) showed that significant coke formation had occurred for Ga-CHA-0.3(550), Ga-CHA-1.0(800), and Ga-MOR-0.3(550). Notably, coke formation was suppressed over Ga-MOR-1.0(800) in the same level of the Ga-MFI-1.0(800) [49]. High Ga loading is also effective in suppressing coke formation over Ga-MOR, improving durability.

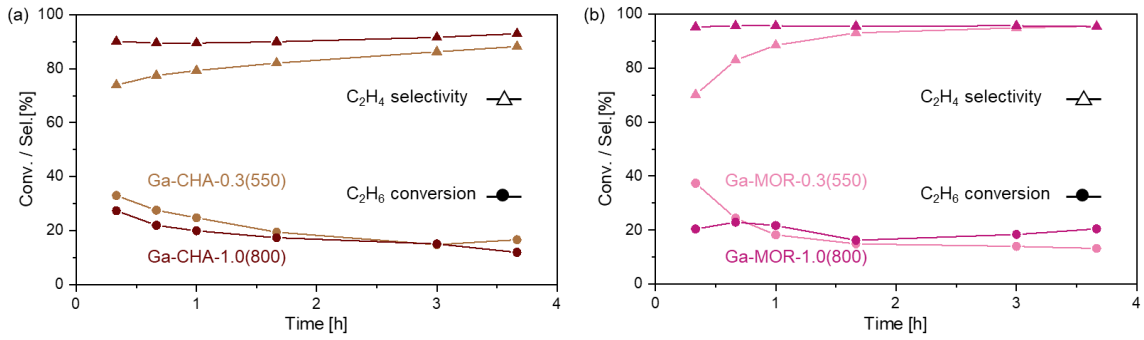

Figure 6 C_2H_6 dehydrogenation by using (a) Ga-CHA and (b) Ga-MOR. Reaction conditions: 100 mg of Ga-exchanged zeolite, 10 mL/min of 10% C_2H_6/He, 660 °C.

Table 1. Conversion, selectivity, carbon balance and deactivation rate (k_d) value in EDH catalyzed by Ga-CHA, MOR, and MFI [a]

Catalyst	Time [min]	Conv. [%][b]	Sel. [%][b]	Carbon balance [%][b]	k_d [h^{-1}][c]
Ga-CHA-0.3(550)	20	33	74	89	0.25
	220	17	88	99	
Ga-CHA-1.0(800)	20	27	90	95	0.28
	220	12	93	100	
Ga-MOR-0.3(550)	20	37	70	76	0.37
	220	14	96	97	
Ga-MOR-1.0(800)	20	20	95	100	0
	220	20	95	97	
Ga-MFI-1.0(800)[d]	20	43	88	85	0.013
	220	42	91	99	

[a]Catalyst: 100 mg of Ga-CHA, Ga-MOR and Ga-MFI. Reactant gas: 10% C_2H_6/He. Total flow rate: 10 mL/min 10%. Temperature: 660 °C. [b]Determined by GC-FID. [c]The determination of the deactivation rate is described in the experimental section. [d]The catalytic test was previously investigated [49]. The results are shown for comparison with those of Ga-CHA and MOR.

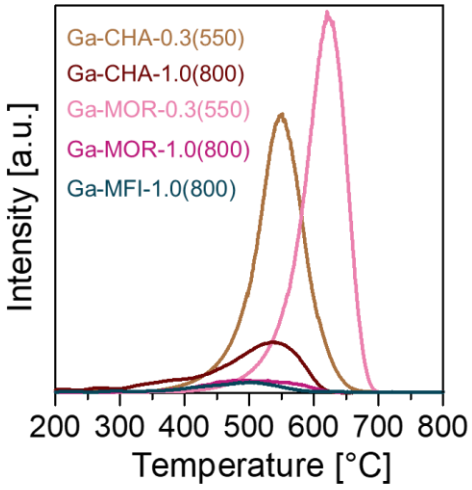

Figure 7 TPO results of a series of Ga-exchanged zeolite after reaction for 2 h.

3.3.3. Kinetic study for high-loading Ga-exchanged zeolites

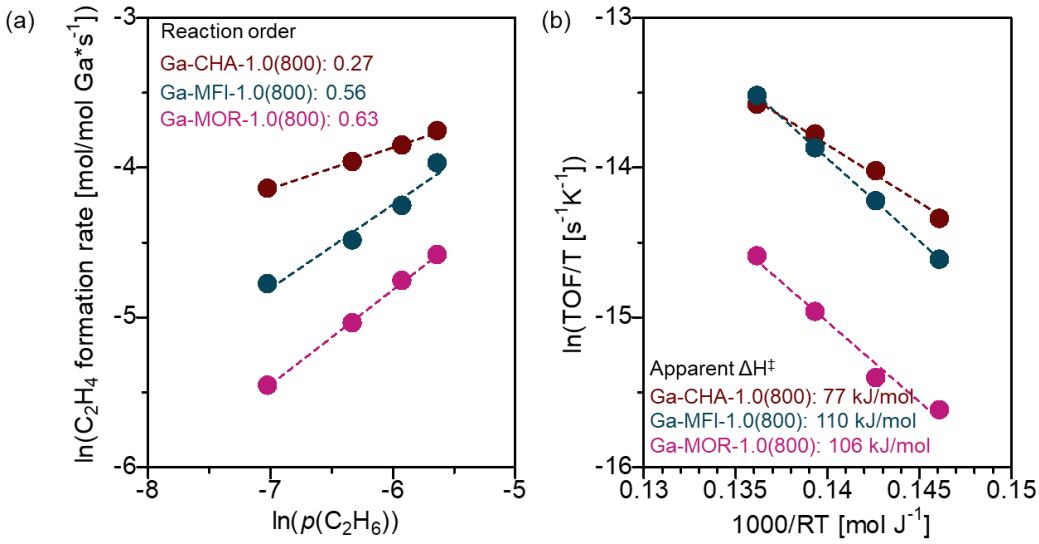

Figure 8. Kinetic study for C_2H_6 dehydrogenation by using Ga-CHA-1.0(800) and Ga-MOR-1.0(800). C_2H_4 formation rate dependency on (a) $p(C_2H_6)$ and (b) reaction temperature. Reaction conditions: 100 mg of catalyst, (a) 50 mL/min of 2-8% C_2H_6/He, 600 °C. (b) 50 mL/min of 4% C_2H_6/He, 550-610 °C. The results for Ga-MFI-1.0(800) were reported in our previous paper [49].

The reaction mechanism for ethane dehydrogenation on isolated Ga species has previously been investigated [37,40,69–71]. Bell's group discussed the reaction mechanisms of $[GaH]^{2+}$ and $[GaH_2]^{+}$ ions for ethane dehydrogenation in a theoretical study [72]. The alkyl mechanism of $[GaH]^{2+}$ ions involve C_2H_4 formation as the rate-determining step (RDS), whereas the RDS can be both C_2H_6 activation and C_2H_4 formation in the carbenium mechanism on $[GaH]^{2+}$ ions. For the $[GaH_2]^{+}$ ions, the alkyl mechanism is most plausible, in which the RDS is C_2H_6 activation. We recently reported a relatively high reaction order of ethane partial pressure ($p(C_2H_6)$) (0.56) for Ga-MFI-1.0(800) possessing $[GaH_2]^{+}$ ions as the dominant Ga-hydrides, whereas a low reaction order of $p(C_2H_6)$ (0.20) was observed for Ga-MFI-0.3(550) having $[GaH]^{2+}$ ions as major Ga-hydrides [49]. Combined with recent literature, the reaction order of $p(C_2H_6)$ would be an indicator to consider active Ga-hydrides, $[GaH]^{2+}$, and $[GaH_2]^{+}$ ions.

Kinetic studies were conducted for Ga-CHA-1.0(800) and Ga-MOR-1.0(800) under the same

reaction conditions as those previously reported to discuss the active Ga species for ethane dehydrogenation. It was difficult to obtain reliable kinetic data for Ga-MOR-0.3(550) (Figure S3), which might be due to rapid deactivation. Hence, kinetic data for the low-loading Ga-exchanged zeolite were excluded from this discussion. The reaction orders of $p(C_2H_6)$ for Ga-MOR-1.0(800) and Ga-CHA-1.0(800) were determined as 0.63 and 0.27, respectively (**Figure 8a**). The reaction temperature dependence of the ethylene formation rate (Eyring plot) was also investigated to evaluate the apparent $\Delta H^{\ddagger}$ (**Figure 8b**). The $\Delta H^{\ddagger}$ values for Ga-MOR-1.0(800) and Ga-CHA-1.0(800) were 106 kJ/mol and 77 kJ/mol, respectively. The reaction order of the $p(C_2H_6)$ and $\Delta H^{\ddagger}$ values for Ga-MOR-1.0(800) are quite similar to those for Ga-MFI-1.0(800) and are consistent with the alkyl mechanism on $[GaH_2]^+$ ions, as proposed by Bell [72]. $[GaH_2]^+$ ions are likely active Ga-hydrides in ethane dehydrogenation on Ga-MOR-1.0(800). In the case of Ga-CHA-1.0(800), the low reaction order of $p(C_2H_6)$ (0.27) indicates that C_2H_4 formation is involved in the RDS, suggesting that $[GaH]^{2+}$ ions are more plausible active Ga-hydrides than $[GaH_2]^+$ ions.

3.3.4. H−D exchange experiment

Although the apparent $\Delta H^{\ddagger}$ for Ga-MFI-1.0(800) was similar to Ga-MOR-1.0(800) and higher than Ga-CHA-1.0(800), the catalytic performance of Ga-MFI-1.0(800) was superior. To determine the reason for the higher catalytic performance, H−D exchange experiments were conducted and monitored by FT-IR spectroscopy for a series of Ga-exchanged zeolites (**Figure 9a**). After the RSSIE reaction (H_2 at 550 or 800 °C) for the IR disk of Ga_2O_3-modified zeolites, recording of background spectra at 50 °C under He, the Ga-zeolites were treated with D_2 at 400 °C to investigate the exchange reactions. The temperature was then decreased to 50 °C and IR spectra recorded. Negative bands derived from the consumption of Ga-hydrides (~2050 cm^{-1}) and positive bands assigned to Ga-deuteride appeared (~1470 cm^{-1}), indicating the occurrence of H−D exchange reactions. This supports the formation of Ga-hydrides in different zeolites. Among the tested catalysts, the highest intensity of the negative band was obtained for Ga-MFI-1.0(800). The relationship between the relative amounts

of Ga-hydrides in zeolites and catalytic performance was plotted. The ethylene yield at 3 h (as an index of steady-state activity) was plotted as a function of negative intensity at 2050 cm^{-1} (**Figure 9b**). A positive linear relationship was observed, which showed that the highest relative amount of Ga-hydrides in Ga-MFI-1.0(800) is one of the main reasons for the superior catalytic performance, although different active Ga-hydrides depending on the zeolite frameworks and Ga loading amounts should also be considered.

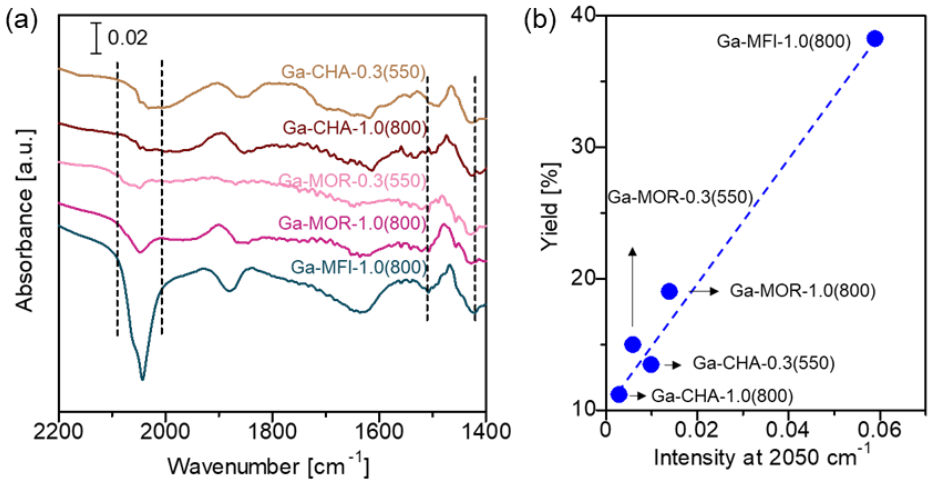

Figure 9. (a) IR spectra of H-D exchange experiments in Ga-CHA, MOR and MFI-1.0(800) at 50 °C. The catalysts were treated with D_2 at 400 °C for 15 mins after H_2 treatment at 800 °C. (b) Plot of ethylene yield value at 3 h in ethane dehydrogenation tests and intensity at 2050 cm^{-1} as a function of amount of the Ga-hydrides.

3.4. Conclusion

We investigated the effect of different zeolite frameworks (CHA and MOR) on Ga speciation and ethane dehydrogenation catalysis for comparison with Ga-MFIs. The formation of Ga-hydrides in CHA and MOR zeolites after RSSIE was confirmed by FT-IR spectroscopy, indicating that Ga-hydrides were more likely to be formed in MOR than CHA. The formation of other isolated Ga species was confirmed by Py adsorption experiments and *in situ* XAS spectroscopy. Increasing the Ga loading was found to be effective in reducing the remaining BASs in both zeolites. These results are similar to those obtained in our recent study of Ga-MFIs [49]. Regarding ethane dehydrogenation catalysis, an increase in Ga loading improved the durability of Ga-MOR, whereas both low- and high-loading Ga-

CHA exhibited low durability. However, the catalytic performances of Ga-CHA and -MOR were inferior to those of the previously developed high-loading Ga-MFI catalyst [49]. The high catalytic performance of MFI was discussed based on kinetic studies and H−D exchange reactions. $[GaH_2]^+$ ions are plausible active Ga-hydrides in the high-loading Ga-MOR, as seen with Ga-MFI, whereas different kinetics were observed for the high-loading Ga-CHA. The H−D exchange reactions over a series of Ga-exchanged zeolites indicate that the highest relative amount of Ga-hydrides is one of the reasons for the high catalytic performance of MFI. This study revealed the formation of Ga-hydrides in other zeolite frameworks other than MFI and suggests that formation of more isolated Ga-hydrides is key to developing more efficient Ga-zeolite-based catalysts for alkane dehydrogenation.

References

1 J. Cejka, A. Corma, S. Zones and Editors., *Zeolites And Catalysis: Synthesis, Reactions And Applications.*, Wiley-VCH Verlag GmbH & Co. KGaA, 2010.

2 A. Marberger, A. W. Petrov, P. Steiger, M. Elsener, O. Kröcher, M. Nachtegaal and D. Ferri, *Nat. Catal.*, 2018, **1**, 221–227.

3 M. Moliner and A. Corma, *React. Chem. Eng.*, 2019, **4**, 223–234.

4 J. Song, Y. Wang, E. D. Walter, N. M. Washton, D. Mei, L. Kovarik, M. H. Engelhard, S. Prodinger, Y. Wang, C. H. F. Peden and F. Gao, *ACS Catal.*, 2017, **7**, 8214–8227.

5 A. A. Battiston, J. H. Bitter and D. C. Koningsberger, *J. Catal.*, 2003, **218**, 163–177.

6 N. Kosinov, C. Liu, E. J. M. Hensen and E. A. Pidko, *Chem. Mater.*, 2018, **30**, 3177–3198.

7 W. Luo, W. Cao, P. C. A. Bruijnincx, L. Lin, A. Wang and T. Zhang, *Green Chem.*, 2019, **21**, 3744–3768.

8 J. W. Harris, W. C. Liao, J. R. Di Iorio, A. M. Henry, T. C. Ong, A. Comas-Vives, C. Copéret and R. Gounder, *Chem. Mater.*, 2017, **29**, 8824–8837.

9 H. Ichihashi and H. Sato, *Appl. Catal. A Gen.*, 2001, **221**, 359–366.

10 K. Nakamura, A. Okuda, K. Ohta, H. Matsubara, K. Okumura, K. Yamamoto, R. Itagaki, S. Suganuma, E. Tsuji and N. Katada, *ChemCatChem*, 2018, **10**, 4113–4119.

11 P. Tomkins, M. Ranocchiari and J. A. Van Bokhoven, *Acc. Chem. Res.*, 2017, **50**, 418–425.

12 J. Shi, Y. Wang, W. Yang, Y. Tang and Z. Xie, *Chem. Soc. Rev.*, 2015, **44**, 8877–8903.

13 M. Dusselier and M. E. Davis, *Chem. Rev.*, 2018, **118**, 5265–5329.

14 U. Deka, I. Lezcano-Gonzalez, B. M. Weckhuysen and A. M. Beale, *ACS Catal.*, 2013, **3**, 413–427.

15 R. Gounder and E. Iglesia, *Acc. Chem. Res.*, 2012, **45**, 229–238.

16 M. H. Mahyuddin, A. Staykov, Y. Shiota, M. Miyanishi and K. Yoshizawa, *ACS Catal.*, 2017, **7**, 3741–3751.

17 M. Lusardi, T. T. Chen, M. Kale, J. H. Kang, M. Neurock and M. E. Davis, *ACS Catal.*, 2020, **10**, 842–851.

18 N. Y. Chen and T. Y. Yan, 1986, 151–155.

19 D. Seddon, *Catal. Today*, 1990, **6**, 351–372.

20 S. M. Al-Zahrani, *Dev. Chem. Eng. Miner. Process.*, 2008, **6**, 101–120.

21 R. Fricke, H. Kosslick, G. Lischke and M. Richter, *Chem. Rev.*, 2000, **100**, 2303–2405.

22 A. Ausavasukhi and T. Sooknoi, *Catal. Commun.*, 2014, **45**, 63–68.

23 G. L. Price and V. Kanazirev, *J. Catal.*, 1990, **126**, 267–278.

24 B. S. Kwak and W. M. H. Sachtler, *J. Catal.*, 1994, 145, 456–463.

25 G. L. Price, V. Kanazirev, K. M. Dooley and V. I. Hart, *J. Catal.*, 1998, **173**, 17–27.

26 A. Biscardi and E. Iglesia, *Catal. Today.*, 1996, **31**, 207–231.

27 P. Meriaudeau and C. Naccache, *J. Mol. Catal.*, , DOI:10.1016/0304-5102(90)85100-V.

28 G. Buckles, G. J. Hutchings and C. D. Williams, *Catal. Letters*, 1991, **11**, 89–93.

29 H. Saito, S. Maeda, H. Seki, S. Manabe, Y. Miyamoto, S. Ogo, K. Hashimoto and Y. Sekine, *J. Japan Pet. Inst.*, 2017, **60**, 203–210.

30 K. Searles, G. Siddiqi, O. V. Safonova and C. Copéret, *Chem. Sci.*, 2017, **8**, 2661–2666.

31 K. Nakagawa, M. Okamura, N. Ikenaga, T. Suzuki and T. Kobayashi, *Chem. Commun.*, 1998, **3**, 1025–1026.

32 V. J. Cybulskis, S. U. Pradhan, J. J. Lovón-Quintana, A. S. Hock, B. Hu, G. Zhang, W. N.

Delgass, F. H. Ribeiro and J. T. Miller, *Catal. Letters*, 2017, **147**, 1252–1262.

33 Y. Cheng, H. Gong, C. Miao, W. Hua, Y. Yue and Z. Gao, *Catal. Commun.*, 2015, **71**, 42–45.

34 P. Castro-Fernández, D. Mance, C. Liu, I. B. Moroz, P. M. Abdala, E. A. Pidko, C. Copéret, A. Fedorov and C. R. Müller, *ACS Catal.*, 2021, **11**, 907–924.

35 E. A. Uslamin, H. Saito, Y. Sekine, E. J. M. Hensen and N. Kosinov, *Catal. Today*, 2020, 1–9.

36 V. B. Kazansky, I. R. Subbotina, R. A. Van Santen and E. J. M. Hensen, *J. Catal.*, 2004, **227**, 263–269.

37 N. M. Phadke, J. Van Der Mynsbrugge, E. Mansoor, A. B. Getsoian, M. Head-Gordon and A. T. Bell, *ACS Catal.*, 2018, **8**, 6106–6126.

38 N. M. Phadke, E. Mansoor, M. Bondil, M. Head-Gordon and A. T. Bell, *J. Am. Chem. Soc.*, 2019, **141**, 1614–1627.

39 N. M. Phadke, E. Mansoor, M. Head-Gordon and A. T. Bell, *ACS Catal.*, 2021, 2062–2075.

40 M. W. Schreiber, C. P. Plaisance, M. Baumgärtl, K. Reuter, A. Jentys, R. Bermejo-Deval and J. A. Lercher, *J. Am. Chem. Soc.*, 2018, **140**, 4849–4859.

41 G. D. Meitzner, E. Iglesia, J. E. Baumgartner and E. S. Huang, *J. Catal.*, 1993, **140**, 209–225.

42 Y. Yuan, C. Brady, R. F. Lobo and B. Xu, *ACS Catal.*, 2021, **11**, 10647–10659.

43 Y. Zhou, H. Thirumalai, S. K. Smith, K. H. Whitmire, J. Liu, A. I. Frenkel, L. C. Grabow and J. D. Rimer, *Angew. Chemie - Int. Ed.*, 2020, **59**, 19592–19601.

44 G. Buckles, G. J. Hutchings and C. D. Williams, *Catal. Letters*, 1991, **8**, 115–123.

45 E. A. Pidko, R. A. van Santen and E. J. M. M. Hensen, *Phys. Chem. Chem. Phys.*, 2009, **11**, 2893–2902.

46 F. J. Machado, C. M. López, Y. Campos, A. Bolívar and S. Yunes, *Appl. Catal. A Gen.*, 2002, **226**, 241–252.

47 D. B. Lukyanov and T. Vazhnova, *Appl. Catal. A Gen.*, 2007, **316**, 61–67.

48 Z. Maeno, S. Yasumura, X. Wu, M. Huang, C. Liu, T. Toyao and K.-I. Shimizu, *J. Am. Chem. Soc.*, , DOI:10.1021/jacs.9b13865.

49 M. Huang, S. Yasumura, L. Li, T. Toyao, Z. Maeno and K. Shimizu, *Catal. Sci. Technol.*, , DOI:10.1039/d1cy01799c.

50 Z. Maeno, X. Wu, S. Yasumura, T. Toyao, Y. Kanda and K. I. Shimizu, *Catalysts*, , DOI:10.3390/catal10070807.

51 N. Katada, H. Tamagawa and M. Niwa, *Catal. Today*, 2014, **226**, 37–46.

52 J. J. H. B. Sattler, J. Ruiz-Martinez, E. Santillan-Jimenez and B. M. Weckhuysen, *Chem. Rev.*, 2014, **114**, 10613–10653.

53 A. I. Serykh and S. P. Kolesnikov, *Phys. Chem. Chem. Phys.*, 2011, **13**, 6892–6900.

54 Y. Yuan, C. Brady, L. Annamalai, R. F. Lobo and B. Xu, *J. Catal.*, 2021, **393**, 60–69.

55 E. J. M. Hensen, M. García-Sánchez, N. Rane, P. C. M. M. Magusin, P. H. Liu, K. J. Chao and R. A. Van Santen, *Catal. Letters*, 2005, **101**, 79–85.

56 G. D. Meitzner, E. Iglesia, J. E. Baumgartner and E. S. Huang, *J. Catal.*, 1993, **140**, 209–225.

57 A. Getsoian, U. Das, J. Camacho-Bunquin, G. Zhang, J. R. Gallagher, B. Hu, S. Cheah, J. A. Schaidle, D. A. Ruddy, J. E. Hensley, T. R. Krause, L. A. Curtiss, J. T. Miller and A. S. Hock, *Catal. Sci. Technol.*, 2016, **6**, 6339–6353.

58 Jeffrey J. Siirola, *AIChE J.*, 2014, **7**, 810–819.

59 L. C. Wang, Y. Zhang, J. Xu, W. Diao, S. Karakalos, B. Liu, X. Song, W. Wu, T. He and D. Ding, *Appl. Catal. B Environ.*, 2019, **256**, 117816.

60 C. Copéret, D. P. Estes, K. Larmier and K. Searles, *Chem. Rev.*, 2016, **116**, 8463–8505.

61 R. S. Vincent, R. P. Lindstedt, N. A. Malik, I. A. B. Reid and B. E. Messenger, *J. Catal.*, 2008, **260**, 37–64.

62 V. Galvita, G. Siddiqi, P. Sun and A. T. Bell, *J. Catal.*, 2010, **271**, 209–219.

63 P. Sun, G. Siddiqi, W. C. Vining, M. Chi and A. T. Bell, *J. Catal.*, 2011, **282**, 165–174.

64 A. Tsyganok, R. G. Green, J. B. Giorgi and A. Sayari, *Catal. Commun.*, 2007, **8**, 2186–2193.

65 U. Olsbye, A. Virnovskaia, O. Prytz, S. J. Tinnemans and B. M. Weckhuysen, *Catal. Letters*, 2005, **103**, 143–148.

66 T. V. M. Rao, E. M. Zahidi and A. Sayari, *J. Mol. Catal. A Chem.*, 2009, **301**, 159–165.

67 Z. Yang, H. Li, H. Zhou, L. Wang, L. Wang, Q. Zhu, J. Xiao, X. Meng, J. Chen and F. S. Xiao, *J. Am. Chem. Soc.*, 2020, **142**, 16429–16436.

68 H. Guo, C. Miao, W. Hua, Y. Yue and Z. Gao, *Microporous Mesoporous Mater.*, 2021, **312**, 110791.

69 E. A. Pidko, V. B. Kazansky, E. J. M. Hensen and R. A. van Santen, *J. Catal.*, 2006, **240**, 73–84.

70 M. S. Pereira, M. Antonio and C. Nascimento, 2005, **406**, 446–451.

71 Z. Feng, X. Liu, Y. Wang and C. Meng, *Molecules*, , DOI:10.3390/molecules26082234.

72 E. Mansoor, M. Head-gordon and A. T. Bell, , DOI:10.1021/acscatal.7b04295.

Chapter 4

In situ Ga K-edge XANES study of Ga-exchanged zeolites at high temperatures under different atmospheres including vacuum, CO, and pressurized H_2

4.1. Introduction

Ga-exchanged zeolites have been recognized as promising catalysts for the transformation of light alkanes. For example, Ga-exchanged MFI zeolites (Ga-MFIs) have been extensively studied for the dehydrocyclodimerization (DHCD) of propane to aromatics (the Cyclar process), which involves propane dehydrogenation to propylene and successive cyclodimerization of the generated propylene.[1–3] Ga-exchanged zeolites were prepared via the reductive solid-state ion-exchange (RSSIE) reaction of Ga_2O_3 with Brønsted acid sites (BASs) in the presence of reductants such as H_2. Reduced Ga species, such as Ga^+ cations and isolated Ga hydrides ($[GaH]^{2+}$/$[GaH_2]^+$), are considered active sites for propane dehydrogenation in the absence of oxidants, while cyclodimerization possibly occurs over BASs.[4–17] Catalysis of the dehydrogenative transformations of other light alkanes by Ga-MFIs has also been studied. Several research groups have investigated the formation of reduced Ga species in different ratios by Fourier transform infrared (FTIR) spectroscopy using probe molecules as well as their relationship with the dehydrogenation catalysis of Ga-exchanged zeolites.[7,8,10,12,13,18] However, the pressure and temperature for catalytic reaction conditions (atmospheric alkane flow conditions and >600 °C) are often different from those for catalyst characterization (vacuum conditions, <300 °C). Besides, unreacted GaOx species often remained especially in the Ga-MFIs prepared under high Ga loading and/or reported temperature (500-600 °C),[11,12] which hinders the elucidation of active Ga species. For the Ga_2O_3-based system, solid-state NMR measurements were performed to observe the surface Ga hydrides on the Ga oxides at relatively high reaction temperatures (relatively low pressure and up to 400 °C).[19] Although the aforementioned spectroscopic studies have provided important insights into the formation and presence of Ga hydrides upon H_2 treatment, the characterization of Ga-exchanged zeolites under operating conditions has rarely been investigated.

X-ray absorption spectroscopy (XAS) is a physicochemical characterization technique used to study the local structure of materials because it is sensitive to the electronic structure of the targeted atoms. One of the advantages of XAS over other characterization techniques is its applicability to in situ spectroscopic studies under operational conditions, such as heterogeneous catalytic reactions.[20] In the context of in situ XAS studies of Ga-exchanged zeolites, the occurrence of a lower-energy shift in the XANES spectra by H_2 activation, including RSSIE, has been reported by a few research groups, regardless of the preparation method.[5,7,11,21–24] Iglesia et al. proposed the formation of Ga-hydride

species based on the energy shift and disappearance of the extended X-ray absorption fine structure (EXAFS) features, [5] whereas the formation of Ga^+ cations was considered by other research groups[22,23]. Hock et al. recently discussed this shift in XANES spectra based on organometallic model Ga complexes where the lower energy shift can be ascribed to the formation of both reduced Ga species[21]. Despite considerable effort devoted to XANES studies on reduced Ga species in zeolites, their speciation (Ga^+ cations or Ga hydrides) remains controversial.

Recently, our research group developed the high-loading Ga-MFIs as an effective catalyst for non-oxidative ethane dehydrogenation (EDH) at 660 °C.[25] High-temperature H_2 treatment (800 °C) is essential to promote RSSIE, where unreacted GaO_X species are not detected, and isolated Ga species are exclusively formed. Isolated Ga-hydride species were present even after high-temperature RSSIE and then decomposed by He treatment above 800 °C. In this work, we first examined in situ XANES measurements under the following two identical conditions: H_2 at 800 °C for RSSIE and hydride formation and He at 850 °C for hydride decomposition. It was found that the absorption edges had equally low energy values, whereas the whiteline intensities depended on the measurement conditions; a higher intensity was obtained under H_2 flow than under He flow. Based on these results, in situ XANES measurements under CO, vacuum, and pressurized H_2 (1-9 atm) conditions were also conducted. The whiteline intensity increased with increasing H_2 pressure from 1 to 6 atm, whereas the CO and vacuum treatments afforded similarly lower whiteline intensities. The present in situ XANES study of Ga-exchanged zeolites showed that the whiteline intensity was responsible for the presence or absence of hydride sources.

4.2. Experimental

4.2.1. Synthesis of Ga_2O_3-modified MFI zeolite

Ga-modified MFI zeolite was synthesized using the impregnation method[25]. One gram of NH_4^+-type MFI zeolite (Tosoh, SiO_2/Al_2O_3 = 22.3) was added to an aqueous solution containing an appropriate amount of $Ga(NO_3)_3 \bullet nH_2O$ (n = 7-9, Wako), and water was evaporated from the mixture. After drying, the resulting solid was calcined at 500 °C for 1 h in air. The loading amount (Ga/Al ratio) was determined to be 1 based on the amounts of zeolite and precursor used in the synthesis. For the other zeolites, NH_4^+-type CHA and H^+-type MOR (SiO_2/Al_2O_3 = 22.3, and 18.3, respectively) were also supplied by Tosoh and used instead of the MFI. Ga_2O_3 modification was performed similarly.[26]

4.2.2. In situ Ga K-edge XANES measurements under normal pressure conditions using a flow-type cell

Ga K-edge XAS measurements under normal pressure conditions were conducted in transmission

mode at the BL14B2 station attached to a Si(311) monochromator at SPring-8 (JASRI), Japan (Proposal No. 2020A1695). A self-supported disk of a Ga_2O_3-modified MFI (80 mg, ϕ = 10 mm) was placed in a flow-type quartz cell. The XANES spectra were continuously recorded during the RSSIE reaction under a 10% H_2/He flow while increasing the temperature from 200 to 800 °C. After the RRSIE, the flow gas was changed to He and then increased to 850 °C. The XANES spectra of the reference samples (β-Ga_2O_3 and $Ga^+Ga^{3+}Cl_4$) were recorded at room temperature. Pellets of $Ga^+Ga^{3+}Cl_4$ were prepared in a glove box filled with Ar and used for measurements without exposure to air. The obtained spectra were analyzed using Athena 0.9.26.[27] The absorption edge (E_0) was defined as the 1st inflection point, whereas the whiteline intensity was compared with the maximum absorption (Ab_{max}) at approximately 13071–13072 eV.

4.2.3. In situ Ga K-edge XAS measurements under pressurized and vacuum conditions using a batch-type cell

XAFS measurements using a batch-type cell were conducted in BL14B1 at SPring-8 (Proposal Nos. 2021B3621 and 2022A3621). Because the maximum temperature of the apparatus is 700 °C, a powder sample of Ga_2O_3-modified MFI was pretreated under H_2 flow at 800 °C to promote the RSSIE reaction. The obtained sample was cooled to ambient temperature and then exposed to air overnight for the XAS measurements. During exposure to air, the reduced Ga species were considerably oxidized (see below). The self-supported disks of oxidized samples were heated from ambient temperature to 700 °C under vacuum conditions to dehydrate samples and then treated with 1 atm of 5% CO/He while recording the XANES spectrum. After the spectra remained unchanged, the CO gas was removed by vacuum treatment, and 1 atm of H_2 was introduced. The measurement conditions were continuously changed to vacuum, C_2H_6 (1 atm), and pressurized H_2 (3, 6, and 9 atm).

4.2.4. EDH reaction over the CO-treated Ga-MFI

The EDH reaction over the CO-treated Ga-MFI was conducted in a flow-type reactor under atmospheric pressure. Before the reaction, 20 mg of Ga_2O_3-modified MFI catalyst was treated with 10% H_2/Ar (10 mL/min) at 800 °C for 1 h. After purging with Ar to remove H_2 and cooling the reactor to room temperature, the catalyst was further treated with 10% O_2/Ar at 200 °C for 30 min to promote the oxidation of reduced Ga species in zeolites. The obtained catalyst was dehydrated under Ar flow (10 mL/min) at 700 °C and then treated with 10% CO/Ar (10 mL/min) for 1 h, affording CO-treated Ga-MFI. Before the EDH reaction, CO was removed by Ar purging, and the temperature was decreased to 600 °C. The EDH reaction was carried out under 10% C_2H_6/Ar flow (10 mL/min) at 600 °C. The conversion and selectivity were determined using a gas chromatography with a flame ionization detector. Note that at 600 °C, the selectivity was kept above 99%, where the main by-

product was methane. No other by-products were detected.

4.3. Results and discussion

In situ XAS measurements of Ga-MFI-1 (Ga/Al = 1, H_2 treatment temperature at 800 °C) were performed under different treatment conditions. The self-supported disk of the Ga_2O_3-modified MFI zeolite was exposed to a 10% H_2/He flow at 200 °C and thereafter heated to 800 °C in a quartz cell to achieve RSSIE. Before the H_2 treatment, the absorption edge of the XANES spectrum was similar to that of bulk Ga_2O_3 (Fig. 1, black solid and gray dashed lines, E_0 = 10374.1 and 10373.9 eV, respectively.)

After H_2 treatment at 800 °C, the absorption edge shifted to a lower energy (red solid line, E_0 = 10370.6 eV), similar to that of Ga^+ in $Ga^+Ga^{3+}Cl_4$ (brown dashed line, E_0 = 10371.6 eV). Notably, the whiteline intensity at 10371.7 eV was significantly strong (Ab_{max} = 3.09). When the H_2-treated sample was treated under He flow at 850 °C, the intensity of the whiteline around 10372 eV decreased (green solid line, Ab_{max} = 2.82), whereas the absorption edge remained unchanged (E_0 = 10370.6 eV). Because He treatment at high temperatures caused the decomposition of Ga hydrides in MFI, as indicated by FTIR spectroscopy in our previous study[25], the change in the whiteline intensity may be ascribed to the decomposition of Ga hydrides. To support the above considerations, the obtained sample was re-treated under a 10% H_2/He flow at 800 °C. The whiteline intensity at approximately 10372 eV returned to the same level as that after the 1st H_2 treatment (blue solid line, Ab_{max} = 3.10), whereas the absorption edge energy was maintained (E_0 = 10371.0 eV). In a separate experiment, Ga hydrides were regenerated by the H_2 treatment of He-treated Ga-MFI-1, as demonstrated by in situ FTIR spectroscopy[25]. These observations indicate that both Ga hydrides and Ga^+ cations exhibit similar absorption edges, whereas the whiteline intensity for the Ga hydrides is higher than that for the Ga^+ cations. In the EXAFS oscillation spectrum of Ga-MFI-1 after the He treatment, the EXAFS feature significantly decreased, and the spectrum pattern was quite different from that of Ga_2O_3[5] (Fig. S1, see the ESI). The FT-EXAFS showed a small scattering peak at 2.7 Å, which is shorter than that for the Ga—Ga shell of Ga_2O_3 at 2.8 Å (Fig. S2, see the ESI), possibly ascribed to the Ga—Al shell of the extra-framework Ga species on the framework Al sites[7,23]. These observations are consistent with our previous results from the FTIR study of pyridine adsorption, where the adsorbed pyridine on unreacted GaO_X was hardly observed[25], supporting the exclusive formation of reduced Ga species.

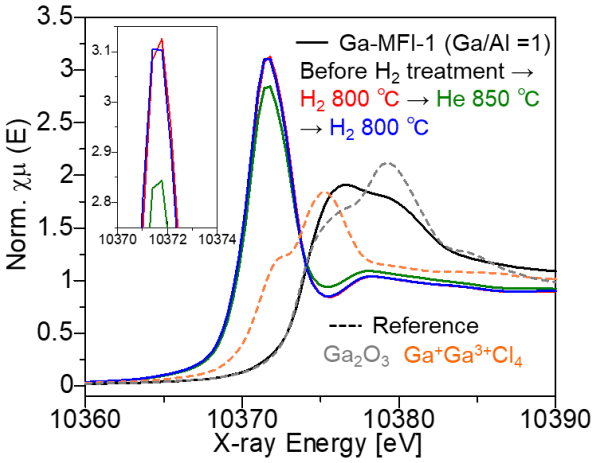

Fig. 1. In situ Ga K-edge XAS spectra of Ga-MFI-1 recorded under various conditions and reference samples (Ga_2O_3, $Ga^+Ga^{3+}Cl_4$). The spectrum before H_2 treatment was obtained at 200 ˚C, whereas other spectra were obtained at the corresponding temperature (solid lines in different colors). For reference, the spectra were recorded at room temperature (dashed lines in different colors).

To further investigate the difference in the whiteline intensity between Ga^+ cations and Ga hydrides, H_2-treated Ga-MFI-1 was exposed to air to oxidize the reduced Ga species on the ion-exchange sites, and then reduced by CO at 700 °C instead of H_2 to suppress the formation of hydride species. The XANES spectrum of air-exposed Ga-MFI-1 exhibits an absorption edge at a high-energy position (Fig. 2, gray solid line, E_0 = 10375.1 eV), confirming the re-oxidation of the reduced Ga species. The CO treatment (1 atm of 5% CO/He) at 700 °C induced the shift of absorption edge to a lower value (red solid line, E_0 = 10370.7 eV), demonstrating that CO serves as the reductant of oxidized Ga species to give reduced Ga species. The Ab_{max} value was determined to be 2.80, which is similar to that of the He-treated Ga-MFI-1, as discussed above.

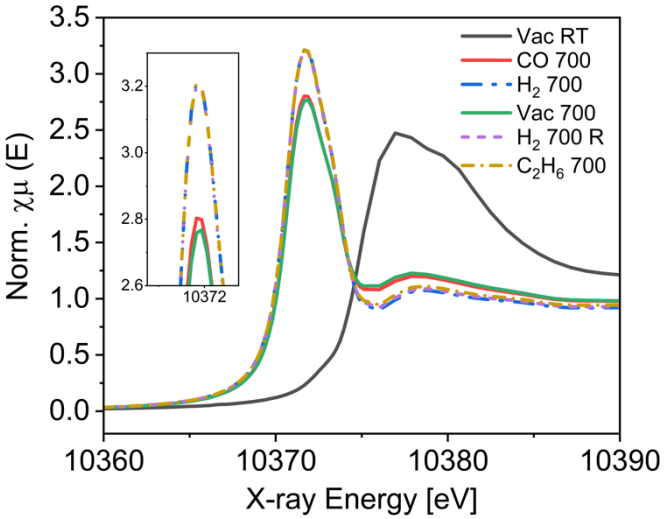

Fig. 2. In situ Ga K-edge XAS spectra of Ga-MFI-1 obtained under different conditions. All the spectra were obtained at 700 ˚C, except for the first spectrum (black solid line), which was taken under room temperature.

Subsequently, 5% CO/He was replaced with H_2 (1 atm) under isothermal conditions to promote the formation of Ga hydride species. The whiteline intensity at approximately 10372 eV increased (blue chain line, Ab_{max} = 3.21), whereas the absorption edge energy was almost the same (E_0 = 10370.7 eV). When the H_2-treated sample was treated under vacuum conditions, the whiteline intensity decreased to the same level as that after CO treatment (green solid line, Ab_{max} = 2.76) while maintaining a low absorption edge energy position. These phenomena indicate that the CO and vacuum treatments afforded similar reduced Ga species (exclusive formation of Ga^+ cations) and that the H_2 treatment induced the formation of hydride-containing Ga species, resulting in higher whiteline intensity.

The vacuum-treated sample was treated with C_2H_6 without exposure to air. The whiteline intensity was similar to that obtained after H_2 treatment (gold chain line, Ab_{max} = 3.21), whereas the absorption energy was maintained (E_0 = 10370.7 eV). Successive H_2 treatment did not change its intensity or absorption edge (purple dashed line), implying that similar hydride-containing Ga species were possibly formed even under a C_2H_6 atmosphere.

In recent studies reported by Bell et al., Ga hydrides were thermodynamically less stable than Ga^+ cations, and a higher H_2 pressure was favorable for the formation of Ga hydrides[7,13]. To further investigate the effect of the H_2 pressure, XAS measurements were performed under a pressurized H_2 atmosphere. Fig. 3a and b show the XANES spectra and corresponding difference spectra (ΔXANES), respectively. The plot of the difference of Ab_{max} (denoted as ΔAb_{max}) as a function of H_2 pressure is also shown in Fig. 3c. An increase in the H_2 pressure from 1 to 3 atm increased the Ab_{max} value from 3.21 to 3.37 (Fig. 3a). A further increase in the H_2 pressure from 3 to 6 atm resulted in a slight increase in the whiteline intensity (Ab_{max} = 3.41). The whiteline intensity did not change when the H_2 pressure reached 9 atm (Fig. 3c). From this H_2-pressure-dependent spectrum change, the increase in the whiteline intensity may be responsible for the formation of hydride-containing Ga species.

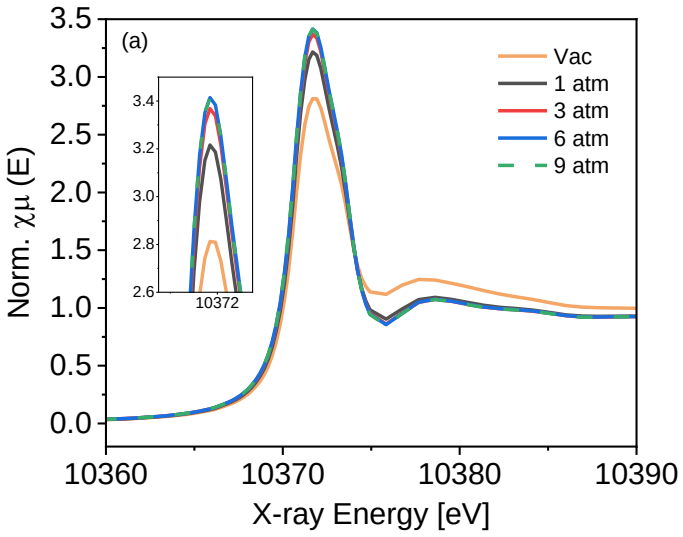

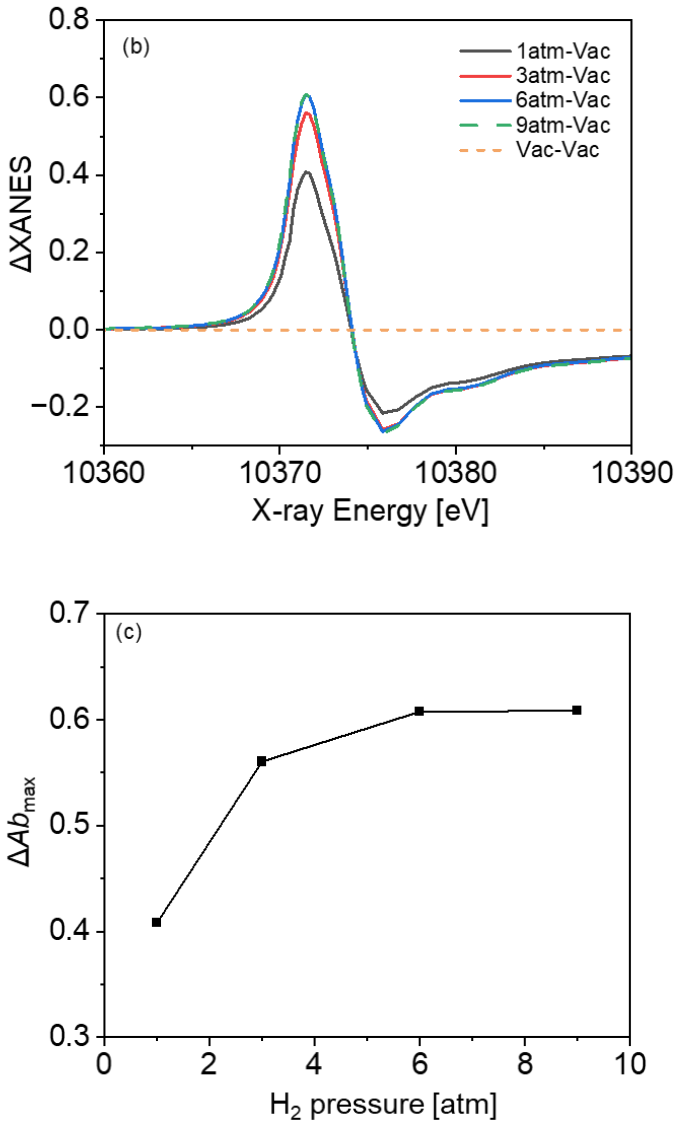

Fig. 3. (a) Comparison of XAS spectra of Ga-MFI-1 under different H_2 pressure (recorded at 700 °C). (b) ΔXANES spectra of the one taken under pressurized H_2 treatment from the one taken under vacuum condition. (c) Plot of ΔAb_{max} as a function of H_2 pressure.

From the above in situ Ga K-edge XANES study, although both H_2 and CO treatments led to the exclusive formation of reduced Ga species (Ga^+ cations and/or Ga hydrides), Ga-hydride species were unlikely to be generated in the CO-treated Ga-MFI-1, resulting in different distributions of reduced Ga species. Therefore, the CO- and H_2-treated Ga-MFIs would exhibit different EDH activities. To examine this hypothesis, we investigated the EDH reaction over the CO-treated Ga-MFI-1 using a flow reactor at 600 °C, and then the activity was compared with the H_2-treated Ga-MFI-1. Notably, the C_2H_4 selectivity was maintained above 99%. The initial C_2H_4 yield (at 5 min) for the CO-treated sample was approximately 6 %, which was lower than that of the H_2-treated sample at the same temperature (approximately 10 %), demonstrating the different distributions of reduced Ga species

between the CO- and H_2-treated Ga-MFIs. When the reaction time was extended to 100 min, the yield value gradually increased from 6% to 9% and then leveled off (Fig. 4), which implies the in situ formation of more active Ga species, possibly hydride-containing ones, from Ga^+ cations during EDH reaction. This result seems consistent with the observed XANES spectral changes under the CO, H_2, vacuum, and C_2H_6 conditions. Although the measurement and treatment temperature were much lower (200 °C) than that in our case, the in situ formation of Ga hydrides from Ga cations with C_2H_6 has been previously reported[18]. Unfortunately, the Ga-hydride species were not detected under the actual operating conditions (10% C_2H_6 flow at 600 °C) at this stage owing to coke formation and the dynamic nature of surface hydride species[12,28].

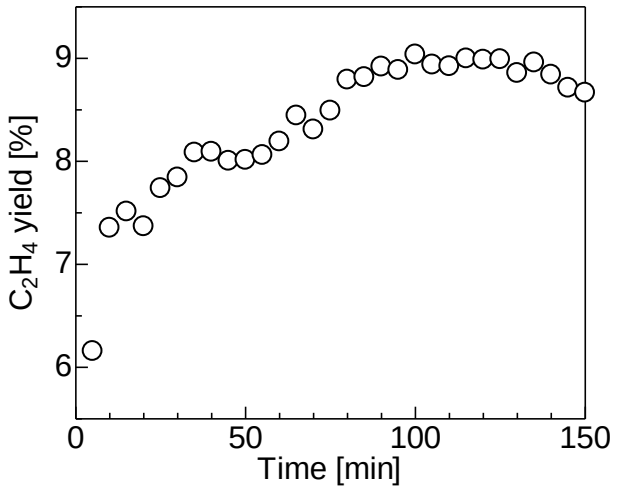

Fig. 4. Time course of C_2H_4 yield in EDH over CO-treated Ga-MFI-1 at 600 °C. The oxidized Ga-MFI-1 was pretreated with 10% CO/Ar at 700 °C and then used for the EDH reaction. The detailed experimental procedure is described in the Experimental section.

Recently, we conducted a comparative study of high-loading Ga-exchanged zeolites with different types of frameworks (CHA and MOR) for the EDH reaction with Ga-MFI.[26] Although the activation energies of the three Ga-exchanged zeolites were similar, the steady-state C_2H_4 yields in the EDH increased in the following order, Ga-MFI-1 > Ga-MOR-1 > Ga-CHA-1. This order is consistent with the relative amount of active Ga hydrides as examined by the H–D exchange reactions between D_2 and H_2-treated Ga-exchanged zeolites, indicating that isolated Ga hydrides are likely the active species for EDH.[29]

In this study, XANES measurements were performed under different conditions (CO, H_2, vacuum, and C_2H_6) for oxidized Ga-CHA-1 and MOR-1, which were prepared similarly to oxidized Ga-MFI-1. For Ga-CHA, a similar spectral change was observed depending on the measurement atmosphere, although the ΔAb_{max} was much smaller (Fig. 5a). For example, the Ab_{max} values obtained under vacuum and C_2H_6 conditions were 3.10 and 3.21, respectively, where ΔAb_{max} was calculated as 0.11.

This value was significantly smaller than that of Ga-MFI (ΔAb_{max} = 0.45). In the case of Ga-MOR, CO treatment was not effective in promoting the reduction of oxidized Ga species in the zeolites (Fig. S3, see the ESI). H_2 treatment effectively reduced the oxidized Ga species, resulting in a sharp absorption peak (Fig. 5b, Ab_{max} = 3.39). Successive vacuum and C_2H_6 treatments induced similar spectral changes, with Ab_{max} values were 3.25 and 3.40, respectively, and ΔAb_{max} was determined as 0.15.

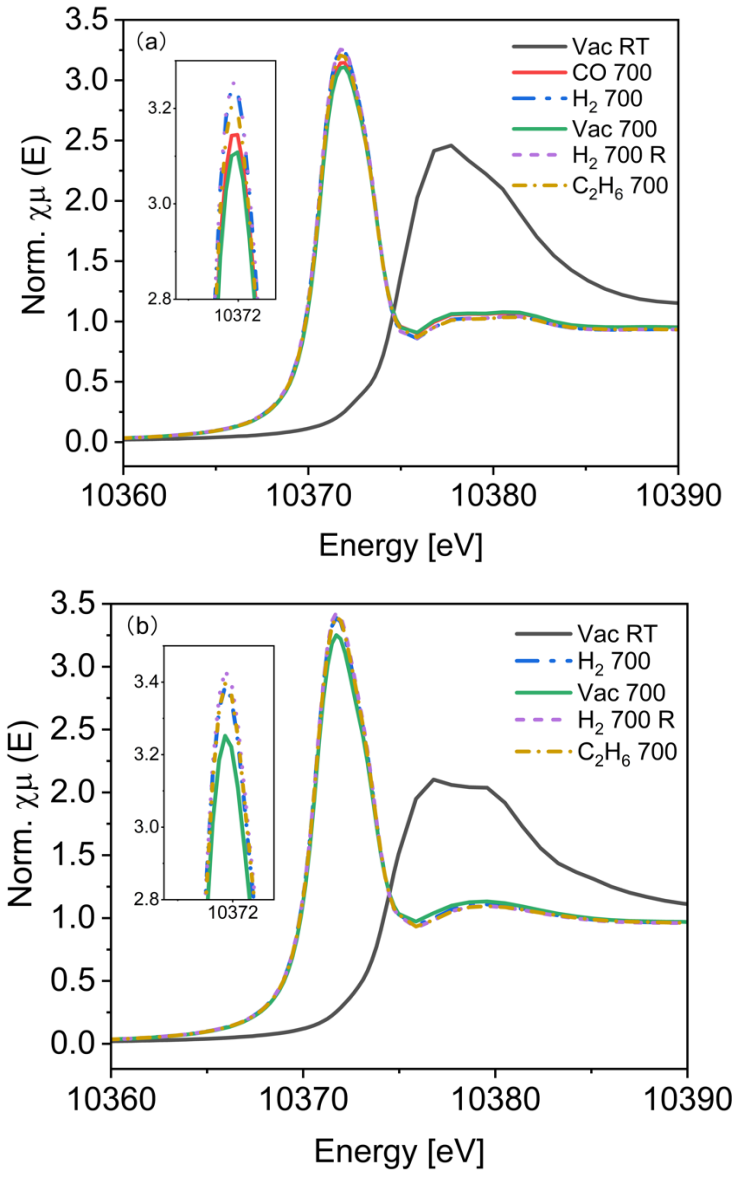

Fig. 5. In situ Ga K-edge XAS spectra of (a) Ga-CHA-1 and (b) Ga-MOR-1 under various conditions. All the spectra were obtained at 700 ˚C, except for the first spectrum (black) taken at room temperature.

The correlation between ΔAb_{max} and the relative amount of Ga hydrides was investigated for the three Ga-exchanged zeolites. The values of Ga-MFI-1, Ga-MOR-1, and Ga-CHA-1 are summarized in Table S1. The negative IR intensity at 2050 cm^{-1} in the H–D exchange reaction (as an index of the relative

amount of Ga hydrides)[26] was plotted as a function of ΔAb_{max} (Fig. 6a). A linear relationship is obtained, showing that the increase in the whiteline intensity is interpreted as the formation of active Ga hydrides. The C_2H_4 yield after 3 h, as an index of the steady-state activity, was also plotted as a function of ΔAb_{max} where a good linear relationship was observed (Fig. 6b), further supporting this interpretation. Although the direct observation of active Ga hydrides under real operating conditions is quite difficult, the above results and findings suggest that the Ga K-edge XANES measurement would be useful for discussing the formation/decomposition of active Ga hydrides under catalytic reaction conditions. Note that during the preparation of our manuscript, Scott and Vila reported that the whiteline intensity of Ga hydrides was predicted to be lower than that of Ga^+ cations in a theory-informed XAS study.[24] They mentioned that the weak coordination of oxygen ligands is one of the key factors affecting the whiteline intensity. The measurement atmosphere may also have affected the coordination environment of the Ga species in our case. A theoretical study for the construction of a more realistic model of the reduced Ga species, considering the coordination environments and measurement temperatures, is required.

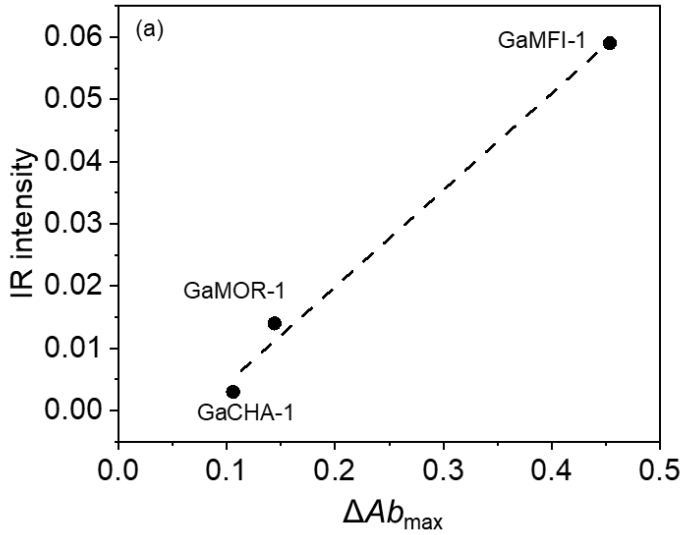

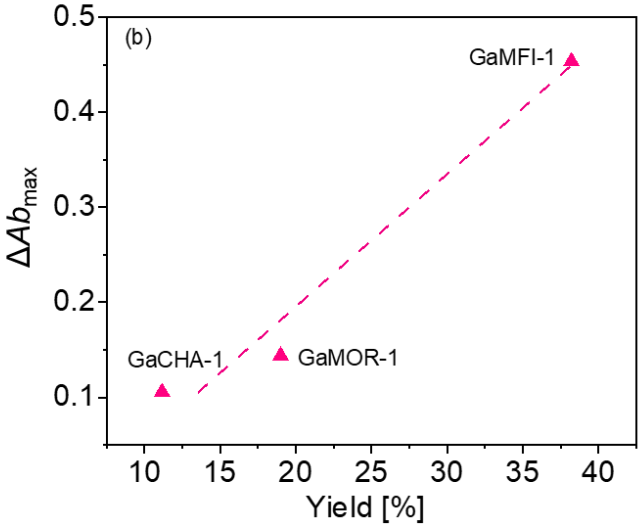

Fig. 6. (a) Plot of negative IR intensity at 2050 cm^{-1} after H–D exchange reaction between D_2 and H_2-treated Ga-CHA, MOR, and MFI (as an index of relative amount of active Ga hydrides) as a function of the difference in maximum whiteline intensity between C_2H_6 and vacuum conditions (ΔAb_{max}). (b) Plot of ΔAb_{max} as a function of C_2H_4 yield after 3 h in EDH (as an index of steady-state activity). The IR intensity and yield values were obtained in our previous report[26].

4.4. Conclusion

We conducted an in situ Ga K-edge XANES study for high-loading Ga-MFI prepared by high-temperature H_2 treatment at high temperatures (> 700 °C) under different atmospheres. In the normal pressure experiment, H_2 treatment afforded a significantly lower energy shift and strong whiteline intensity at the absorption edge of the XANES spectrum. Successive high-temperature He treatment decreased the whiteline intensity while maintaining the absorption edge position in energy, and the XANES spectrum returned to almost its original intensity. In situ XANES measurements of oxidized Ga-MFI under CO, pressurized H_2, and vacuum conditions showed that the whiteline intensity increased with the increase of H_2 pressure while the similary lower intensities were obtained under CO and vacuum onditions. These results indicated that the increase in the whiteline intensity is interpreted as the formation of active Ga hydrides. Notably, the C_2H_6 treatment resulted in a higher intensity similar to that of the H_2 treatment, suggesting the presence of hydride-containing Ga species under real operation conditions. Similar spectral changes depending on the measurement conditions were observed for Ga-CHA and Ga-MOR. The degree of spectral change correlated well with the relative amount of Ga hydrides estimated by IR, as well as the steady-state EDH activity.

References

1 Y. Ono, *Catal. Rev.*, 1992, **34**, 179–226.

2 N. Y. Chen and T. Y. Yan, *Ind. Eng. Chem. Process Des. Dev.*, 1986, **25**, 151–155.

3 D. Seddon, *Catal. Today*, 1990, **6**, 351–372.
4 K. M. Dooley, C. Chang and G. L. Price, *Appl. Catal. A Gen.*, 1992, **84**, 17–30.
5 G. D. Meitzner, E. Iglesia, J. E. Baumgartner and E. S. Huang, *J. Catal.*, 1993, **140**, 209–225.
6 V. B. Kazansky, I. R. Subbotina, R. A. van Santen and E. J. M. Hensen, *J. Catal.*, 2004, **227**, 263–269.
7 N. M. Phadke, J. Van der Mynsbrugge, E. Mansoor, A. B. Getsoian, M. Head-Gordon and A. T. Bell, *ACS Catal.*, 2018, **8**, 6106–6126.
8 N. M. Phadke, E. Mansoor, M. Bondil, M. Head-Gordon and A. T. Bell, *J. Am. Chem. Soc.*, 2019, **141**, 1614–1627.
9 L. Ni, R. Khare, R. Bermejo-Deval, R. Zhao, L. Tao, Y. Liu and J. A. Lercher, *J. Am. Chem. Soc.*, 2022, **144**, 12347–12356.
10 Y. Yuan, J. S. Lee and R. F. Lobo, *J. Am. Chem. Soc.*, 2022, **144**, 15079–15092.
11 M. W. Schreiber, C. P. Plaisance, M. Baumgärtl, K. Reuter, A. Jentys, R. Bermejo-Deval and J. A. Lercher, *J. Am. Chem. Soc.*, 2018, **140**, 4849–4859.
12 Y. Yuan, C. Brady, L. Annamalai, R. F. Lobo and B. Xu, *J. Catal.*, 2021, **393**, 60–69.
13 E. Mansoor, M. Head-Gordon and A. T. Bell, *ACS Catal.*, 2018, **8**, 6146–6162.
14 Y. V Joshi and K. T. Thomson, *Catal. Today*, 2005, **105**, 106–121.
15 M. S. Pereira and M. A. C. Nascimento, *Chem. Phys. Lett.*, 2005, **406**, 446–451.
16 E. A. Pidko, E. J. M. Hensen and R. A. van Santen, *J. Phys. Chem. C*, 2007, **111**, 13068–13075.
17 E. A. Pidko, V. B. Kazansky, E. J. M. Hensen and R. A. van Santen, *J. Catal.*, 2006, **240**, 73–84.
18 V. B. Kazansky, I. R. Subbotina, N. Rane, R. A. van Santen and E. J. M. Hensen, *Phys. Chem. Chem. Phys.*, 2005, **7**, 3088–3092.
19 H. Chen, P. Gao, Z. Liu, L. Liang, Q. Han, Z. Wang, K. Chen, Z. Zhao, M. Guo, X. Liu, X. Han, X. Bao and G. Hou, *J. Am. Chem. Soc.*, 2022, **144**, 17365–17375.
20 G. T. Whiting, F. Meirer and B. M. Weckhuysen, in *XAFS Techniques for Catalysts, Nanomaterials, and Surfaces*, eds. Y. Iwasawa, K. Asakura and M. Tada, Springer International Publishing, Cham, 2017, pp. 167–191.
21 A. "Bean" Getsoian, U. Das, J. Camacho-Bunquin, G. Zhang, J. R. Gallagher, B. Hu, S. Cheah, J. A. Schaidle, D. A. Ruddy, J. E. Hensley, T. R. Krause, L. A. Curtiss, J. T. Miller and A. S. Hock, *Catal. Sci. Technol.*, 2016, **6**, 6339–6353.
22 A. C. Jr. Faro, V. de O. Rodrigues and J.-G. Eon, *J. Phys. Chem. C*, 2011, **115**, 4749–4756.
23 E. J. M. Hensen, M. García-Sánchez, N. Rane, P. C. M. M. Magusin, P.-H. Liu, K.-J. Chao and R. A. van Santen, *Catal. Lett.*, 2005, **101**, 79–85.
24 L. Li, J. A. Chalmers, S. R. Bare, S. L. Scott and F. D. Vila, *ACS Catal.*, 2023, **13**, 6549–6561.
25 M. Huang, S. Yasumura, L. Li, T. Toyao, Z. Maeno and K. Shimizu, *Catal. Sci. Technol.*, 2022, **12**, 986–995.
26 M. Huang, Z. Maeno, T. Toyao and K. Shimizu, *Catal. Today*, 2023, **411–412**, 113824.
27 B. Ravel and M. Newville, *J. Synchrotron Radiat.*, 2005, **12**, 537–541.
28 C. Copéret, D. P. Estes, K. Larmier and K. Searles, *Chem. Rev.*, 2016, **116**, 8463–8505.
29 H. Mengwen, S. Yasumura, T. Toyao, K. Shimizu and Z. Maeno, *Phys. Chem. Chem. Phys.*, 2023, **25**, 10211–10230.

Chapter 5

Anaerobic ammodehydrogenation of ethane to acetonitrile over Ga-loaded H-FER zeolite catalysts

5.1. Introduction

Currently, CH_3CN is commercially produced as a byproduct of propylene ammoxidation to acrylonitrile (CH_2=CHCN), and the production of CH_3CN strongly depends on the demand for CH_2=CHCN.[1,2] Therefore, an on-purpose technique for selective CH_3CN production from abundant C_2H_6[3–11] or C_2H_4[12–14] could be an important alternative to the current industrial process.[15] Previously, pioneering works by Li and Armor[7,16,17] showed the selective formation of CH_3CN by the ammoxidation of C_2H_6 ($C_2H_6 + NH_3 + O_2$ reaction) over Co-exchanged zeolites. Recently, Xiang et al. developed an alternative route: direct CH_3CN synthesis by the anaerobic ammodehydrogenation of C_2H_6 ($C_2H_6 + NH_3$ reaction) over Pt- and Co-Pt-loaded MFI zeolites.[15,18] Although the formation of CH_3CN from C_2H_6 and NH_3 is thermodynamically less favorable than the ammoxidation of C_2H_6, Xiang et al. demonstrated that the ammodehydrogenation method affords higher activity and selectivity to CH_3CN than the conventional ammoxidation process[18]. To date, only two catalysts (Pt/MFI and Co-Pt/MFI) have been reported for the ammodehydrogenation of C_2H_6.[15,18] This highlights the challenges in developing efficient catalysts for this new catalytic reaction.

Mechanistic studies by Xiang et al. showed a tandem dehydrogenation–amination–dehydrogenation mechanism; the initial C_2H_6 dehydrogenation over the metal sites was followed by amination between C_2H_4 and NH_3 to form ethylamine ($CH_3CH_2NH_2$), which underwent further dehydrogenation on the metal sites.[18] Our group reported a series of studies on the anaerobic dehydrogenation of C_2H_6 over Ga- and In-loaded zeolites.[19–21] Knowing the high dehydrogenation activity of these catalysts, we hypothesized that Ga- and In-loaded zeolites could be effective catalysts for C_2H_6 dehydrogenation.

In this study, we investigated the selective CH_3CN production from C_2H_6 and NH_3 using Ga-loaded zeolites under anaerobic conditions. Various zeolite supports, including MFI, MOR, Y, BEA,

and FER, were compared for their catalytic activities, and the Ga-loaded FER zeolite exhibited the highest activity. The Ga/HFER catalyst notably outperformed all the reported catalysts.

5.2. Experimental section

5.2.1. Catalyst preparation

The Ga/HFER catalysts were prepared using a conventional impregnation method. The Ga precursor, $Ga(NO)_3 \cdot nH_2O$ (n = 7–9, Wako), was mixed with H^+-type FER zeolite (SiO_2/Al_2O_3 = 18.3, Tosoh) in deionized water. Subsequently, water was removed from the mixture using a rotary evaporator, followed by drying in an oven (100 °C, 12 h) and calcinating at 500 °C for 1 h under an air flow to yield Ga_2O_3-loaded HFER. Other Ga_2O_3-loaded zeolites were prepared in a similar manner using NH_4^+-type MOR (SiO_2/Al_2O_3 = 18.3, Tosoh), MFI (SiO_2/Al_2O_3 = 22.3, Tosoh), BEA (SiO_2/Al_2O_3 = 17.5, Tosoh), and Y (SiO_2/Al_2O_3 = 10.6, Tosoh). Ga_2O_3 was purchased from FUJIFILM Wako Pure Chemical Co. (Osaka, Japan).

5.2.2. Catalytic testing

Catalytic tests were performed at atmospheric pressure using a fixed-bed flow reactor (Pyrex glass tube) with an inner diameter of 12 mm. The catalyst powder (typically 0.1 g) placed in the reactor was purged with He at 550 °C (0.5 h) before the reaction. The reaction temperature was measured inside the catalyst bed using a thermocouple with a tip on the upper side of the catalyst bed. The gas stream was fed into the reactor using mass-flow controllers. For ammodehydrogenation of C_2H_6 or C_2H_4, the reactor was fed with 2% C_2H_6 (C_2H_4) + 2.5% NH_3/He mixture with a total flow rate of 20 mL min^{-1}. The products in the outlet gas were analyzed using a gas chromatography (GC) with flame ionization detector and a Porapak Q column. The yield, conversion and selectivity values were determined based on the following equations.

$$\text{Acetonitrile yield [\%]} = \frac{[\text{acetonitrile}]}{[\text{ethane}]_{\text{init}}} \times 100$$

$$\text{Methane yield [\%]} = \frac{[\text{methane}]}{2 \times [\text{ethane}]_{\text{init}}} \times 100$$

$$\text{Hydrogen cyanide yield [\%]} = \frac{[\text{Hydrogen cyanide}]}{2 \times [\text{ethane}]_{\text{init}}} \times 100$$

$$\text{Ethylene yield [\%]} = \frac{[\text{ethylene}]}{[\text{ethane}]_{\text{init}}} \times 100$$

$$\text{Ethane yield [\%]} = \frac{[\text{ethane}]}{[\text{ethane}]_{\text{init}}} \times 100$$

$$\text{Conv. [\%]} = \frac{[\text{ethane}]_{\text{init}} - [\text{ethane}]}{[\text{ethane}]_{\text{init}}} \times 100$$

$$\text{Selec. [\%]} = \frac{[\text{acetonitrile}]}{[\text{ethane}]_{\text{init}} - [\text{ethane}]} \times 100$$

A transient catalytic experiment and temperature-programmed surface reaction (TPSR) were performed using a flow reactor connected to a mass spectrometer (BELMass, MicrotracBEL Corp.) to analyze the outlet gas.

5.2.3. Catalyst Characterization

Ga K-edge extended X-ray absorption fine structure (EXAFS) and X-ray absorption near-edge structure (XANES) spectra were recorded in the transmission mode at the BL01B1 station attached to a Si(311) monochromator at SPring-8 (JASRI), Japan (Proposal No. 2023A1931). Seventeen milligrams of the samples (φ:7 mm) were pelletized into self-supported disks. Curve-fitting analyses were performed using the REX version 2.5 program (RIGAKU).

5.3. Result and discussion

5.3.1 Catalysts screening for C_2H_6 ammodehydrogenation

Various metal-loaded MFI zeolite catalysts with similar loadings (M/Al = 1.0) were screened for C_2H_6 ammodehydrogenation. The lower-loading Pt-MFI was also tested as a previously reported catalyst. The reactions were conducted by flowing 2% C_2H_6+2.5% NH_3/He (total flow rate: 20 mL min^{-1}) over 0.1 g of the catalyst at 650 °C. The product yields and amount of unreacted C_2H_6 after a reaction time of 25 min are shown in Fig. 1A. The CH_3CN yield strongly depended on the loaded metal and changed in the following order: Ga > Zn > Pt > In. The time course of CH_3CN yield is shown in Fig. 1B. The yield gradually decreased with increasing reaction time. Hereafter, the yields

at a reaction time of 25 min are compared to discuss the effects of the catalyst type and reaction conditions on the catalytic activity.

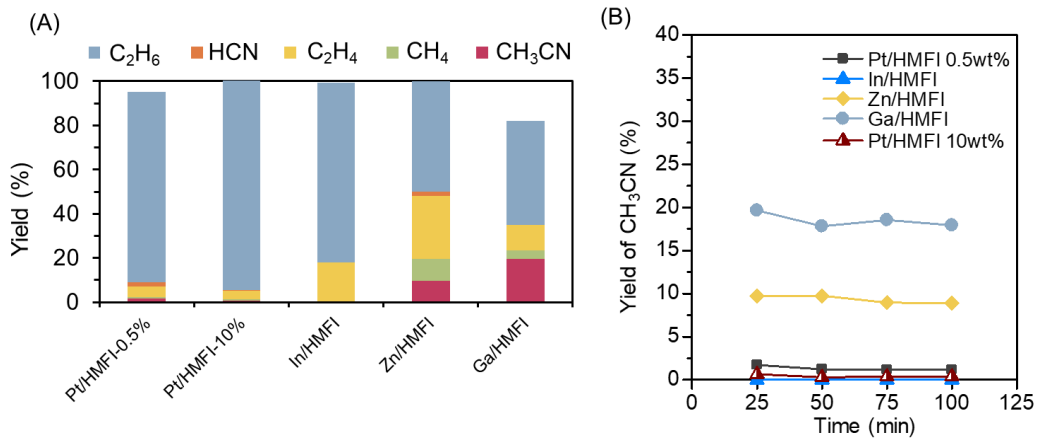

Fig. 1. C_2H_6 ammodehydrogenation by metal-loaded zeolites. (A) Yields of products and unreacted C_2H_6. (B) Time course of CH_3CN yields. Reaction conditions: 100 mg of catalyst, 650 °C, 2% C_2H_6 + 2.5% NH_3/He (total flow rate: 20 mL min^{-1}).

Various Ga-loaded zeolites with similar Ga loadings (9.4–12.1 wt.%) and then tested for the ammodehydrogenation of C_2H_6 at 650 °C. The compositions and pore sizes of the tested Ga-loaded zeolites are summarized in Table 1. Ga/HFER, Ga/HMFI, Ga/HBEA, and Ga/HMOR had similar SiO_2/Al_2O_3 ratios (18.3, 22.3, 17.5, and 18.3, respectively), with the same Ga/Al ratio of 1.0. For Ga/HY, the SiO_2/Al_2O_3 ratio was 10.6, and the Ga/Al ratio was 0.5. Fig. 2A shows a comparison of the yields of the products and unreacted C_2H_6 observed at 25 min. The results showed that the CH_3CN yield depended strongly on the zeolite type and changed in the following order: Ga/HFER > Ga/HMFI > Ga/HBEA > Ga/HMOR > Ga/HY. The CH_3CN yield decreases with increasing zeolite pore size (Table 1). Fig. 2B shows the time course of CH_3CN yield over the Ga-loaded zeolites. The yield gradually decreased with increasing reaction time.

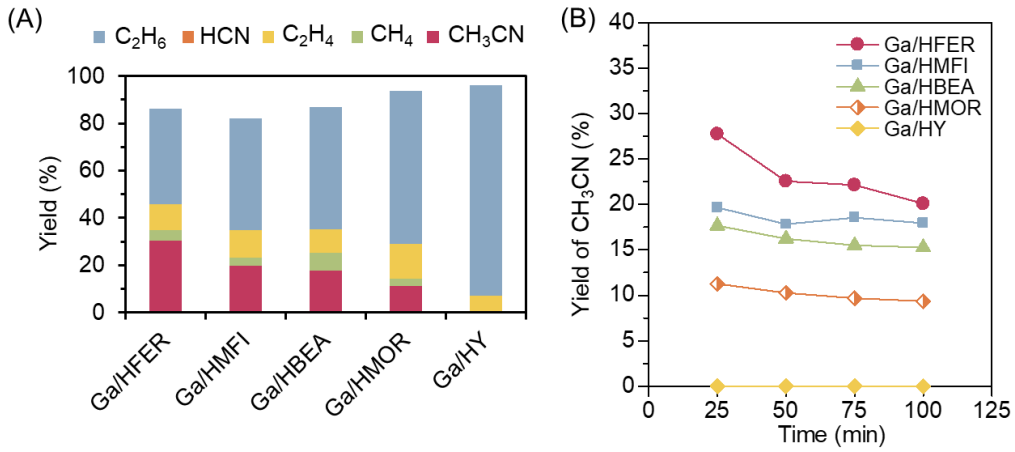

Fig. 2. C_2H_6 ammodehydrogenation using various Ga-loaded zeolites. (A) Yields of products and unreacted C_2H_6. (B) Time course of CH_3CN yields. Conditions are the same as in Fig. 1.

Table 1. Characteristics and porosity of different Ga-zeolites.

Catalyst	Si/Al$_2$	Ga/Al	Ga loading/ wt%	Pore size/ Å
Ga/HFER	18.3	1	11.8	4.2 x 5.4
Ga/HMFI	22.3	1	9.7	5.1 x 5.5
Ga/HBEA	17.5	1	12.1	6.6 x 6.7
Ga/HMOR	18.3	1	11.8	6.5 x 7.0
Ga/HY	10.6	0.5	9.4	7.4 x 7.4

Ga/HFER catalysts with different Ga loadings and Ga-free HFER were prepared and tested under standard conditions. Fig. 3 shows the effect of the Ga/Al ratio on the product yield. The Ga-free HFER catalyst showed no activity in the dehydrogenation of C_2H_6, and C_2H_4 (2.9% yield) was produced as a main product. For the Ga/HFER catalysts, the CH_3CN yield increased with increasing Ga/Al ratio, whereas the C_2H_4 yield decreased with increasing Ga/Al ratio. These results indicate that Ga is the main active species for the dehydrogenation of C_2H_6 to CH_3CN. Based on the aforementioned

results for catalyst screening, we adopted Ga/HFER with a Ga/Al ratio of 1.0 as the standard catalyst for subsequent structural and catalytic studies.

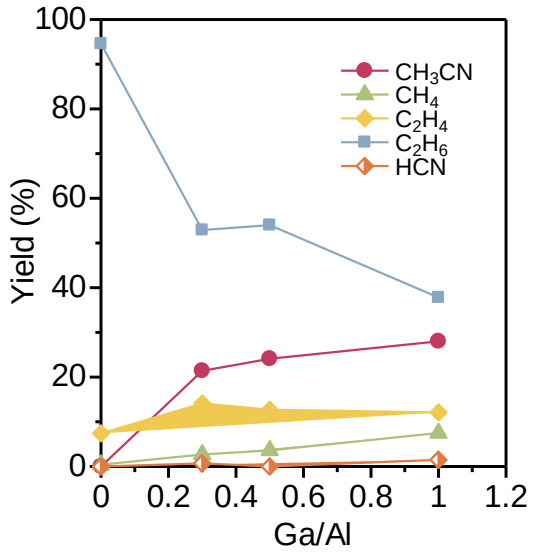

Fig. 3. Yields of products and unreacted C_2H_6 versus the Ga/Al ratio of Ga/HFER catalysts. Conditions are the same as in Fig. 1.

5.3.2. Characterization of Ga species in Ga/HFER

In the literature, atomically dispersed Ga-exchanged zeolites have been prepared by loading Ga_2O_3 on zeolites using a conventional impregnation method, followed by H_2 treatment at high temperatures (500–800 °C) to promote reductive solid-state ion exchange (RSSIE) reactions.[22,23] The precursors of the Ga-zeolites catalysts tested in the current study were also prepared by a conventional impregnation method, followed by calcination. However, Ga(III) oxide species can be transformed into isolated Ga species by RSSIE during the ammodehydrogenation of C_2H_6, which continuously produces H_2 at 650 °C. To study the structural changes in Ga species, we performed Ga K-edge EXAFS/XANES measurements of Ga/HFER before and after the ammodehydrogenation of C_2H_6 at 650 °C. The results are summarized in Table 2. Two comparative catalysts were prepared to identify the Ga species in the standard catalyst. The first was a Ga(III) oxide-loaded KFER (H^+-free FER) prepared using the impregnation method, followed by calcination. Another comparative catalyst, Ga_2O_3 + HFER, was prepared by physically mixing Ga_2O_3 (10 wt.%) with HFER. As shown in Table 2, the physically

mixed Ga_2O_3 + HFER catalyst exhibited a slightly higher CH_3CN yield than the Ga/HFER catalyst. By contrast, Ga/KFER showed significantly lower CH_3CN yields than Ga/HFER and Ga_2O_3 + HFER.

Table 2. C_2H_6 ammodehydrogenation by various catalysts.[a]

C_2H_6 ammodehydrogenation				
Catalyst	Yield (%)	Conversion (%)	Selectivity (%)	Rate of CH_3CN formation ($\mu mol\ g^{-1}\ min^{-1}$)
Ga_2O_3 + HFER	31.5	65.5	48.1	112.5
Ga/HFER	25.3	49.9	50.8	90.5
Ga/KFER	0.7	29.7	2.2	2.3
HFER	0.4	11.3	3.2	1.3

[a] Conditions are the same as in Fig. 1.

The Fourier transforms (FTs) of the k^3-weighted EXAFS before and after the catalytic reaction are shown in Fig. 4A, together with the results for a reference compound Ga_2O_3. The structural parameters, coordination number (CN), and interatomic distance (R) derived from the curve-fitting analysis of the Ga K-edge EXAFS are listed in Table 3. The EXAFS spectrum of Ga/HFER shows two peaks owing to the Ga–O and Ga–Ga shells. The curve-fitting analysis for Ga/HFER revealed 6.5 Ga–O bonds at 1.90 Å and 2.3 Ga–Ga bonds at 3.05 Å. The Ga–Ga shell parameters were nearly identical to those of Ga_2O_3. After the catalytic reaction at 650 °C, the EXAFS spectrum of Ga/HFER (Ga/HFER_R) showed a peak owing to a Ga–O shell (5.6 Ga–O bonds at 1.87 Å) and a Ga–Al shell (1.2 Al atoms at 3.14 Å). These results indicate that the Ga_2O_3 species in Ga/HFER are converted to isolated Ga^{n+} species at the cation exchange sites in the zeolite. The EXAFS spectrum of the physically mixed Ga_2O_3 + HFER showed two peaks corresponding to Ga–O and Ga–Ga shells. According to the curve-fitting analysis of Ga_2O_3 + HFER, the CN and R of Ga–O are 5.5 and 1.87 Å, respectively, while those for the Ga–Ga shell are 2.7 and 3.08 Å, respectively. The Ga–Ga shell parameters were nearly identical to those of Ga_2O_3. After the catalytic reaction at 650 °C, the EXAFS spectrum of Ga_2O_3 +

HFER (Ga_2O_3+HFER_R) showed only the peak corresponding to a Ga–O shell (4.6 Ga–O bonds at 1.84 Å). Fig. 4B shows the XANES spectra of the catalysts and reference compound Ga_2O_3. The XANES features of Ga_2O_3 + HFER before the reaction are similar to those of Ga_2O_3. The XANES spectrum after the reaction (red spectrum) has different features from those before the reaction. The low-energy peak owing to the tetrahedral Ga(III) species is observed as the main peak. These results indicate that the Ga_2O_3 species in Ga_2O_3 + HFER were converted to isolated Ga^{n+} species, possibly on the cation exchange sites in the HFER zeolite. To discuss the role of the cation exchange sites (Brønsted acid sites), we performed EXAFS analysis of Ga/KFER after the reaction. The EXAFS spectrum of Ga/KFER after the reaction showed both Ga–O and Ga–Ga shells, which indicates that the Ga_2O_3 species in Ga/K-FER do not undergo solid-state ion exchange during the reaction. This implies that the Brønsted acid sites, that is, the cation exchange sites of FER, act as anchoring sites of the isolated Ga^{n+} species. Combined with the catalytic results (Table 2) that Ga/KFER showed a significantly lower CH_3CN yield than Ga/HFER and Ga_2O_3 + HFER, we conclude that the isolated Ga sites formed by solid-state ion exchange during the reaction act as active sites for C_2H_6 ammodehydrogenation.

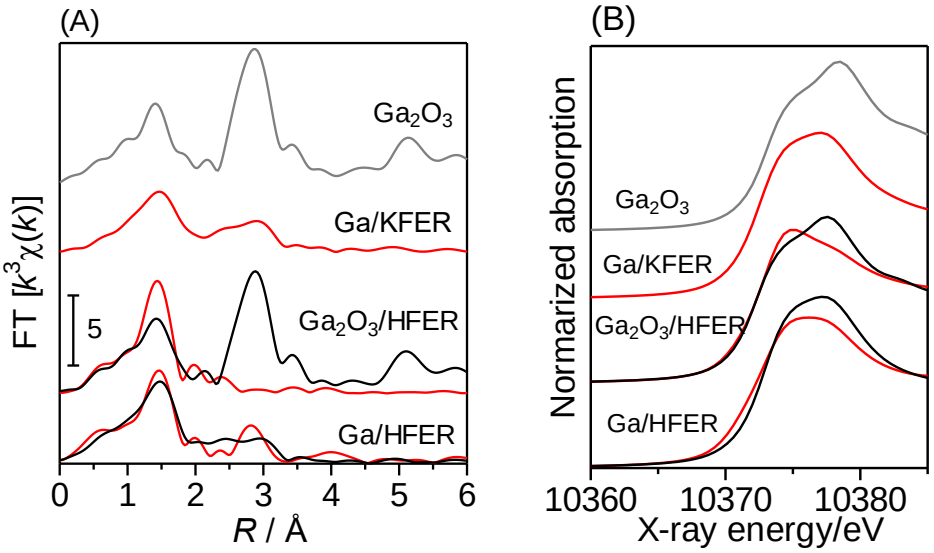

Fig. 4. (A) FT of k^3-weighted EXAFS oscillations measured at room temperature (25 °C) for Ga/KFER, Ga_2O_3/HFER, and Ga/HFER before and after reaction (red and black lines, respectively). (B) In situ Ga K-edge XAS spectra of Ga/KFER, Ga_2O_3/HFER, and Ga/HFER before and after reaction and the

reference Ga_2O_3.

Table 3. Curve-fitting analysis of Ga K-edge EXAFS.

Sample	Shell	CN [a]	*R* /Å [b]	σ /Å [c]	R_f /% [d]
Ga_2O_3 + HFER	O	5.5	1.87	0.114	2.1
	Ga	2.7	3.08	0.031	
Ga_2O_3 + HFER_R	O	4.6	1.84	0.081	1.3
Ga/HFER	O	6.5	1.90	0.114	1.3
	Ga	2.3	3.05	0.098	
Ga/HFER_R	O	5.6	1.87	0.099	1.8
	Al	1.8	3.14	0.032	
Ga/KFER_R	O	5.4	1.90	0.119	1.7
	Ga	3.4	3.06	0.106	
GaMFI_H_2	O	3.9	1.91	0.119	2.0
	Al	1.2	2.92	0.094	
	Ga	0.4	3.21	0.075	
Ga_2O_3	O	5.5	1.86	0.113	2.2
	Ga	2.7	3.07	0.024	

[a] Coordination numbers. [b] Bond distance. [c] Debye-Waller factor. [d] Residual factor.

5.3.3. Catalytic performance on Ga/HFER

The reaction conditions were screened for C_2H_6 ammodehydrogenation over Ga/HFER. Fig. 5A shows the effect of the C_2H_6/NH_3 ratio on the catalytic performance. The C_2H_6/NH_3 ratio increased from 0.8 to 2, where the NH_3 concentration was constant at 2.5%, and concentration of C_2H_6 increased from

2% to 5%. The CH_3CN yield (based on C_2H_6) decreased from 28.0% to 17.9%, even though the formation rate of CH_3CN increased from 5.0 to 8.0 mmol·$g^{-1}$$min^{-1}$. Fig. 5B shows the effect of reaction temperature on product yield. The CH_3CN yield increases with temperature. Based on these results, we adopted the reaction conditions in Fig. 1 (C_2H_6/NH_3 ratio of 0.8, 650 °C) as the standard conditions.

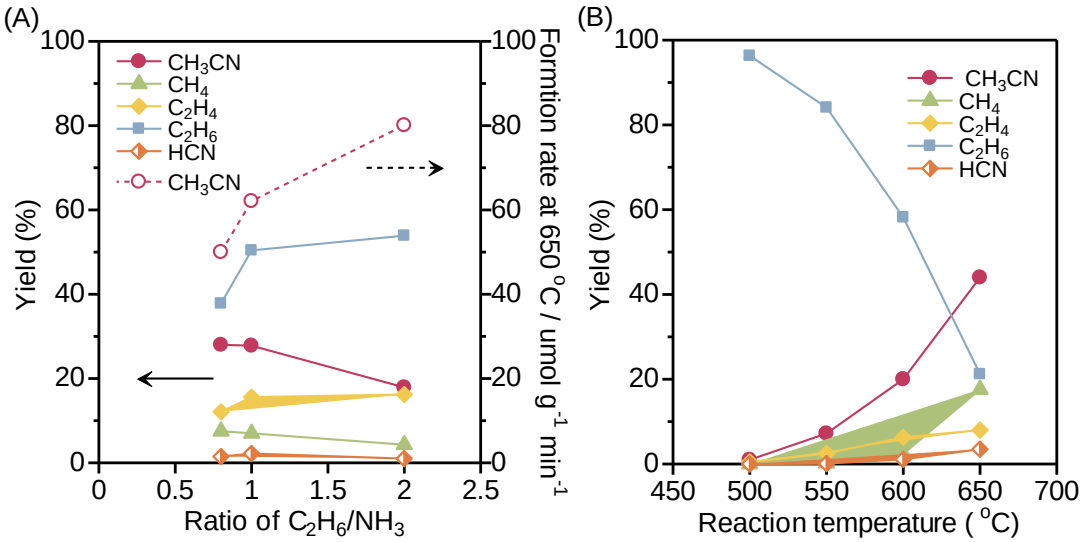

Fig. 5. Reaction condition screening for C_2H_6 ammodehydrogenation by Ga/HFER: (A) C_2H_6/NH_3 ratio (650 °C, when NH_3 is 2.5%, C_2H_6 2-5%) (B) reaction temperature.

The Ga/HFER-catalyzed C_2H_6 + NH_3 reactions under oxidative and nonoxidative conditions were investigated. Under anaerobic conditions (Fig. 6A), CH_3CN was produced as the main product, with an initial yield of 28.0%. Under oxidative conditions (Fig. 6B), the C_2H_6 + NH_3 + $2O_2$ reaction afforded CO_2 as the main product, and the initial yield of CH_3CN was only 3.4%. Cofeeding of O_2 increased the yields of CO_2, CO, CH_4, and C_2H_4. This indicates that O_2 promotes the C_2H_6 combustion and oxidative dehydrogenation of C_2H_6. The combustion of C_2H_6 to CO_2 and CO is one of the main reasons for low CH_3CN yields under oxidative conditions. Interestingly, most previous studies on the catalytic C_2H_6 + NH_3 transformation to CH_3CN were based on the ammoxidation of C_2H_6 (C_2H_6 + NH_3 + $2O_2$ reaction); hence, the presence of O_2 significantly increased the CH_3CN yield. [4–11] The current catalytic system is a rare example of the significant negative effect of O_2 on C_2H_6 + NH_3 transformation to CH_3CN.

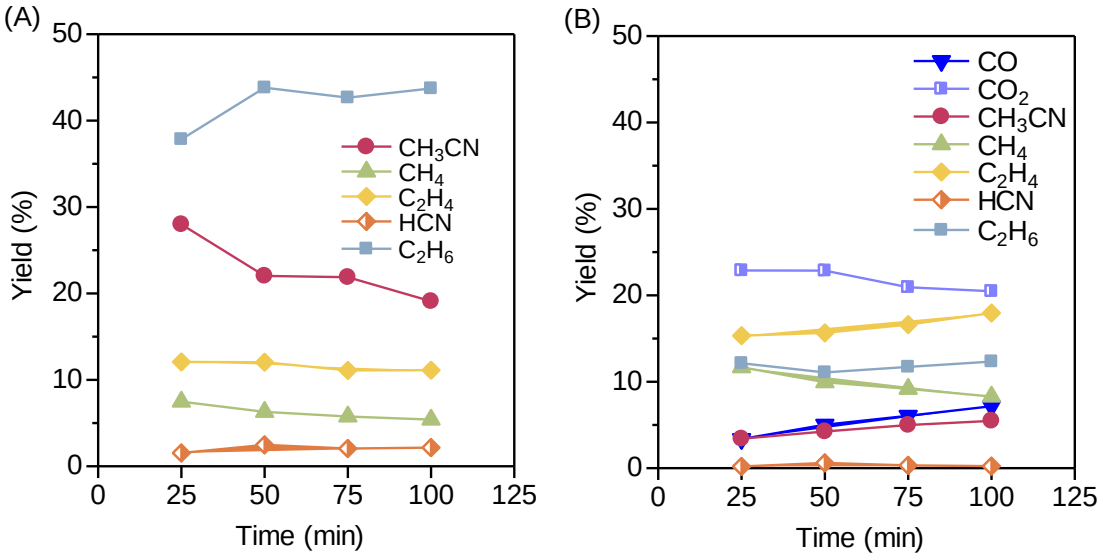

Fig. 6. Time dependence of product yields for (A) ammodehydrogenation (2% C_2H_6/2.5% NH_3/He) and (B) ammoxidation (2% C_2H_6/2.5% NH_3/8.6% O_2/He) by Ga/HFER (0.1 g) at 650 °C.

Fig. 7 shows a plot of the selectivity of CH_3CN versus the conversion of C_2H_6 based on the results of previous reports on the $C_2H_6 + NH_3 + O_2$ [4–11] and $C_2H_6 + NH_3$ reactions [15,18]. Most of these studies were conducted under oxidative conditions. Li et al. reported that Co-beta catalysts can achieve a high CH_3CN yield of up to 26.4% with a CH_3CN selectivity of 55.3% at 475 °C.[17] The Co-BEA zeolites from the impregnation method exhibit a high selectivity towards CH_3CN up to 90% and a high conversion of C_2H_6 up to 48% at 450 °C.[11] Direct CH_3CN formation from C_2H_6 and NH_3 under anaerobic conditions was reported only by two groups. Denton et al. first investigated CH_3CN production from C_2 to C_5 hydrocarbons ~70 y ago, and only 3 % yield of CH_3CN from C_2H_6 was achieved.[3] Xiang et al. recently reported that Pt/HZSM5 showed a CH_3CN selectivity of 99% with a conversion of 1% at 350 °C.[18] They also showed that Co-loaded Pt/HZSM5 shows 18% CH_3CN selectivity with 20% conversion at 600 °C. [15] We compared the catalytic performance of a reported catalyst with that of Ga/HFER. The Ga/HFER, under optimized conditions, achieves a good selectivity for CH_3CN (55.6%) at 78.8% conversion, which supersedes all the reported catalysts.

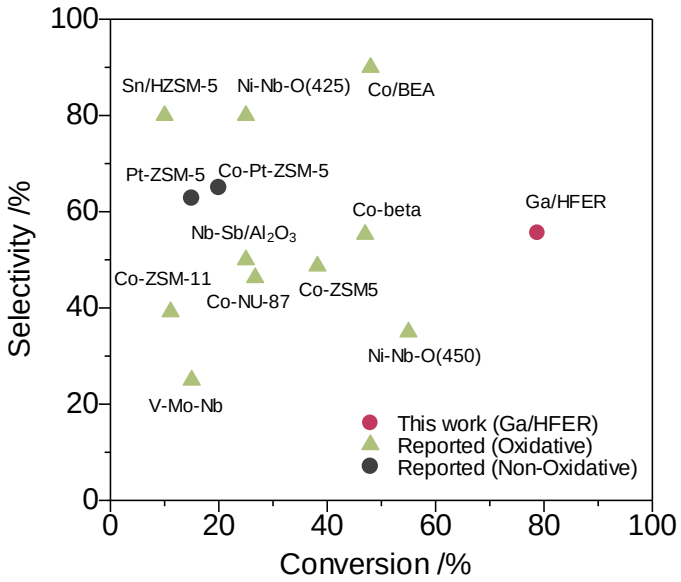

Fig. 7. Catalytic performance comparison of the reference catalysts and Ga/HFER.

5.3.4. Mechanistic study

In this section, we report the kinetic and spectroscopic results and discuss the reaction mechanism. Fig. 8 shows the yields of various products as a function of contact time for C_2H_6 ammodehydrogenation on Ga/HFER. The reactions were conducted using different amounts of catalyst. As the contact time increased, the yield of C_2H_4 decreased, and the yield of CH_3CN increased. This suggests that CH_3CN is produced via a consecutive reaction pathway: dehydrogenation of C_2H_6 to C_2H_4, which then reacts with NH_3 to afford CH_3CN.

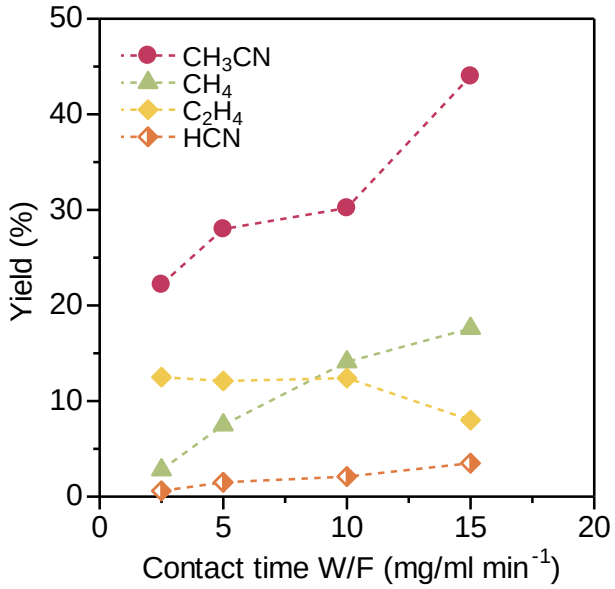

Fig. 8. Product yields vs. contact time for C_2H_6 ammodehydrogenation on Ga/HFER. Conditions: 50–300 g catalyst, 650 °C, 2% C_2H_6 + 2.5% NH_3/He (total flow rate: 20 mL min^{-1}).

The results of the kinetic studies of C_2H_6 ammodehydrogenation on Ga/HFER are shown in Fig. 9. Fig. 9A and B show the dependence of the CH_3CN formation rate on the C_2H_6 ($p(C_2H_6)$) and NH_3 partial pressures ($p(NH_3)$), respectively. The reaction order with respect to C_2H_6 was 0.27, which was slightly higher than that of NH_3 (0.17). This suggests that C_2H_6 is involved in a kinetically relevant step, while NH_3 is not involved in the slow step. The reaction rates of the model reactions (C_2H_4 ammodehydrogenation and C_2H_6 dehydrogenation) and main reaction (C_2H_6 ammodehydrogenation) are compared in Table 4. For Ga/HFER, the reaction rates changed in the following order: C_2H_4 + NH_3 reaction to CH_3CN > C_2H_6 dehydrogenation to C_2H_4 > C_2H_6 + NH_3 reaction to CH_3CN. This result is consistent with the consecutive reaction pathway suggested by the results shown in Fig. 8. C_2H_6 was dehydrogenated to C_2H_4, which reacted with NH_3 to yield CH_3CN. The C_2H_6 dehydrogenation step was slower than the CH_3CN formation step. The Arrhenius plots for these reactions are shown in Fig. 9C. In the temperature range tested (610–580 °C), the rates change in the following order: C_2H_4 + NH_3 > C_2H_6 dehydrogenation > C_2H_6 + NH_3. From the slope of the plots, apparent activation energies for C_2H_4 + NH_3 (62 kJ mol^{-1}), C_2H_6 dehydrogenation (177 kJ mol^{-1}), and C_2H_6 + NH_3 (81 kJ mol^{-1}) were estimated. The highest activation energy observed for C_2H_6 dehydrogenation suggests that the dehydrogenation of C_2H_6 is the rate-limiting step in the C_2H_6 + NH_3 reaction. By contrast, the relatively low activation energy for C_2H_4 + NH_3 (62 kJ mol^{-1}) suggests that the CH_3CN formation by the C_2H_4 + NH_3 reaction is a relatively facile process. These mechanistic considerations are consistent with those derived from the reaction order analyses: C_2H_6 is involved in a kinetically relevant step, while NH_3 is not involved in the slow step.

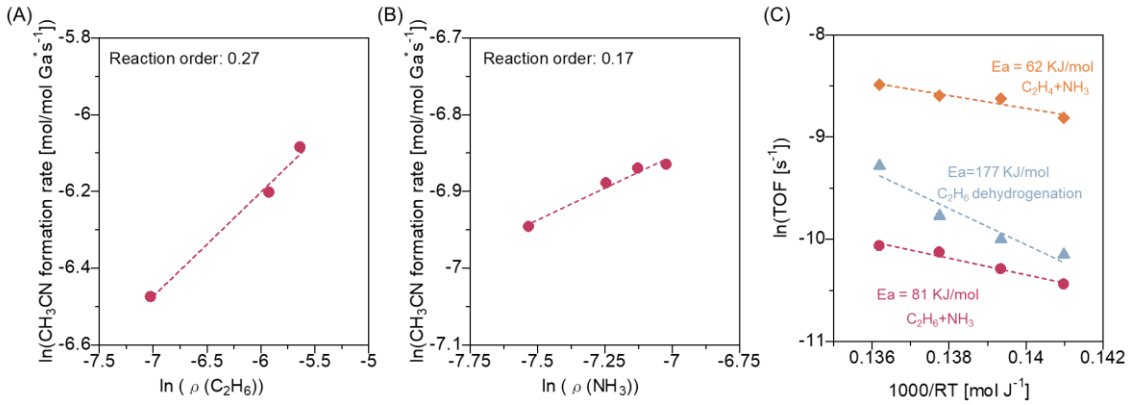

Fig. 9. Kinetic study for C_2H_6 ammodehydrogenation by Ga/HFER: (A) C_2H_6 reaction order and (B) NH_3 reaction order. (C) Arrhenius plot for Ga/HFER-catalyzed C_2H_6 dehydrogenation, C_2H_6 ammodehydrogenation, and C_2H_4 ammodehydrogenation.

The reaction rates over Ga/HFER and HFER for the model reactions are compared in Table 4. The Ga/HFER catalyst showed higher activity than HFER for the C_2H_4 + NH_3 reaction to give CH_3CN. For the C_2H_6 dehydrogenation to C_2H_4, Ga/HFER showed higher activity than HFER. Combined with the EXAFS results, these results indicate that the isolated Ga species act as active sites for the initial C_2H_6 dehydrogenation step and the C_2H_4 ammodehydrogenation step.

Table 4. Rates of three reactions by Ga/HFER and HFER.

Formation rate of main product (CH_3CN or C_2H_4) at 650 °C/ umol g^{-1} min^{-1}			
Reaction	Ga-FER	H-FER	Ga/K-FER
C_2H_6 ammodehydrogenation	90.5	1.3	2.3
C_2H_4 ammodehydrogenation	183.8	43.7	
C_2H_6 dehydrogenation	110.5	26.4	

The reaction of C_2H_4 with NH_3 produces $CH_3CH_2NH_2$ as an intermediate that can be dehydrogenated to CH_3CN. We conducted transient reactions using Ga/HFER to elucidate the possible

reaction pathway. First, NH_3 was adsorbed on Ga/HFER by exposing it to a flow of 10% NH_3/He at 400 °C (10 min). The system was then purged with He (30 min) to remove gaseous NH_3. Thereafter, C_2H_4 was fed to the catalyst at 400 °C while monitoring the mass signals of the gas phase products as a function of the time (Fig. 10A). Mass signals corresponding to C_2H_4 (m/z = 28), CH_3CN (m/z = 41), and $CH_3CH_2NH_2$ (m/z = 45) were observed during transient reactions. Notably, $CH_3CH_2NH_2$ initially formed was subsequently transformed into CH_3CN. This suggests that C_2H_4 reacted with the adsorbed NH_3 to yield $CH_3CH_2NH_2$, which was then converted into CH_3CN. We also performed a temperature-programmed surface reaction (TPSR) experiment on NH_3-preadsorbed Ga/HFER in C_2H_4 (Fig. 10B). The catalyst, preexposed to a 10% NH_3/He flow at 300 °C (10 min), followed by He purge (30 min), was exposed to a C_2H_4 flow while ramping up the temperature from 300 to 700 °C at a ramping rate of 10 °C min^{-1}. Mass signals corresponding to CH_3CN (m/z = 41) were recorded during the temperature ramping. The observation of CH_3CN formation by the reaction between C_2H_4 and adsorbed NH_3 further confirms the proposed reaction pathway.

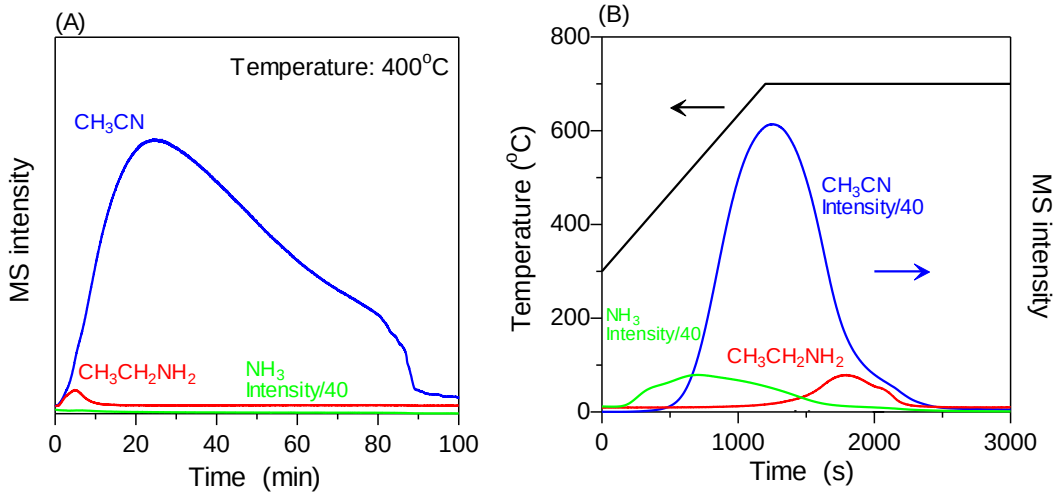

Fig. 10. (A) Mass intensity of the gas phase products during the transient reaction of NH_3 preadsorbed Ga/HFER under 5% C_2H_4 at 400 °C. (B) TPSR profile for the reaction of NH_3 preadsorbed Ga/HFER under 5% C_2H_4.

5.4. Conclusion

The findings of this study revealed that Ga/HFER is an effective catalyst for CH_3CN synthesis via the

anaerobic ammodehydrogenation of C_2H_6. A Ga-free HFER and Ga-loaded K-exchanged FER (Ga/KFER) are nearly inactive for this reaction, indicating that both Ga and Brønsted acid sites are indispensable elements. EXAFS results showed that the Ga_2O_3 species in the as-prepared Ga/HFER catalyst are converted to isolated Ga cations after the C_2H_6 ammodehydrogenation at 650 °C, while the Ga_2O_3 species in Ga/KFER remain unchanged after the reaction. The results indicate that the Brønsted acid sites (exchangeable H^+ sites) of HFER act as the anchoring sites of the isolated Ga cations, possibly formed by reductive solid-state ion exchange during the reaction, and the isolated Ga sites act as active sites for C_2H_6 ammodehydrogenation. Kinetic analysis suggests that CH_3CN is produced via a consecutive reaction pathway: the dehydrogenation of C_2H_6 to C_2H_4, which reacts with NH_3 to yield CH_3CN. The cofeeding of O_2 to $C_2H_6 + NH_3$ significantly decreased the CH_3CN yield and formation of CO_2 and CO as the main products, suggesting the importance of reductive conditions in the current catalytic system. These findings have important implications for the development of novel catalysts and processes for the synthesis of value-added chemicals from inexpensive feedstocks.

Reference

1. Deepa, H. A., Anusha, R. & Asha, P. Evaluation on Production and Economics of Acrylonitrile by Sohio Process. *Int. J. Eng. Res. Technol.* **4**, 1–6 (2016).
2. Bell, A. T. Insights into the mechanism and kinetics of propene oxidation and ammoxidation over bismuth molybdate catalysts derived from experiments and theory. *J. Catal.* **408**, 436–452 (2022).
3. Denton, W. I. & Bishop, R. B. Production of Acetonitrile and Other Low Molecular Weight Nitriles. *Ind. Eng. Chem.* **45**, 282–286 (1953).
4. Catani, R. & Centi, G. Selective ethane ammoxidation to acetonitrile on alumina-supported niobium-antimony oxides. *J. Chem. Soc. Chem. Commun.* 1081–1083 (1991) doi:10.1039/C39910001081.
5. Liang, T. *et al.* Highly selective Sn/HZSM-5 catalyst for ethane ammoxidation to acetonitrile and ethylene. *Appl. Catal. A Gen.* **610**, 117942 (2021).

6. Liu, X. *et al.* Ammoxidation of Ethane to Acetonitrile and Ethylene: Reaction Transient Analysis for the Co/HZSM-5 Catalyst. *ACS Omega* **5**, 1669–1678 (2020).

7. Li, Y. & Armor, J. N. A reaction pathway for the ammoxidation of ethane and ethylene over Co-ZSM-5 catalyst. *J. Catal.* **176**, 495–502 (1998).

8. Bondareva, V. M. *et al.* Ammoxidation of ethane on V-Mo-Nb oxide catalysts. *React. Kinet. Catal. Lett.* **87**, 377–386 (2006).

9. Rojas, E., Guerrero-Pérez, M. O. & Bañares, M. A. Direct ammoxidation of ethane: An approach to tackle the worldwide shortage of acetonitrile. *Catal. Commun.* **10**, 1555–1557 (2009).

10. Rubio-Marcos, F. *et al.* Tuning of Active Sites in Ni-Nb-O Catalysts for the Direct Conversion of Ethane to Acetonitrile or Ethylene. *ChemCatChem* **3**, 1637–1645 (2011).

11. Essid, S. *et al.* Improvement of the conventional preparation methods in Co/BEA zeolites: Characterization and ethane ammoxidation. *Solid State Sci.* **93**, 13–23 (2019).

12. Peeters, I. *et al.* Structure-activity relationships in the ammoxidation of ethylene in the absence of molecular oxygen over γ-Al2O3-supported molybdenum oxide catalysts. *J. Catal.* **173**, 28–42 (1998).

13. Ayari, F. *et al.* Effect of the chromium precursor nature on the physicochemical and catalytic properties of Cr-ZSM-5 catalysts: Application to the ammoxidation of ethylene. *J. Mol. Catal. A Chem.* **339**, 8–16 (2011).

14. Rhimi, B., Mhamdi, M., Kalevaru, V. N. & Martin, A. Synergy between vanadium and molybdenum in bimetallic ZSM-5 supported catalysts for ethylene ammoxidation. *RSC Adv.* **6**, 65866–65878 (2016).

15. Chen, G. *et al.* Acetonitrile formation from ethane or ethylene through anaerobic ammodehydrogenation. *Catal. Today* 113751 (2022) doi:10.1016/j.cattod.2022.05.016.

16. Li, Y. & Armor, J. N. Ammoxidation of Ethane to Acetonitrile over Metal–Zeolite Catalysts. *J. Catal.* **173**, 511–518 (1998).

17. Li, Y. & Armor, J. N. Ammoxidation of ethane to acetonitrile over Co-beta zeolite. *Chem. Commun.* 2013–2014 (1997).

18. Chen, G. *et al.* Catalytic Light Alkanes Conversion through Anaerobic Ammodehydrogenation. *ACS Catal.* **11**, 7987–7995 (2021).

19. Huang, M. *et al.* High-loading Ga-exchanged MFI zeolites as selective and coke-resistant catalysts for nonoxidative ethane dehydrogenation. *Catal. Sci. Technol.* (2022) doi:10.1039/d1cy01799c.

20. Huang, M., Maeno, Z., Toyao, T. & Shimizu, K. ichi. Ga speciation and ethane dehydrogenation catalysis of Ga-CHA and MOR: Comparative investigation with Ga-MFI. *Catal. Today* **411**–**412**, 113824 (2022).

21. Maeno, Z. *et al.* In-exchanged cha zeolites for selective dehydrogenation of ethane: Characterization and effect of zeolite framework type. *Catalysts* **10**, (2020).

22. Kazansky, V. B., Subbotina, I. R., Van Santen, R. A. & Hensen, E. J. M. DRIFTS study of the chemical state of modifying gallium ions in reduced Ga/ZSM-5 prepared by impregnation I. Observation of gallium hydrides and application of CO adsorption as a molecular probe for reduced gallium ions. *J. Catal.* **227**, 263–269 (2004).

23. Serykh, A. I. & Kolesnikov, S. P. On the nature of gallium species in gallium-modified mordenite and MFI zeolites. A comparative DRIFT study of carbon monoxide adsorption and hydrogen dissociation. *Phys. Chem. Chem. Phys.* **13**, 6892–6900 (2011).

Chapter 6

General conclusions

In this thesis, the author described the studies on the Ga-hydrides in zeolites for dehydrogenative transformation of light-alkane. General conclusions are summarized as follows.

In **Chapter 1**, a brief introduction of Ga-hydrides in various zeolites for light-alkane transformation.

In **Chapter 2**, we prepared a series of Ga-MFIs with different Ga loading amounts and H_2 treatment temperature and examined the generated Ga species and catalysis for EDH. *In situ* FTIR spectroscopy revealed that $[GaH]^{2+}$ ions were preferentially formed in low-loading Ga-MFI (Ga-MFI-0.3(550)), prepared under conventional conditions, whereas both $[GaH]^{2+}$ and $[GaH_2]^+$ ions were moderately formed in the middle-loading Ga-MFI (Ga/Al = 0.5). In contrast, $[GaH_2]^+$ ions were formed as the major Ga hydride in Ga-MFI-1.0(800). The characterization of other Ga species and BASs indicated that high-temperature H_2 treatment was required to promote the RSSIE sufficiently for high-loading Ga-MFI. In Ga-MFI-1.0(800), monovalent Ga species ($[GaH_2]^+$ ions and Ga^+ cations) are mainly formed. The difference of H_2 treatment temperature between 700 and 800 ˚C also affects the proportion of $[GaH]^{2+}$ and $[GaH_2]^+$ ions in high-loading Ga-MFI. In EDH, Ga-MFI-1.0(800) exhibited high selectivity owing to much less coke formation, resulting in the highest durability. Under the optimized reaction conditions, the highest C_2H_4 formation rate was achieved among the reported Pt-free catalyst systems. The kinetic study revealed that isolated Ga hydrides serve as active sites rather than Ga^+ cations. The main reason for the high catalytic performance of Ga-MFI-1.0(800) is a low amount of the remaining BASs by introducing the high loading amount of isolated Ga species. Based on the comparison of high-loading Ga-MFIs treated with different temperature (700 or 800 ˚C), the different proportion of active Ga hydrides ($[GaH_2]^+$ and $[GaH]^{2+}$ ions) also influences their catalysis in EDH.

In **Chapter 3**, we investigated the effect of different zeolite frameworks (CHA and MOR) on

Ga speciation and ethane dehydrogenation catalysis for comparison with Ga-MFIs. The formation of Ga-hydrides in CHA and MOR zeolites after RSSIE was confirmed by FT-IR spectroscopy, indicating that Ga-hydrides were more likely to be formed in MOR than CHA. The formation of other isolated Ga species was confirmed by Py adsorption experiments and *in situ* XAS spectroscopy. Increasing the Ga loading was found to be effective in reducing the remaining BASs in both zeolites. These results are similar to those obtained in our recent study of Ga-MFIs. Regarding ethane dehydrogenation catalysis, an increase in Ga loading improved the durability of Ga-MOR, whereas both low- and high-loading Ga-CHA exhibited low durability. However, the catalytic performances of Ga-CHA and -MOR were inferior to those of the previously developed high-loading Ga-MFI catalyst. The high catalytic performance of MFI was discussed based on kinetic studies and H−D exchange reactions. $[GaH_2]^+$ ions are plausible active Ga-hydrides in the high-loading Ga-MOR, as seen with Ga-MFI, whereas different kinetics were observed for the high-loading Ga-CHA. The H−D exchange reactions over a series of Ga-exchanged zeolites indicate that the highest relative amount of Ga-hydrides is one of the reasons for the high catalytic performance of MFI. This study revealed the formation of Ga-hydrides in other zeolite frameworks other than MFI and suggests that formation of more isolated Ga-hydrides is key to developing more efficient Ga-zeolite-based catalysts for alkane dehydrogenation.

In **Chapter 4**, we conducted an in situ Ga K-edge XANES study for high-loading Ga-MFI prepared by high-temperature H_2 treatment at high temperatures (> 700 °C) under different atmospheres. In the normal pressure experiment, H_2 treatment afforded a significantly lower energy shift and strong whiteline intensity at the absorption edge of the XANES spectrum. Successive high-temperature He treatment decreased the whiteline intensity while maintaining the absorption edge position in energy, and the XANES spectrum returned to almost its original intensity. In situ XANES measurements of oxidized Ga-MFI under CO, pressurized H_2, and vacuum conditions showed that the whiteline intensity increased with the increase of H_2 pressure while the similarly lower intensities were obtained under CO and vacuum conditions. These results indicated that the increase in the whiteline intensity is interpreted as the formation of active Ga hydrides. Notably, the C_2H_6 treatment resulted in a higher intensity similar to that of the H_2 treatment, suggesting the presence of hydride-containing

Ga species under real operation conditions. Similar spectral changes depending on the measurement conditions were observed for Ga-CHA and Ga-MOR. The degree of spectral change correlated well with the relative amount of Ga hydrides estimated by IR, as well as the steady-state EDH activity.

In **Chapter 5**, the findings of this study revealed that Ga/HFER is an effective catalyst for CH_3CN synthesis via the anaerobic ammodehydrogenation of C_2H_6. A Ga-free HFER and Ga-loaded K-exchanged FER (Ga/KFER) are nearly inactive for this reaction, indicating that both Ga and Brønsted acid sites are indispensable elements. EXAFS results showed that the Ga_2O_3 species in the as-prepared Ga/HFER catalyst are converted to isolated Ga cations after the C_2H_6 ammodehydrogenation at 650 °C, while the Ga_2O_3 species in Ga/KFER remain unchanged after the reaction. The results indicate that the Brønsted acid sites (exchangeable H^+ sites) of HFER act as the anchoring sites of the isolated Ga cations, possibly formed by reductive solid-state ion exchange during the reaction, and the isolated Ga sites act as active sites for C_2H_6 ammodehydrogenation. Kinetic analysis suggests that CH_3CN is produced via a consecutive reaction pathway: the dehydrogenation of C_2H_6 to C_2H_4, which reacts with NH_3 to yield CH_3CN. The cofeeding of O_2 to C_2H_6 + NH_3 significantly decreased the CH_3CN yield and formation of CO_2 and CO as the main products, suggesting the importance of reductive conditions in the current catalytic system. These findings have important implications for the development of novel catalysts and processes for the synthesis of value-added chemicals from inexpensive feedstocks.

Throughout all the studies, the author extensively investigated the catalytic properties of Ga-hydrides in zeolites for dehydrogenative transformation of light alkanes. The study covered various aspects, including the preparation of Ga-hydrides in MFI zeolites with different Ga loading amounts and H_2 treatment temperatures, the influence of zeolite frameworks (CHA and MOR) on Ga speciation, and an in-depth analysis of high-loading Ga-MFI using in situ Ga K-edge XANES studies. Additionally, the author explored the effectiveness of Ga/HFER as a catalyst for CH_3CN synthesis through anaerobic ammodehydrogenation of C_2H_6. Throughout the thesis, the focus was on understanding the formation and behavior of Ga-hydrides in zeolites and their impact on catalytic

performance, shedding light on the development of efficient Ga-zeolite catalysts for alkane dehydrogenation and the synthesis of value-added chemicals.

Acknowledgement

I would like to extend my deepest gratitude to my supervisor Prof. Ken-ichi Shimizu for providing me with the chance of being a part of his laboratory. I could not complete the thesis without his great support and valuable. I grew up from a beginner to a person who has gained scientific thinking and experimental skills with his guidance. I never forget his valuable guidance.

I greatly appreciate Prof. Dr. Zen Maeno for his daily support and kind encouragement. His patient guidance and kind advice make me a researcher. His warm-hearted attitude makes me feel at home though I study alone in Japan. I remember his kindness forever.

I also appreciate Prof. Dr. Takashi Toyao for his great help to complete this work. I could always discuss with him thanks to his kindness to give me time for discussion. I would like to be thankful to Prof. Dr. Shinya Furukawa, Prof. Dr. S.M.A. Hakim Siddiki, their kindness in assisting with this thesis and invaluable suggestion and the great help to complete this work.

I also would like to thank all other members of Prof. Shimizu's laboratory.

Finally, I would like to express my best regards to my family and friends for their kind support, understanding, and encouragement all the time.

Huang Mengwen